MEASUREMENT OF THERMODYNAMIC PROPERTIES OF RARE EARTH CHLORIDES IN MOLTEN LiCl-KCl EUTECTIC SALT FOR WASTE MINIMIZATION FROM PYROCHEMICAL PROCESSING OF SPENT NUCLEAR FUEL

by

Prashant Bagri

A dissertation submitted to the faculty of
The University of Utah
in partial fulfillment of the requirements for the degree of

Doctor of Philosophy

Department of Metallurgical Engineering

The University of Utah

August 2017

The University of Utah Graduate School

STATEMENT OF DISSERTATION APPROVAL

The dissertation of **Prashant Bagri**

has been approved by the following supervisory committee members:

Michael F. Simpson ,	Chair(s)	**25 April 2017** Date Approved
Michael L. Free ,	Member	**25 April 2017** Date Approved
Hojong Kim ,	Member	Date Approved
Jan D. Miller ,	Member	**25 April 2017** Date Approved
Anil V. Virkar ,	Member	**25 April 2017** Date Approved

by **Manoranjan Misra** , Chair/Dean of

the Department/College/School of **Metallurgical Engineering**

and by **David B. Kieda** , Dean of The Graduate School.

ABSTRACT

The thermodynamic and electrochemical properties of rare earth chlorides in molten salt solutions are of interest from the standpoint of both pyrochemical processing of spent nuclear fuel and for the development of Generation IV nuclear reactors. Knowledge of key properties like activity coefficients, phase diagrams and reliable waste disposal methods will accelerate the development of safe reliable carbon free energy. In this work, three conduits of research have been pursued and reported within the larger theme of minimization of waste in spent fuel reprocessing and associated technology development.

First a novel process for the disposal of chloride salts using H-Y zeolite has been studied. In this process, a protonated Y zeolite is used to occlude the LiCl-KCl eutectic salt. In the process, the proton and the chloride ions react to evolve HCl gas that can be easily captured and neutralized. Hence the final waste form will be lighter compared to the baseline process. Results indicate that the proton and chloride react to form HCl gas which was captured and neutralized. Up to 50 % of theoretical ion exchange was achieved based on the total HCl evolution.

The activity of four rare earth chlorides was determined electrochemically in LiCl-KCl eutectic salt. These rare earth chlorides are: $LaCl_3$, $NdCl_3$, $GdCl_3$, and $CeCl_3$. The activity was determined using two distinct experimental set-ups: using a Ag/AgCl reference electrode and an analyte reference electrode. Broadly it is noted that the activity coefficient of the rare earth chlorides changes with concentration of the analyte in solution. From the data of all of the four rare earth chlorides it was concluded that as the ionic size of the rare earth reduces, the species shows a larger negative deviation from ideal solution behavior. The presence of large concentrations of CsCl seems to influence the activity of some of the rare earths.

The solidus and liquidus temperatures for quaternary LiCl-KCl-CsCl-$RECl_3$ systems were determined using a differential scanning calorimetry. It is observed that the presence of CsCl depresses the melting temperature for all of the rare earth chlorides tested. The

LiCl-KCl-CsCl-$LaCl_3$ system departs from eutectic behavior and manifests peritectic behavior. The LiCl-KCl-CsCl-$GdCl_3$ system shows peritectic behavior at only low $GdCl_3$ and high CsCl concentrations. The LiCl-KCl-CsCl-$NdCl_3$ system continues to exhibit purely eutectic behavior for all of the concentration windows tested for this work.

For my Mom!

CONTENTS

LIST OF FIGURES

LIST OF TABLES

NOTATION AND SYMBOLS

Symbol	Assignment
μ	Chemical Potential
γ	Activity Coefficient
X	Mole Fraction
μ^E	Excess Chemical Potential
E^0	Standard Reduction Potential
R	Universal Gas Constant
E	Electrochemical Potential
n	Number of Electrons Transferred
$\bar{G^E}$	Excess Chemical Potential
α	Ion Size Parameter
$\bar{G}$	Chemical Potential
a	Activity
C_p	Heat Capacity
S	Entropy
H	Enthalpy
T	Temperature
$E^{0'}$	Apparent Potential
G	Gibbs Free Energy
N_i	Total Moles of ’i’

ACKNOWLEDGEMENTS

This work does not only belong to the author alone. A vast number of people have made contributions to make this possible. First and foremost, I would like to thank my adviser Dr. Michael F. Simpson for taking me as a graduate student, his patience, guidance, support and mentoring. I would also like to thank the committee, Dr. Anil V. Virkar, Dr. Hojong Kim, Dr. Jan D. Miller, and Dr. Michael F. Free, for firstly agreeing to be on the committee, for their suggestions and input. Special thanks to Dr. Arthur D. Pelton at Polytechnique Montréal for his continued guidance with thermodynamics and always entertaining my questions.

I would also like to thank all of my lab mates, past and present, without whom this work would not have been possible. The scientific help, discussions, friendly banter and camaraderie made this experience one I will always cherish. Thank you to you all: Adam Burak, Aliaksei Minko, Avi Jurovitzki, Chao Zhang, David Horvath, Devin Rappleye, Lauryan Hansen, Manish Wasnik, Mario Gonzalez, Milan Stika, Parker Okabe, Silvia Padilla, Tarciso Bastos.

Further, I would like to thank all of my friends in Salt Lake City over all of these years. This time in Salt Lake City has been a life changing experience and will always be memorable. Special thanks to Gita for cooking all of the food for so many years, Anshul and Hari for always being there.

Finally, I would like to thank my family both in the US and in India who have been the bedrock of my life. Your unwavering support has been the foundation upon which I stand always. My Grandparents without whose blessing none of this would have ever happened. My parents and sisters whom I miss every single day, hoping that they would be here with me.

Last but not the least, I would like to thank my wife Ankita. It is safe to say that without your encouragement and support this would not have been possible. Thank you for being patient, understanding, encouraging, supportive. Thank you for marrying me!!

CHAPTER 1

INTRODUCTION

Over the course of human history, distinct civilizations have used the Earth's natural resources in abundance in a given epoch. Those epochs have been named for the namesake materials like the Stone Age, Bronze Age and the Iron Age. It is an interesting thought experiment to question the *Age* the 21^{st} century represents. As Eric Roston[3] discussed so eloquently in his book of the same title, the Twenty-First century represents the *Carbon Age*. Every facet of modern life is predominantly powered by carbon energy sources. Carbon is in fact the foundation upon which modern lifestyles and the global economy have been built since the advent of the steam engine. Carbon sources of energy have in the recent decades come under increasing scrutiny. The effect of emitting large quantities of carbon and other greenhouse gases into the Earth's atmosphere has contributed to the warming of the global climate. The science of global climate change is undisputed.[4] The effects of the carbon already in the atmosphere will linger on for many centuries to come. The United Nations' Intergovernmental Panel on Climate Change (IPCC) in its Fifth Assessment Report[5] completed in 2014 states amongst other things that, *"Warming of the climate system is unequivocal, and since the 1950s, many of the observed changes are unprecedented over decades to millennia."* Such dire predictions should serve as a wake-up call to the world leaders for urgent action. As President Obama has stated on many occasions the solution to the energy problem is *All of the above*. This *All of the above* must include safe, sustainable and proliferation resistant nuclear energy.

The International Energy Agency (IEA) estimates that in 2013, the total world energy consumption was about 12.3 terra watts.[6] With the continued growth in the world population as expected, this number is only likely to increase. At the same time, the per capita energy consumption is also going up, as reported by the IEA. An upward trend in these key metrics means that for the foreseeable future, there is going to be a continued demand for increased

energy worldwide. This reality coupled with the unyielding evidence on climate change means that there is going to be an increasing need to develop carbon free sources of energy. This must include the large scale adaptation and deployment of clean, sustainable, safe and proliferation resistant nuclear energy. Nuclear energy since its advent has been a politically challenging and socially sensitive issue for large scale deployment. The attitudes towards nuclear energy are well entrenched in society and hard to change. Only with the advent of newer, safer nuclear reactors can the public at large be educated to have a more favorable view of having a nuclear reactor in their backyard and lead to a renaissance in the nuclear energy industry.

In recent years, there have been conflicting attitudes in various countries about the use of nuclear energy. The Fukushima Daiichi nuclear disaster was an important event in shaping the public policy and public opinion. In the first decade of the twenty-first century, there was an increasing interest in the developing world from countries like India to satiate their energy demands with nuclear energy which resulted in the landmark Indo-US Civilian Nuclear Agreement under the George W. Bush administration. Similarly, China has been looking into expanding its nuclear energy infrastructure to move away from coal to help mitigate the increasing pollution observed in many parts of China. Since the Fukushima Daiichi nuclear disaster in 2011, Germany, Belgium, Spain and Switzerland currently have policies on phasing out nuclear power. There is a much larger group of countries that currently do not have any operating nuclear power plants and remain in continued opposition to nuclear energy.

In the United States, the state of the nuclear industry is somewhat mixed. In the 2000s, there was definitely a renewed and sustained interest in nuclear power in the US as the cost of fossil fuels skyrocketed. The US government in 2010 announced loan guarantees for two new nuclear reactors to be built.

While the many challenges associated with the nuclear industry have been briefly touched on above, public opinion is something that can be altered with a sustained public discourse about the improved safety benefits of the new up-coming Generation IV reactors. To meet that eventual target, it is important that the research and development of the new generation of reactors be actively pursued with the enthusiastic financial support of governments around the world and the technical safety of these reactors be well established before such

a campaign can be embarked upon.

1.1 Spent Fuel Management

The management of spent fuel presents an important challenge that needs to be adequately addressed when a nuclear power plant is built. The current practice in the United States is to store nuclear waste in a long term geological repository like the Waste Isolation Pilot Plant (WIPP). WIPP is primarily used to store waste generated from defense applications. Commercial nuclear power plants currently store their waste in dry casks at the plant site. Three options exist with regard to management of spent fuel: long term storage, disposal of the waste, and recycling. For any decision about the adaptation of an open versus closed fuel cycle many competing considerations play a role in the decision making process. Some of these considerations are to prevent excessive exposure of ionizing radiation to the population, prevent nuclear weapons proliferation, ensure an adequate supply of nuclear fuel, and cost of reprocessing.

Convincing arguments can be made for the merits of both an open fuel cycle and a closed fuel cycle. However the above factors must be considered before any long term policy decision is made. In terms of reprocessing technology, there are two major technology options, viz. aqueous reprocessing and pyrochemical reprocessing. The commercialized aqueous reprocessing option is the PUREX process and its derivative process options. PUREX is a nitric acid based solvent extraction process. The other alternative is high temperature electrochemical separation of the fuel, i.e., pyrochemical processing. The research presented in this work has applications to the waste minimization within the pyroprocessing flowsheet.

1.2 Pyrochemical Processing

The International Atomic Energy Agency (IAEA) estimated in a review[7] that in the year 2010, the cumulative waste generated from global energy production would be about 340,000 tons heavy metals (tHM) rising to a projected value of about 445,000 tHM by the year 2020. These large volumes of generated waste call for new strategies for the treatment of both new reactor systems and supporting fuel cycle options to enable waste reduction and maximum utilization of the precious fuel.

Research and development into pyrochemical reprocessing alternatives date back to the

1950s, with metal electrorefining and oxide reduction drawing interest from researchers in the United States and Russia. Electrorefining now draws considerable research interest in the United States, Republic of Korea, Japan, India and Europe. Pyrochemical processing encompasses a wide spectrum of technologies including chemical, electrochemical and physical treatments for separations of nuclear materials. They include oxidation/reduction between metal and salt phase, electrorefining, electrowinning and oxide reduction.

One of the advantages of using the pyroprocessing scheme is that molten salts are very radiation resistant solvents, hence the cooling times before reprocessing can be significantly shortened. Cooling times of a few months are a vast improvement over the approximately five years or longer needed for aqueous reprocessing. A pyrochemical processing facility can also be made relatively compact compared to a PUREX facility. A further advantage of using molten salt is the reduced risk of criticality hazards and a more proliferation resistant process due to relatively impure product fractions. Some of the challenges are that molten salts and liquid metals are very aggressive media and their use at high temperature can pose significant operational challenges. The need for an inert atmosphere begets the need for highly sophisticated technology and automation. This work deals mainly with electrorefining based processes which is discussed in more detail in the next section.

1.3 Electrorefining

Electrorefining is a high temperature, molten salt based extraction process used for the separation of the spent fuel within the pyroprocessing flowsheet. A schematic diagram of an electrorefining cell is shown in Figure 1.1. The electrorefining of metallic spent fuel is a batch process performed in a molten LiCl-KCl eutectic (59 mol % LiCl, 41 mol % KCl) salt bath generally at a temperature of 773 K. In electrorefining, the spent fuel is anodically dissolved and uranium and transuranics are deposited on the cathode. The cathode can be an inert metal (steel), a reactive metal (aluminum) or liquid metal cathode (cadmium). Inert solid cathodes are excellent at recovering pure uranium deposit,[8] reactive solid metal cathodes are good at collecting uranium and transuranic elements with less rare earth impurities[9] whereas liquid metal cathodes allow for the co-deposition of uranium and transuranic elements during the electrorefining process but can result in high levels of rare earth impurities in the cathode deposit.[10] The use of a reactive aluminum or cadmium

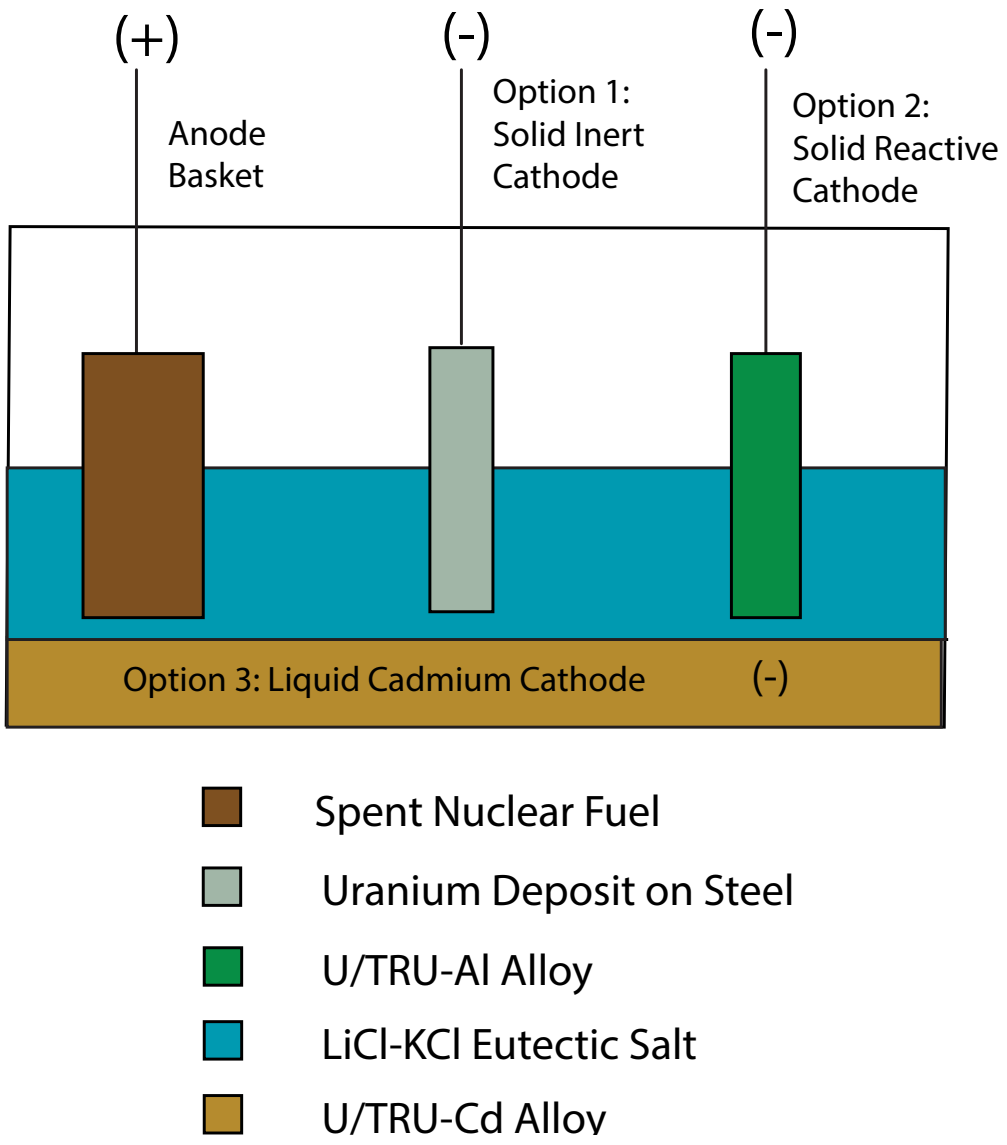

Figure 1.1. Schematic of an electrolytic electrorefining cell for pyroprocessing.

cathode results in an Al-An/Cd-An alloy (An: Actinide). During electrorefining, plutonium and other minor actinides (MAn) and reactive fission products convert to chlorides and accumulate in the salt. Unreactive fission products, nonmetals and residual oxides from the reduction step accumulate as metallic or oxide solids in the anode basket to form anode sludge. Recovery of the actinides from the deposited product is completed using a cathode processor.

Over the last two decades, a considerable body of literature has been published on each of the unit operations in the electrorefining process. Many of the challenges associated

with large scale commercialization have been overcome, while some obstacles remain. Engineering scale developments have continued to progress as greater emphasis is placed on industrialization and new design concepts. The Idaho National Laboratory (INL) continues to operate the Mark IV and Mark V electrorefiners for treating fuel from the Experimental Breeder Reactor-II.[11] Korean Atomic Energy Research Institute (KAERI) continues to advance innovative new concepts in electrorefining.[12,13]

Minimizing the total volume of waste generated also remains an overall goal of the partitioning and transmutation (P&T) strategies,[14] which are being developed as an alternative waste management option to the direct geological disposal of spent nuclear fuel. Presently there are quite a few organizations in various countries working actively to develop various technology elements of pyrochemical electrorefining process. However at this point, there is no consensus on an agreed flow sheet or agreement on the key steps for this process. Figure 1.2 shows the generic flow sheet for an electrorefining process published by Lewin and Harrison.[1] It can be observed from Figure 1.2 that once the fuel has been processed through the oxide reduction, electrorefining processing unit operations, salt clean-up needs to be performed for both the oxide reduction and electrorefining unit operations. The waste generated from the whole process needs to be disposed of safely.

1.3.1 Product Processing

1.3.1.1 Cathode Processing

Cathode processing is essentially a high temperature vacuum distillation process. The solid cathode product removed from the electrorefiner is comprised of metallic uranium

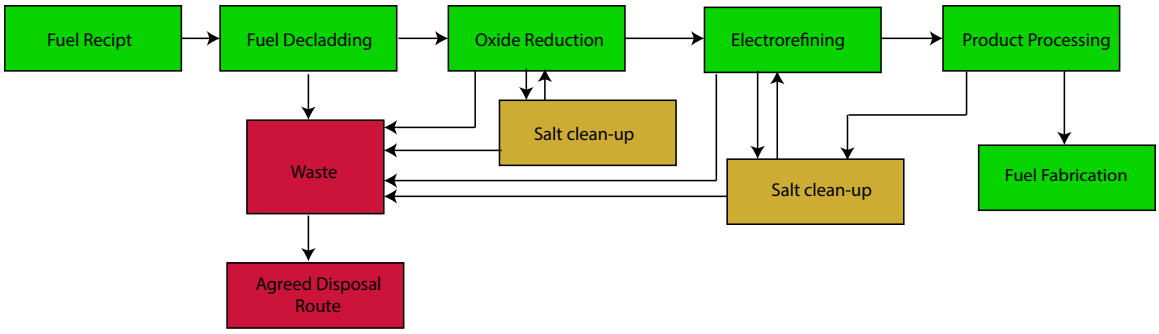

Figure 1.2. Schematic of the electrorefining process flowsheet adapted from Lewin and Harrison[1]

dendrites coated with salt. Using the processor, the salt is vaporized and condensed under vacuum, while the metal dendrites melt and coalesce to form a uranium metal ingot. In the case of a liquid metal cadmium cathode, product from the electrorefiner containing uranium and transuranics is again heated under vacuum. In this process, the cadmium is distilled, condensed and collected while the uranium and TRU product remain as a solid metal ingot in the process vessel. Both the separated salt and the cadmium can be returned and reused in the electrorefiner.

1.3.1.2 Anode Processing

At the anode, fuel fines, nonreactive metals including the cladding hulls and inert matrix materials (zirconium) are retained with the anode after electrorefining. These materials are removed from the electrorefiner and loaded into a vacuum distillation unit to remove any residual salt. The metals are melted and consolidated in the process to produce a metal waste form for disposal in a high level waste disposal repository.

1.3.2 Salt Clean-up

Over time, the unwanted products in the electrorefiner electrolyte will begin to accumulate. These unwanted products include rare earths chlorides (lanthanides) and alkaline earth fission products. These unwanted products when present in high enough concentrations will begin to interfere with the electrorefining unit operation. The working electrolyte in the electrorefiner will then need to be cleaned of these unwanted products. There are a few stages in this salt clean-up process. Each of them has been discussed briefly below.

1.3.2.1 Actinide Recovery

The salt clean-up process is a critical operation in the flowsheet to minimize the amount of radionuclide that exits a pyroprocessing facility for final waste disposal. An efficient salt clean-up process should reduce the costs associated with waste disposal and mitigate concerns of environmental contamination. After the electrorefining step, any residual actinides present in the molten LiCl-KCl eutectic salt must be removed prior to the salt being sent further for fission product clean-up and recycle. A few different options have been presented for salt clean-up that are currently being developed and evaluated. These are discussed briefly below.

One of the proposed options is exhaustive electrolysis on a solid aluminum cathode.[15,16] This is an electrolysis process in which an inert anode is used on which chlorine gas generated during the process, while the actinides are deposited on a solid cathode forming an An-Al alloy (An = actinide). This An-Al alloy can be further processed via either vacuum distillation or chlorination. Song et al.[17] proposed the use of an inert anode along with a liquid cadmium cathode followed by chlorination of the reduced lanthanide fission products. In this two-step process, the first step is the reduction of all actinides and some lanthanides fission products to form a Cd-An-Ln alloy. In the second step, $CdCl_2$ is added to the cadmium alloy. This causes the lanthanide elements to be selectively chlorinated and redissolved back into the LiCl-KCl. The actinides can then be removed from the cathode using the distillation process.

Other processes like a multistage reductive extraction process have been proposed[18] and investigated for the treatment of salt containing actinides, lanthanides and alkaline earth fission products. This process consists of addition of Li-Bi alloy to the molten salt melt at about 500°C.

This causes the actinides to be preferentially extracted into the liquid metal (Bi) phase due to the difference in distribution coefficients between the molten LiCl-KCl electrolyte and bismuth metal according to Equation 1.1.

$$3\,Li_{(Bi)} + UCl_3 \rightleftharpoons U_{(Bi)} + 3\,LiCl_{(S)} \tag{1.1}$$

Once the actinides have been removed from the salt to a satisfactory level, this molten eutectic electrolyte now needs to be sent for final waste disposal. This salt still contains high levels of lanthanides and alkaline earth fission products that can lead to contamination, and hence a safe sustainable salt disposal option must be developed. At this stage of the process, there are two potential flow sheets options for the further treatment of the salt, as shown in Figure 1.3. Figure 1.3 shows the two options for further treatment of the salt. One option is the disposal of the salt into an appropriate waste form (Option # 1). The current technology for salt disposal is absorption of the salt into zeolite-4A. This is followed by mixing with a glass frit and pressureless consolidation process to generate a glass-bonded sodalite waste form. A portion of this work will look into a novel method to replace this

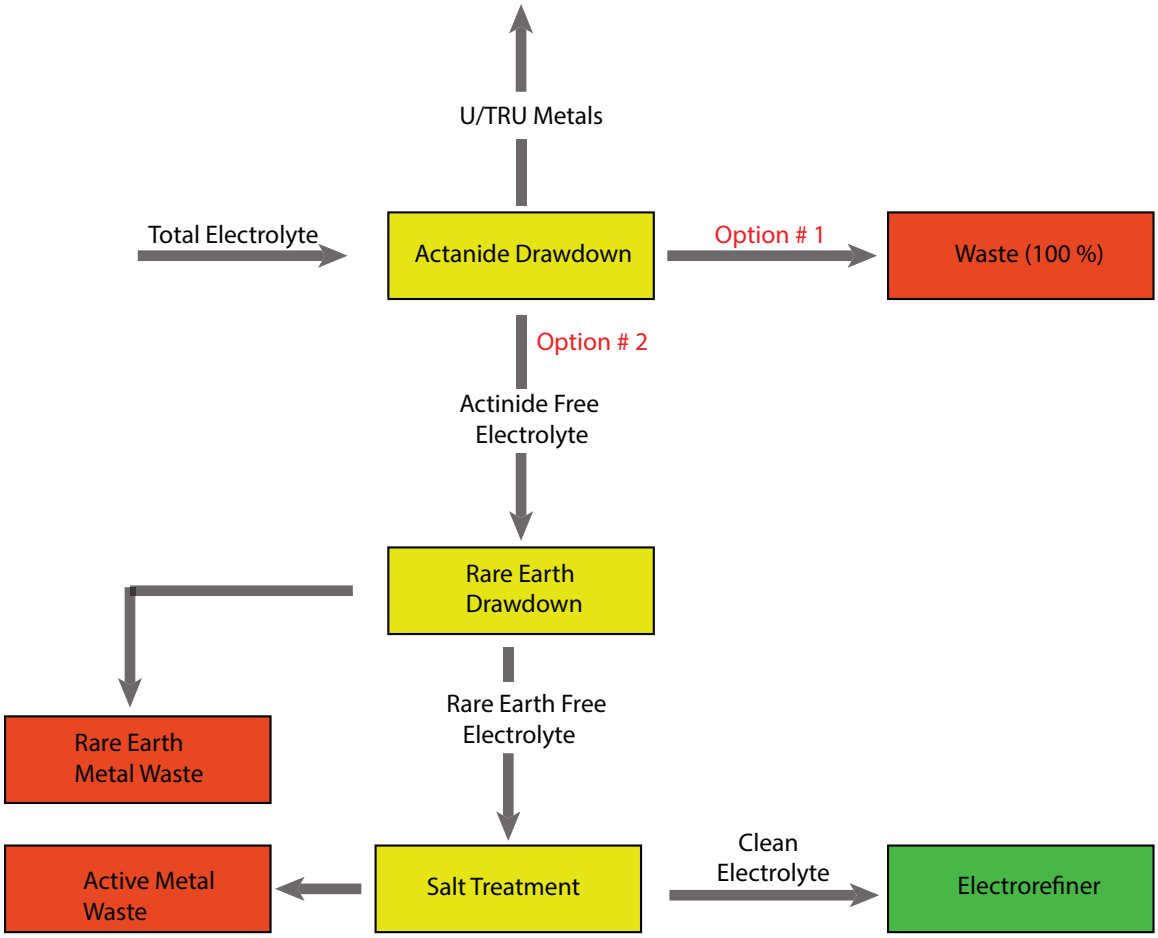

Figure 1.3. Process options for treatment of electrorefiner waste salt.

current process with an ion exchange process using H-Y zeolite. Hence the current waste disposal technology will be discussed later.

The other option (Option # 2) as shown in Figure 1.3 is to further process the molten salt via electrolysis for the removal of the rare earth products from the molten salt. This second process option is known as the Rare Earth Drawdown (REDD) process. After the removal of the rare earth products, the salt can be recycled back to the electrorefiner for further use. The rare earth drawdown process is discussed in more detail in the next section. There are other options like phosphate precipitation and carbonate precipitation that are being discussed in the literature. However in this work, the discussion is limited to the electrochemical separation processes yielding a metal product at the end.

1.4 Rare Earth Drawdown

The Rare Earth Drawdown (REDD) process was recently proposed by Williamson and Willit[19] for separating rare earth fission products from ER waste salt. This process is an electrolytic reduction step which is very similar to the actinide recovery unit operation where an inert anode is used at which chlorine gas is evolved. Rare earths are now deposited on a cathode from this actinide free salt to yield a solid rare earth metallic product at the cathode. The rare earth drawdown can be performed in the same vessel as the actinide recovery. After the drawdown process, the salt will contain only some alkaline earth fission products that cannot be readily reduced on the cathode. Alkaline earth fission products like CsCl that are present in the salt have a standard reduction potential (Cs^+/Cs) that is more negative than the standard reduction potential of Li^+/Li.[20] Once the rare earths have been selectively removed from the molten salt electrolyte, this actinide free, rare earth free electrolyte can now be sent back to the electrorefiner to be reused. This recycling of the molten salt electrolyte back to the electrorefiner in the Option # 2 presented in Figure 1.3 will help reduce the overall volume of waste that will eventually have to be disposed of safely.

As previously mentioned, alkaline earth metals species like CsCl cannot be readily reduced since it has a reduction potential that is more negative than the Li^+/Li reduction potential. Hence as the salt is continuously recycled, over time appreciable quantities of CsCl will begin to accumulate in the molten salt, increasing in quantity with every cycle. It is anticipated that at significant quantities, this CsCl present will begin to affect all of the upstream processes: electrorefining, actinide drawdown and the rare earth drawdown. It is anticipated that the CsCl will influence the important thermodynamic properties like apparent potentials, activity coefficients of actinides and rare earths present in the molten salts. Additionally, it is important to study the phase diagram of these systems to determine if the solidus and liquidus temperatures are affected due to the presence of the alkaline earth metals. To date, there have been no papers published in the open literature on the effect alkaline earths metals on the thermodynamic properties of rare earth chlorides and/or actinides.

Studying the effect of all alkaline earths on the large number of actinides and rare earths is a formidable task. Hence this work has been limited to a few rare earth metals which

have been studied in detail to lay the foundation for a future study of other rare earths and actinides in molten eutectic salt. In real spent nuclear fuel, there can be a very large number of elements present, upwards of 15 species including actinides, lanthanides and other fission products. In such a case, during both electrorefining and rare earth drawdown operations, knowledge of important thermodynamic properties like activity and activity coefficients will enable better predictions of the reduction potentials of species in solution. Comprehension of activity coefficients will help operators develop accurate sophisticated models to better control the operating potentials in these electrochemical cells to get high quality product at the cathode, relatively free of impurities. This is more pertinent if the species in the molten salt systems show a significant deviation from ideal solution behavior as reported in the literature.

Another aspect that requires further understanding is the interaction of other fission products like CsCl with the rare earth chlorides. This is of interest from the standpoint of the rare earth drawdown process. As the salt electrolyte is circulated between the electrorefiner and the rare earth drawdown process, other fission products like Cs and Sr will accumulate in the salt. As these other fission products increase in concentration in the salt over time, it will begin to interact and influence of the properties of the rare earth chlorides. A part of the electrochemical work performed in this dissertation will examine the influence of CsCl on the activity coefficient of the rare earth chlorides. The activity/activity coefficients of $LaCl_3$, $GdCl_3$, $CeCl_3$ and $NdCl_3$ were studied in this dissertation.

1.5 Scope of Work

Having reviewed the background information on pyroprocessing, in this section the scope of work for this dissertation will be discussed. The scope of this work can be succinctly captured by the process options presented in Figure 1.3. This works explores the waste minimization and salt disposal options for the electrorefiner salts. Within this larger paradigm, the main subtopics have been explored. The first is a novel waste disposal process to replace the current scheme. The second is electrochemical testing to determine the thermodynamic behavior of the rare earths as a function of concentration and study the influence of CsCl on them. Third is the development of phase diagram to examine the influence of CsCl on the solidus and liquidus temperatures. Each of these topics has been

elaborated upon in the next subsections.

1.5.1 Zeolite Waste Disposal

The working electrolyte from the electrorefiner will eventually have to be disposed safely after the concentration of nonreactive fission products has reached unsustainable levels. Part of this work is dedicated to the research and development of a novel waste disposal waste form using an H-Y zeolite to reduce the final volume of waste.

1.5.2 Electrochemical Testing

In this work, the activity of four rare earths ($LaCl_3$, $NdCl_3$, $GdCl_3$ and $CeCl_3$) have been studied as a function of concentration. Further, the effect of presence of CsCl on the activity coefficient was evaluated for three rare earth chlorides: $LaCl_3$, $GdCl_3$ and $CeCl_3$.

1.5.3 Phase Diagram Development

Ternary and quaternary phase diagrams were developed for $LiCl-KCl-RECl_3$ and LiCl-KCl-CsCl-$RECl_3$ systems. For the quaternary phase diagrams, for every rare earth chloride, two concentrations of CsCl were evaluated. The phase diagrams were developed using thermal testing available at the University of Utah.

1.6 Literature Review

In this section, the existing literature relating to the activity coefficient of rare earths in molten salts will be briefly reviewed. For each of the rare earth chlorides studied here, the previously published literature will be examined. While the literature for the rare earths in LiCl-KCl eutectic salt will be reviewed, there seem to be no reports in the literature of the effect of the presence of other salts like CsCl have on the electrochemical and thermodynamic properties for all of the rare earths studies as a part of this dissertation.

1.6.1 Activity Coefficient of Rare Earths

First, the literature regarding the activity coefficients of the rare earth chlorides will be reviewed individually.

1.6.1.1 Lanthanum Chloride

There have been a number of studies looking at the activity coefficient of lanthanum chloride in molten LiCl-KCl eutectic salt. Lanthanum chloride serves as a typical representative element for the lanthanide series, and hence has been studied extensively. Most of these studies have been reported at single concentrations and activity coefficient has not been reported as a function of concentration of $LaCl_3$. Previously various authors[21–24] have calculated the activity coefficients of $LaCl_3$ from experimental measurements.

Tang and Pesic[21] reported the value of γ_{LaCl_3} as 0.278 at a concentration of 1.07×10^{-4} mol/cm^3 at 783 K. Lantelme and Berghoute[22] studied the thermodynamic behavior of $LaCl_3$ for a concentration up to 1.81 mol % $LaCl_3$ for a whole host of temperatures. They modeled the activity coefficient as a second order polynomial function of mole fraction of $LaCl_3$. If the activity coefficients are computed based on the model presented for 750 K, activity coefficient value of 1.01 for 0.152 mol % $LaCl_3$ is obtained, going up to 1.21 for 1.81 mol % $LaCl_3$.

Masset et al.[23] reported the value of γ_{LaCl_3} as 0.0057 at a concentration of 20×10^{-5} mol/cm^3 at 733 K. Castrillejo et al.[24] reported values at 723K and 823 K, not at 773 K as reported here. At 723 K, they reported a value of 0.0053 for the activity coefficient of $LaCl_3$. The concentration at which this measurement was made is not clear from the paper. A brief summary is shown in Table 1.1. It is clear from Table 1.1 that there is quite a large discrepancy in the reported literature.

Table 1.1. Activity coefficient of $LaCl_3$ in LiCl-KCl eutectic salt reported in the literature

Reference	T (K)	[$LaCl_3$]	γ_{LaCl_3}
Lantelme and Berghoute[22]	750	0.152 to 1.81 mol %	1.01 to 1.21
Tang and Pesic[21]	783	1.07×10^{-4} mol cm^{-3}	0.278
Masset et al.[23]	733	20×10^{-5} mol cm^{-3}	0.0057
Castrillejo et al.[24]	723	N/A	0.0053

1.6.1.2 Gadolinium Chloride

The activity coefficient of $GdCl_3$ in molten eutectic LiCl-KCl has been reported by three main studies in the literature.[22,25,26] Tang and Pesic[25] reported the activity coefficient of $GdCl_3$ at a concentration of 2.0 wt. % $GdCl_3$. Caravaca et al.[26] reported the activity coefficient of gadolinium chloride in LiCl-KCl eutectic salt at a single concentration of 0.166 mol % $GdCl_3$. Caravaca et al.[26] in calculating their activity coefficients used two different standard states for their calculations reporting two vastly different activity coefficient values for the same concentration of gadolinium chloride. Lantelme and Berghoute[22] determined the activity coefficient as a function of concentration up to 1.44 mol % $GdCl_3$. Lantelme and Berghoute[22] for their work used a definition of standard state with unit activity at infinite dilution and reported activity coefficients of $GdCl_3$ that are vastly different from the other two studies cited here.[25,26] A summary of the reported findings from these three studies is shown in Table 1.2.

From the data reported in the three main studies cited here, two key areas remain with substantial knowledge gaps. First is expanding the concentration range and concentration dependence of the activity coefficient of $GdCl_3$ above and beyond the 1.44 mol % $GdCl_3$ reported in the single study by Lantelme and Berghoute.[22] A second and key area where knowledge gaps remain and further advancements can be made is the selection of an adequate standard state. The choice of two different standard states by Caravaca et al.[26] in a single study and a completely unique standard state by Lantelme and Berghoute[22] to

Table 1.2. Activity coefficient of $GdCl_3$ in LiCl-KCl eutectic salt reported in the literature

Reference	T (K)	[$GdCl_3$]	γ_{GdCl_3}
Lantelme and Berghoute[22]	750	0.16 to 1.44 mol %	1.04 to 1.54
Tang and Pesic[25]	773	2.0 wt. %	1.749×10^{-4}
Caravaca et al.[26]	771	0.166 mol %	4.60×10^{-3}
Caravaca et al.[26]	771	0.166 mol %	1.50×10^{-4}

report activity coefficients of $GdCl_3$ greater than unity shows that clearly there is room to develop a better experimental and theoretical framework to define standard states and activity coefficients of rare earth chlorides in general and gadolinium chloride in particular.

1.6.1.3 Cerium Chloride

For cerium chloride, the only studies in the literature for the activity coefficient of cerium chloride in have been reported by Marsden and Pesic,[27] Castrillejo et al.,[24] and Zhang et al..[28] Marsden and Pesic[27] report the activity coefficient of cerium chloride as a function of temperature (673 K - 973 K). In their work, the concentration of cerium chloride at which these measurements were made is not reported. At 773 K, Marsden and Pesic[27] reported the activity coefficient of $CeCl_3$ to be 1.18×10^{-2}. Apart from the work by Marsden and Pesic,[27] there is one additional study in the literature on the activity coefficient cerium chloride. Castrillejo et al.[24] reported the activity coefficient ($\log \gamma$) of cerium chloride at two temperatures of 723 and 823 K to be 2.87×10^{-3} and 7.87×10^{-3}, respectively, (on the mole fraction scale). Again the concentration of $CeCl_3$ at which such measurements were made is not clear from the paper.

Zhang et al.[28] also studied the activity coefficient of $CeCl_3$ in a temperature range of 823 to 923 K at a concentration of 0.125 mol L^{-1} $CeCl_3$. For their calculations of the activity coefficient of cerium chloride, Zhang et al.[28] used data generated from cyclic voltammograms rather than equilibrium measurements. They reported values in the range of 9.14 x 10^{-3} at 823 K to 7.78 x 10^{-3} at 923 K. Another point to note in their data is the choice of standard state. They state in their paper that the standard state chosen for their calculations is the Gibbs free energy of formation of $CeCl_3$ at standard states. This value at the operating temperatures of 823 to 923 K would represent the Gibbs free energy of formation of solid cerium chloride. The appropriate standard states for such calculations would be represented by the Gibbs free energy of supercooled liquid $CeCl_3$. A brief summary of the data has been presented Table 1.3.

1.6.1.4 Neodymium Chloride

The chemistry of $NdCl_3$ in molten LiCl-KCl eutectic salt is different from the other rare earth chlorides studied here. $NdCl_3$ is present in two stable oxidation states of +2 and +3 in the molten LiCl-KCl eutectic salts. Due to the existence of the two oxidation states

Table 1.3. Activity coefficient of $CeCl_3$ in LiCl-KCl eutectic salt reported in the literature

Reference	T (K)	[$CeCl_3$]	γ_{CeCl_3}
Marsden and Pesic[27]	773	N/A	1.18×10^{-2}
Castrillejo et al.[24]	723	N/A	2.87×10^{-3}
Castrillejo et al.[24]	823	N/A	7.87×10^{-3}
Zhang et al.[28]	823	0.125 mol L^{-1}	9.14×10^{-3}
Zhang et al.[28]	923	0.125 mol L^{-1}	7.78×10^{-3}

of neodymium, the experimental determination of activity coefficient of $NdCl_3$ is more challenging than the other rare earths in this work.

Masset et al.[23] determined the activity coefficient of $NdCl_3$ at a concentration of 70 x 10^{-5} mol cm^{-3} at 733 K. For these measurements, Masset et al.[23] used cyclic voltammograms rather than equilibrium measurements. Further they derived a relationship between the two reduction peaks (Nd(III)/Nd(II) and Nd(II)/Nd(0)) that are observed. They reported an activity coefficient of $NdCl_3$ of 8×10^{-5}.

Castrillejo et al.[24] also studied the activity coefficient of the $NdCl_3$. They concede in their paper that due to the existence of Equation 1.2, potentiometric methods cannot be used to determine the standard potential (and by extension the activity coefficient) of Nd(III)/Nd(0) system. For such calculations, various assumptions need to be made as noted by Castrillejo et al..[24] These assumptions listed by Castrillejo et al.[24] are reproduced here.

$$2Nd(III) + Nd(0) \rightleftharpoons Nd(II) \tag{1.2}$$

- *Reversible behavior of the electrochemical systems. Then voltammetric curves obtained at low sweep rates (<200 mV s^{-1}) were analyzed.*

- *Both systems are separate enough to consider them as independent electrochemical*

exchanges. As it was shown previously, this is not strictly correct in the case of the eutectic LiCl-KCl melt, so in this case we will obtain an approximate value.

- *The absence of perturbation phenomena, such as nucleation and crystal growth, that introduces an additional overpotential.*

As noted in the assumptions made by Castrillejo et al.,[24] this is a very inexact method to determine the standard potentials laced with assumptions and are not necessarily completely accurate. However with these assumptions embedded into their calculations, Castrillejo et al.[24] reported the activity coefficient of $NdCl_3$ at two temperatures of 723 and 823 K to be 3.04×10^{-4} and 4.41×10^{-4} respectively (on the mole fraction scale). The concentration of $NdCl_3$ at which such measurements/calculation were made was 1.21 mol cm^{-3} $NdCl_3$. A brief summary of the data has been presented Table 1.4.

1.6.2 Phase Diagram Studies

The phase diagrams of rare earth chlorides are not as well studied and reported on as the electrochemical properties of rare earth chlorides. Ternary phase diagrams of $LiCl-KCl-RECl_3$ have been studied by Sridharan et al..[29] They studied three common rare earth chlorides: $LaCl_3$, $NdCl_3$ and $CeCl_3$ up to a concentration of about 25 mol%. For studying this system, the mixture was treated as a pseudo binary system since the concentration of the eutectic salt is always fixed at its eutectic composition of 59 mol % LiCl and 41 mol % KCl.

Sridharan et al.[29] also studied the LiCl-KCl-$LaCl_3$ ternary system up to a concentration of 22 mol % $LaCl_3$. They reported that the LiCl-KCl-$LaCl_3$ system departs from eutectic

Table 1.4. Activity coefficient of $NdCl_3$ in LiCl-KCl eutectic salt reported in the literature

Reference	T (K)	$[NdCl_3]$ mol cm^{-3}	γ_{NdCl_3}
Masset et al.[23]	733	70×10^{-5}	8×10^{-5}
Castrillejo et al.[24]	723	1.21×10^{-4}	3.04×10^{-4}
Castrillejo et al.[24]	823	1.21×10^{-4}	4.41×10^{-4}

melting to peritectic melting at a concentration above 6 mol % $LaCl_3$. Sridharan et al.[29] also studied the LiCl-KCl-$NdCl_3$ ternary system up to a concentration of 22 mol % $NdCl_3$. They reported that the LiCl-KCl-$NdCl_3$ system departs from eutectic melting to peritectic melting at a concentration above 8 mol % $NdCl_3$. The solidus line shifts upwards at concentrations of between 20 to 22 mol % $NdCl_3$. Sridharan et al.[29] further studied the LiCl-KCl-$CeCl_3$ ternary system up to a concentration of 22 mol % $CeCl_3$. They reported that the LiCl-KCl-$CeCl_3$ system departs from eutectic melting to peritectic melting at a concentration above 6 mol % $CeCl_3$. For these three rare earth systems, the data reported by Sridharan et al.[29] were very similar to previous literature.[30]

To the best knowledge of this author, there are no works published in the open literature that have studied the LiCl−KCl−CsCl−$RECl_3$ quaternary systems. There is published literature on a number of the possible binary systems and even some ternary systems in thermochemical databases like the Factsage. From these binary and ternary systems, it is theoretically possible to derive the behavior and phase diagrams of the quaternary systems. However no available published literature has attempted to do so both experimentally and theoretically.

1.6.3 Salt Waste Disposal

The disposal of the final waste salt is an important technology towards the goal of safe, sustainable nuclear energy. Disposal of the radioactive salt containing a whole host of heavy metals can be a challenging process. Any final waste form must not be susceptible to radiation over the long term, resistant to leaching of the metals to prevent ground water contamination.

From 1996 to 1999, DOE directed Argonne National Laboratory to demonstrate the electrometallurgical treatment technology for EBR-II fuel treatment, which features the electrorefiners. At that time, Argonne National Laboratory developed and successfully demonstrated a process for immobilizing waste salt from the electrorefiner into a ceramic waste form with a matrix of glass-bonded sodalite.[31–33] This process starts with the high temperature absorption of the salt into zeolite-4A.[34] The salt-loaded zeolite is then blended with glass frit and heated to form a sintered, glass-bonded sodalite.[31,35–37] Substantial research and development has been performed in support of the baseline process, which

includes salt grinding and milling, zeolite preparation (milling and drying), high temperature salt/zeolite blending, glass/zeolite blending, and pressureless consolidation (PC). All of these steps have been developed and demonstrated at production scale, in some cases with real electrorefiner salt waste.[35] In other cases, such as pressureless consolidation, the demonstration has only involved nonradioactive surrogates.[32] While the ceramic waste process (CWP) has been demonstrated to produce highly leach resistant ceramics that exceed the benchmark standard of high-level waste glass, this comes at the expense of high volumes of waste and high waste processing cost.

Recently, it was proposed by Wang et al.[38] from Sandia National Laboratory that the electrorefiner salt could be an excellent candidate for disposal in a geological repository without any encapsulation or stabilization in a waste form. Some experiments were performed to assess the stability of surrogate electrorefiner salt in the presence of simulated brine that would be present in a salt dome. Those studies indicated reduced solubility and rates of dissolution. And this was followed up by a detailed performance assessment calculation that indicated no appreciable impact to the surrounding environment for direct disposal of the ER salt into a generic salt repository. However, there are very significant potential problems with this approach. For one, it is likely that the salt would be placed into temporary storage for a number of years prior to being shipped to final disposal in the repository. The electrorefiner salt primarily consists of LiCl-KCl, which is highly hygroscopic. It may be very difficult to store untreated salt for long periods of time while insuring no pickup of ambient moisture. If there is pickup of moisture, the salt becomes extremely corrosive and can rapidly degrade even stainless steel containers. Additionally this waste form would not be proliferation resistant as radioactive species present in the salt can be easily recovered from the salt through aqueous processing.

1.7 Structure of Dissertation

The structure of this dissertation and sequence of chapters is as follows:

1. Introduction: This chapter has the general background information and literature review.

2. Occlusion and Ion Exchange of Eutectic LiCl-KCl in H-Y Zeolite: In this chapter,

the entire work done for Option # 1 including literature review, experimental section and results is presented.

3. Thermodynamics of Molten Salt Solutions: In this chapter some basic thermodynamics will be reviewed in the first part of this chapter. In the second part of this chapter, the theoretical work done to support the electrochemical experiments is presented.

4. Experimental Section: In this chapter the experimental methods for the electrochemical and phase diagram work is presented.

5. Activity of Rare Earth Chlorides: In this chapter the experimental results for all of the electrochemical work for four rare earth chlorides; $LaCl_3$, $GdCl_3$, $NdCl_3$, and $CeCl_3$ in molten LiCl-KCl eutectic salt is presented.

6. Application of Thermodynamic Behavior of $Gd/GdCl_3$ for Galvanic Drawdown of Uranium(III) Chloride: In this chapter, preliminary experimental data are presented on a novel method for the galvanic drawdown of uranium(III) chloride from LiCl-KCl eutectic salt.

7. Liquidus and Solidus Data for LiCl-KCl-CsCl-$RECl_3$ Mixtures: In this chapter, all of the phase diagram work performed for this dissertation is presented.

8. Conclusions: In this chapter, the findings and conclusions drawn from this dissertation are presented.

9. Appendix A: In this appendix, the raw experimental data for the electrochemical work are tabulated.

10. Appendix B: In this appendix, the thermograms for the phase diagram work are documented.

CHAPTER 2

OCCLUSION AND ION EXCHANGE OF EUTECTIC LiCl-KCl IN H-Y ZEOLITE

In this chapter, the results from the salt waste using using H-Y zeolite will be presented and discussed. This work was published in the Journal of Nuclear Fuel Cycle and Waste Technology (Bagri, Prashant, and Michael F. Simpson. "Occlusion and Ion Exchange of Eutectic LiCl-KCl in HY Zeolite" Journal of Nuclear Fuel Cycle and Waste Technology 13(S) (2015): 45-53). The findings from that publication have been adapted here.

2.1 Introduction

The US Department of Energy's (DOE) Idaho National Laboratory (previously Argonne National Laboratory until 2005) has been operating molten salt electrorefiners at their Fuel Conditioning Facility (FCF) since 1996 for the purpose of treating spent fuel from the Experimental Breeder Reactor-II.[39] The electrolyte used in these electrorefiner (ER) systems is a molten eutectic LiCl-KCl mixture. As a result of processing the spent fuel, a number of fission products and other metals form soluble chlorides that partition into the salt and lead to increasing contamination of the salt. After the completion of the fuel treatment campaign in FCF, the salt will have become highly contaminated with radioactive fission products and actinides. Due to the high solubility of this salt in aqueous systems and the presence of long-lived radionuclides, it should be stabilized for long-term disposal in a geologic repository. From 1996 to 1999, DOE directed Argonne National Laboratory to demonstrate the electrometallurgical treatment technology for EBR-II fuel treatment, which features the electrorefiners. At that time, ANL developed and successfully demonstrated a process for immobilizing waste salt from the ER into a ceramic waste form with a matrix of glass-bonded sodalite.[31–33] This process starts with the high temperature absorption of the salt into zeolite-4A.[34] The salt-loaded zeolite is then blended with glass frit and heated to form a sintered, glass-bonded sodalite.[31,35–37] Substantial research and development

have been performed in support of the baseline process, which includes salt grinding and milling, zeolite preparation (milling and drying), high temperature salt/zeolite blending, glass/zeolite blending, and pressureless consolidation (PC). All of these steps have been developed and demonstrated at production scale, in some cases with real electrorefiner salt waste.[35] In other cases, such as PC, the demonstration has only involved nonradioactive surrogates.[32]

While the ceramic waste process (CWP) has been demonstrated to produce highly leach resistant ceramics that exceed the benchmark standard of high-level waste glass, this comes at the expense of high volumes of waste and high waste processing cost. The maximum loading of salt into the sodalite waste form is approximately 7.5 wt%. For 1700 kg of electrorefiner waste salt, this corresponds to 22.7 metric tons of ceramic waste would need to be generated. The two primary in-cell process steps are the salt/zeolite blending (using V-blender) and the PC. It is estimated that 10 kg of salt could be processed in the V-blender each week, and one 400-kg ceramic waste form could be generated in the PC furnace each month. Based on the V-blender processing rate, this would require at least 3.3 years. Based on the PC furnace capacity, 4.7 years would be required.

Recently, it was proposed by Wang et al.[38] from Sandia National Laboratory that the electrorefiner salt could be an excellent candidate for disposal in a geologic salt formation without any encapsulation or stabilization in a waste form. Some experiments were performed to assess the stability of surrogate electrorefiner salt in the presence of simulated brine that would be present in a salt dome. Those studies indicated reduced solubility and rates of dissolution. And this was followed up by a detailed performance assessment (PA) calculation that indicated no appreciable impact to the surrounding environment for direct disposal of the ER salt into a generic salt repository.

Given that direct salt disposal operationally involves only the draining and cooling of several canisters of salt, this would seem like the preferred disposal option for salt moving forward. However, there are very significant potential problems with this approach. For one, it is likely that the salt would be placed into temporary storage for a number of years prior to being shipped to final disposal in the repository. The electrorefiner salt primarily consists of LiCl-KCl, which is highly hygroscopic. It may be very difficult to store pure, untreated salt for long periods of time while insuring no pickup of ambient moisture. If

there is pickup of moisture, the salt becomes extremely corrosive and can rapidly degrade even stainless steel containers. This might ultimately result in great difficulty containing radioactive fission products, water, and actinides. Risk of contamination of the environment and even nuclear criticality would increase. Another problem is that there is no current disposition path for the plutonium from EBR-II other than to leave it in the electrorefiner salt and dispose of it as waste. With a significant amount of plutonium in the EBR-II spent fuel inventory, disposing of the salt without any sort of immobilization may pose a nuclear security risk. Without immobilization in a chemically resistant solid matrix, the salt is in a form that can be readily dissolved and subjected to separations processes, which might be effective at isolating the plutonium from the salt matrix that contains other actinides and radioactive fission products. Thus, there is significant motivation to seek out a compromise between an expensive and time-consuming baseline CWP approach and a higher-risk minimal direct disposal approach.

Zeolites are attractive absorption/ion exchange materials for nuclear waste application because of their high thermal stability and radiation resistance coupled with extremely high sorption surface area. Study of the interaction of anhydrous chloride salts with zeolites has not been limited to the above-mentioned ceramic waste process. Numerous other studies have been done that investigate the sorption and diffusion of these salts into the zeolite lattice.[40,41] Various zeolite types have been studied for this process, including zeolite-A, faujasite, and beta zeolite. When protonated zeolite was used instead of alkali metal-substituted zeolite, it was found that the metals contained in the salt can replace the protons in the zeolite. This results in the evolution of HCl gas via the following reaction.

$$\mathrm{LaCl_3(s)} + 3H - zeolite(s) \rightleftharpoons La - zeolite(s) + 3HCl(g) \tag{2.1}$$

A viable candidate zeolite for this application is H-Y, a synthetic, widely manufactured zeolite which has the faujasite structure. Faujasitic zeolites have pores and cages like the zeolite-A that is used in the baseline ceramic waste process. But the pore sizes of faujasites are larger (7-8 angstroms versus 4 angstroms for zeolite-4A). While zeolite-4A has a Si/Al ratio of 1.0, that ratio has a wide range for faujasites. Zeolite-X is the only faujasite with a Si/Al ratio of 1.0. Zeolite Y has Si/Al ratios ranging from about 2 up to infinity. The

removal of Al from the structure tends to thermally stabilize the faujasite structure, but it comes at the expense of a reduction in ion exchange site concentration. As the Si/Al ratio increases, the maximum concentration of exchanged ions in the zeolite decreases. From the standpoint of producing an optimal waste form, it has been initially assumed that low Si/Al ratios of around 2-3 are optimal.

Commercially available H-Y zeolite is available with a Si/Al ratio of 2.6. It is estimated that an effective loading of 22 wt% can be achieved for the salt in the zeolite via ion exchange with the H-ions as with the reaction shown above. The 1700 kg of salt waste would need to be blended with 6134 kg of zeolite. Since all of the chlorine is being evolved as HCl, the final total mass of salt-loaded zeolite would only be 6824 kg. Assuming one week to process a 120 kg batch of salt-loaded zeolite in the blender (similar design to zeolite dryer would be appropriate), it would take 65 weeks to process all of the salt from both electrorefiners. This is 2.6 times faster than the time required to run the V-blender for the baseline process and 3.8 times faster than the time required to run the PC furnace.

While the conventional ceramic waste form requires very high temperature final processing (1188 K) to form the glass-bonded sodalite, it is proposed to consolidate the fission product-loaded zeolite with a binder consisting of fine metal powders. It has been shown that zeolite powder can form strong agglomerates with metal (Al, for example) powders at temperatures less than 473 K.[42] Such an agglomeration process could be tailored to optimize waste form geometry based on heat rejection requirements. The use of metallic binders should result in very high thermal conductivity, which will also aid in the rejection of heat from the waste forms. With the expected 10% binder addition, the final mass of waste from the electrorefiners would be about 7.5 MT (a reduction of 3x compared to the baseline). A process flowsheet for the proposed process is shown in Figure 2.1.

While this process appears to be highly promising, there is little experimental data to support evaluation of the exchange reaction between actual electrorefiner salt mixtures with H-Y zeolites. Achieving a high degree of ER salt exchange with the H^+ ions in the zeolite with a high processing rate is critical for the viability of this new process. The first stage of this study involves testing of the ion exchange reaction with eutectic LiCl-KCl without any added contaminants. This is deemed relevant, because LiCl-KCl comprises 70 wt% plus of the ER salt and largely dictates the phase behavior and other physical properties of the ER

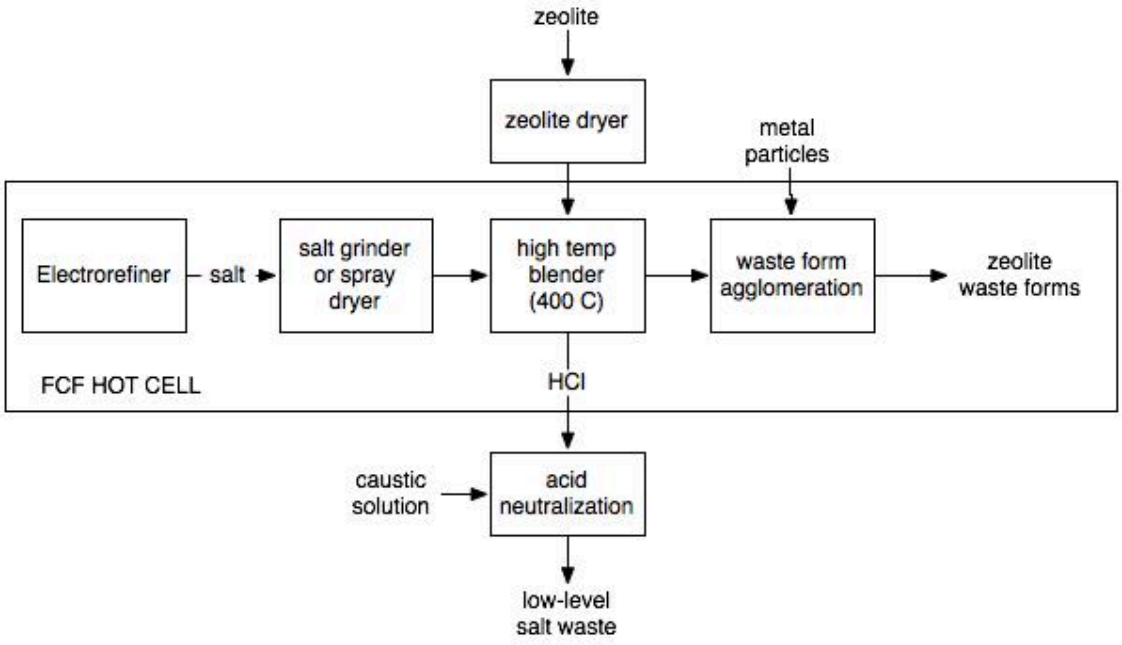

Figure 2.1. Proposed new process for stabilizing ER waste salt for permanent disposal.

salt.

2.2 Experimental Methods

For this study, two different H-Y zeolites were used with Si/Al ratios of 2.55 and 15 (Zeolyst International) CBV-400 and CBV-720, respectively. To determine the mass of salt to mix with the dried zeolite, the crystal lattice of the zeolites used in these experiments was assumed to be of the form $H(SiO_2)(2.55)\,AlO_2$ for CBV-400 and $H(SiO_2)(15)\,AlO_2$ for CBV-720. Based on the above chemical formulae, the molecular weight of the zeolites was calculated to be 213.20 g/mole and 961.2 g/mole for CBV-400 and CBV-720, respectively. The stoichiometric ratio of salt to zeolite for each test was 80%. In other words, the zeolite was present in 20% excess in the powder mixture of salt and zeolite. For all experiments, the zeolite was first heated and dried in a Lindberg tube furnace (Thermo Scientific) under flowing ultra high purity argon.

The surface area was measured using a Micromeritics ASAP 2020 instrument. For BET measurements, a full isotherm was performed under liquid nitrogen. Degassing was performed at 5 μm of Hg for 180 minutes. Then the temperature was raised to 673 K for

240 minutes.

Powder X-ray diffraction was performed using a Phillips X'pert instrument. The diffraction scan was run from 2°to 80°2θ. Before performing the measurement, the zeolite powder was spread on a glass slide. Subsequently sample and detector alignment was performed. The scan rate was chosen to be 2°/min.

For the purpose of measuring the generation of HCl from the reaction of LiCl-KCl with the H-Y zeolites, two different kinds of experiments were setup and performed. One involved heating very small (15 mg) samples of the salt/zeolite mixture as prepared above in a thermogravimetric analyzer (TGA). This approach yielded mass change of the sample versus temperature. For every gram of LiCl-KCl, there is up to 0.65 gram of mass loss from HCl evolution. This allows one to calculate the percentage of LiCl-KCl that has reacted based on the sample mass loss. For the TGA measurements, a Q600 TGA/DSC from TA Instruments was employed. Alumina sample pans were loaded in the glove box with approximately 15 mg of salt/zeolite sample and quickly transferred into the instrument to avoid the pick-up of moisture from the air. Temperature range for these measurements was room temperature to 800°C. The temperature profile for the samples was as follows. The sample was ramped from room temperature to 300°C at a rate of 5°C/min. It was then held at 300°C for 6 hours. The temperature was then again ramped (5°C/min) to 650°C, where the sample was held for 12 hours. Finally the sample was ramped (5°C/min) to the final temperature of 800°C and held for 60 minutes.

The second type of experiment was designed to verify that mass loss from the TGA could be directly attributed to HCl evolution. Samples of salt/zeolite (7-10 grams) were placed in a small crucible and heated in a 1-inch diameter quartz tube heated by a tube furnace (Thermo Scientific Lindberg Blue M) with a carrier gas of argon directed into an acid-base titration cell. The flow of argon in the tube was controlled using a mass flow controller (MKS Instruments). This mass flow controller was calibrated using a 100 ml soap film meter. The gas coming out of the tube was diverted into a titration cell held as a fixed pH of 10. The pH of the cell was controlled using an autotitrator (Synergy Titroline 7000) via controlled addition of 1 N NaOH. The gas was sparged into the titration cell solution using a glass frit for enhanced mass transfer and reaction. A diagram of the system configuration is given in Figure 2.2.

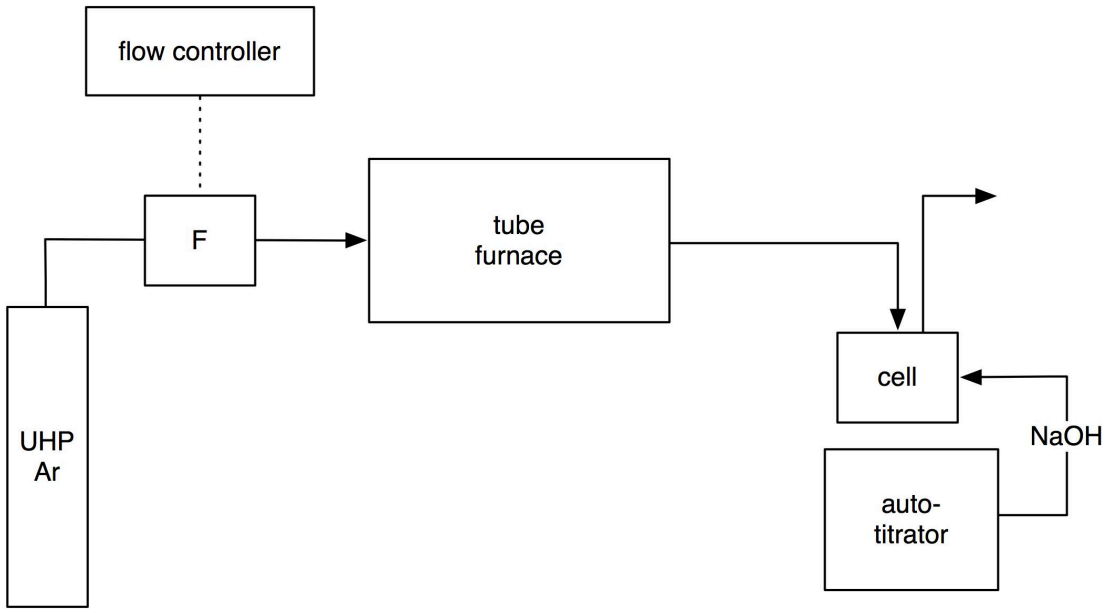

Figure 2.2. System design of the solid-state ion exchange test system.

After each solid-state ion exchange run, an additional analysis was performed on the remaining solid powder. The objective was to measure the amount of unabsorbed LiCl-KCl. Hypothetically, after each experiment the salt is either (1) reacted to form HCl, (2) absorbed in the zeolite but still present as chloride salt, or (3) not absorbed at all. In case (3), a quick water wash will dissolve the salt, and the resulting Cl^- ions can be quantified via an ion selective electrode. The method developed at Argonne National Laboratory to measure this "free salt" is the free chloride test (FCT).[34] For each FCT, three weighed samples of salt/zeolite powder are mixed with a known quantity of nanopure water (18.2 MΩ). The wash solutions are filtered using a 0.45 μm PTFE syringe filter (VWR). Three 1:100 dilutions are made from each of the three leachates with 2 volume % ionic strength adjuster ($NaNO_3$) added. An ion selective electrode (Cole Parmer) is calibrated and used to measure the concentration of Cl^- ions in these solutions. Those concentrations are then used to calculate the percentage of the original LiCl-KCl that can be removed via water wash and is, by definition, considered to be free salt.

2.3 Results and Discussion

BET and XRD measurements were made on the zeolite samples received. Table 2.1 shows the BET surface area results, and Figure 2.3 shows the XRD patterns. Both results are consistent with highly crystalline faujasitic zeolites.

These zeolites were dried by ramping the temperature to 150°C at 2°C/min and holding for 48 hours under flowing ultra high purity argon. Initially, the plan was to dry the zeolites at 375°C, but that was found to result in complete loss in crystallinity. This is shown in the XRD patterns found in Figure 2.4

The results of TGA analysis of the LiCl-KCl + CBV-400 mixture are shown in Figure 2.5. In this plot, it is shown that there is an initial drop of approximately 10% in mass of the sample from heating to 300°C. The mass further decreases to a cumulative loss of 18% by the time the temperature reaches 650°C. The changes in mass could be due to either off-gassing of residual water or release of HCl formed via the ion exchange reaction or a combination of the two processes.

While the TGA yields somewhat ambiguous results in that weight changes can be attributed to multiple processes, the ion exchange experiments with off-gas passed through the autotitrator could be used to directly monitor the process in which H^+ ions are replaced with metal ions and HCl is evolved (Equation 2.1). Figure 2.6 shows the data from the ion exchange experiments involving both zeolite samples (CBV-400 and CBV-720). It was observed that as the temperature in the furnace increased to about 300°C, there was minimal evolution of HCl. During the temperature ramp from 300°C to 650°C, there is a dramatic spike in HCl production. The curve then tapers off under isothermal conditions at 650°C.

Table 2.1. Measured BET surface area of H-Y zeolite samples used in this study.

Zeolite Name	Si/Al Ratio	Unit Cell	Formula Weight (gram/mole)	Surface Area m^2/gram
CBV-400	2.55	$H(SiO_2)(2.55)\,AlO_2$	213.20	680
CBV-720	15	$H(SiO_2)(15)\,AlO_2$	961.2	843

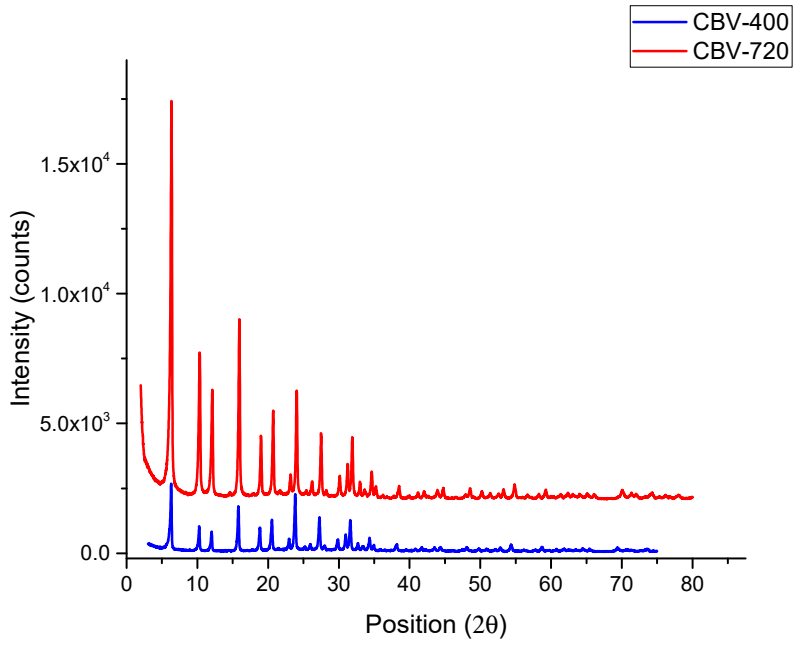

Figure 2.3. X-ray diffraction pattern of the as received H-Y zeolites.

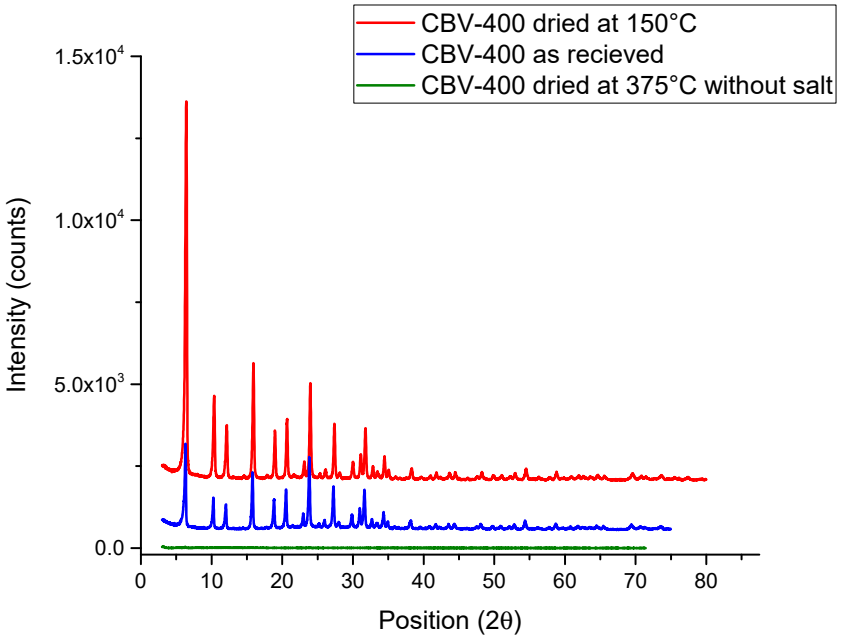

Figure 2.4. X-ray diffraction pattern of as received zeolite (CBV-400) compared to zeolite dried at 150°C and 375°C.

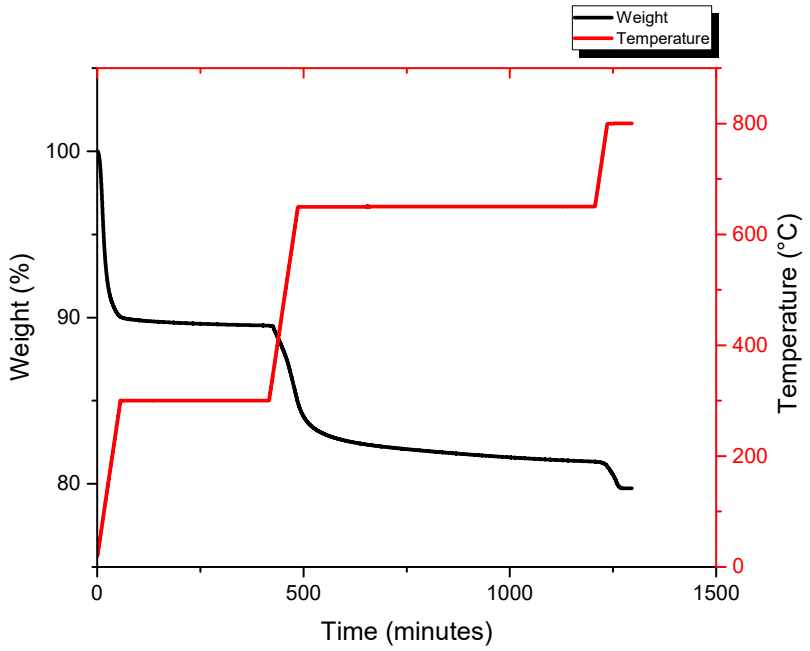

Figure 2.5. Results of TGA test for mixture of LiCl-KCl and H-Y zeolite (CBV-400).

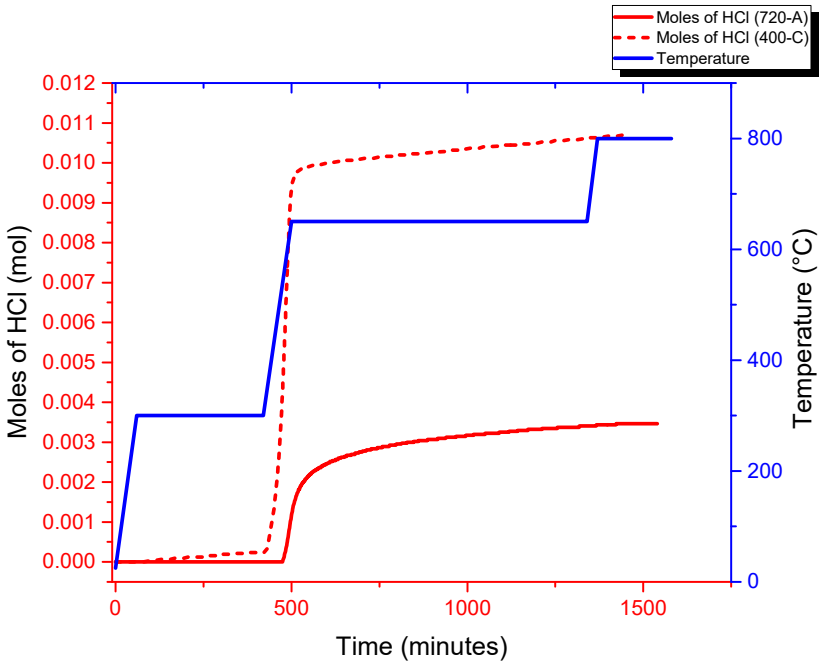

Figure 2.6. Titration curves for ion exchange tests 400-C and 720-A.

These results indicate that the reaction 2.1 proceeds in the forward direction at temperatures ranging from 300°C to 650°C. This temperature range is consistent with that used for the baseline ceramic waste process to occlude the salt into zeolite-A. Thus, existing equipment designs would be compatible with this new process. Based on the total NaOH titrated for each test, the cumulative moles of HCl evolved were calculated. Percent conversion given in Table 2.2 simply represents the numerical value of the fraction (moles of HCl evolved)/(total moles of HCl evolution possible). Total moles of HCl can be calculated from knowing the moles of Cl^- that is present in the system and assuming that all of the Cl^- will react with the zeolite to evolve HCl as shown in Equation 2.1.

Table 2.2 summarizes the results from all of the solid ion-exchange experiments with the dried zeolite. It can be seen that the zeolite with a higher Si/Al ratio of 15 (CBV-720) shows better ion-exchange behavior as compared to the zeolite with a lower Si/Al ratio.

Free chloride tests were performed on the post-test salt-zeolite residue from the solid-state ion exchange experiments. This was used to determine what fraction of the unreacted salt was not absorbed (occluded) in the zeolite. Theoretically, after the salt and zeolite have been contacted at high temperature, the original salt either did not absorb, absorbed but did not react, or absorbed and reacted. It is hypothesized that the salt must first absorb into the pores of the zeolite in order to react and form HCl. A summary of the free chloride test results for samples taken from the solid-state ion exchange tests is also presented in Table 2.2.

Several aspects of the results in Table 2.2 are considered to be readily meaningful. First, there is good repeatability demonstrated for the estimated degree of ion exchange as measured via titration volumes for both sets of duplicate runs (400-A/400-C and 720-A/720-B). There is a significant difference (40%) in the free chloride results for the duplicates, though. In previous studies, it has been observed that the measured free chloride concentration values can be subject to high variance.[34,37] Improvement in the repeatability of the free chloride analysis results possibly requires optimization of the sample size or an increase in the number of samples analyzed and statistically averaged. Note that for both runs in which the temperature was raised only to 300°C, it appears that all of the salt was leached via the free salt test. This suggests that either a higher temperature or longer contact time is needed to achieve significant salt occlusion in the zeolite. Since the melting point of the

Table 2.2. Summary of results of salt-zeolite solid-state ion exchange experiments with H-Y zeolite dried at 150°C. Heating rate of 5°C/min for all runs. For runs that went to 650°C, a 6 hour hold at 300°C was used. For CBV-400 Si/Al = 2.55, CBV-720 Si/Al = 15.

Test No.	Zeolite Sample	T_{max} (°C)	% Free Chloride	% Conversion Ion Exchange	Estimated % Salt Occluded But Not Reacted
400-A	CBV-400	650	25.0	32.0	43
400-B	CBV-400	300	121.2	0	0
400-C	CBV-400	650	14.5	34.7	51
720-A	CBV-720	650	26.3	49.6	24
720-B	CBV-720	650	14.0	45.7	40
720-C	CBV-720	300	99.6	0	0.4

salt is 350°C, it may be that absorption is delayed until the salt actually melts. In previous studies with zeolite-A, solid-state adsorption was inferred from particular test results.[43] But in the case of the H-Y zeolites, more study of this phenomenon is needed. The last column in Table 2.2 is the difference between the starting amount of salt and what was estimated to be either "free salt" or reacted with the zeolite. This is the estimated percentage of salt that has been absorbed into the zeolite but has not reacted with protons to form HCl. Given the small particle size of the zeolite (estimated to be <10 μm), the time scale for diffusion through the zeolite crystals is likely to be very low. Thus, it is inferred that the reaction to form HCl is kinetically limited rather than diffusion limited.

Note that the free chloride test has only been validated using zeolite-A. It is possible that the larger pore faujasites are susceptible to having the salt leached from the pores even with very short contact times with water. To test whether some of the chloride measured in the leach solutions is actually HCl, the pH was measured. It was found to have a pH value of about 7, confirming that little to no HCl was in the solution and that the Cl^- ions come from LiCl or KCl.

From this initial investigation, much of the key to achieving high degree of ion exchange

appears to relate to maintaining the crystalline structure of the zeolite. Figure 2.7 shows X-ray diffraction patterns for three zeolite samples that appear to have maintained their faujasitic structure: CBV-400 dried at 150°C, CBV-400 after heating to 300°C with salt, and CBV-400 after heating to 650°C with salt). Recall from Figure 2.4 that without salt present, heating CBV-400 to 375°C resulted in complete loss in its faujasite structure. This collapse does not occur when the zeolite is heated to only 150°C. And, interestingly, it does not occur if the zeolite is heated to 300°C or even 650°C in the presence of salt. The salt appears to be providing a stabilizing effect to the structure. The key to ultimately optimizing this process may be found in first determining the highest temperature that the zeolite can be heated without salt being present to maximize its dryness and then followed by mixing with salt and heating to 650°C to maximize exchange of the H^+ with ions from the ER waste salt. This is considered to be the most logical basis for follow-on investigation of this process.

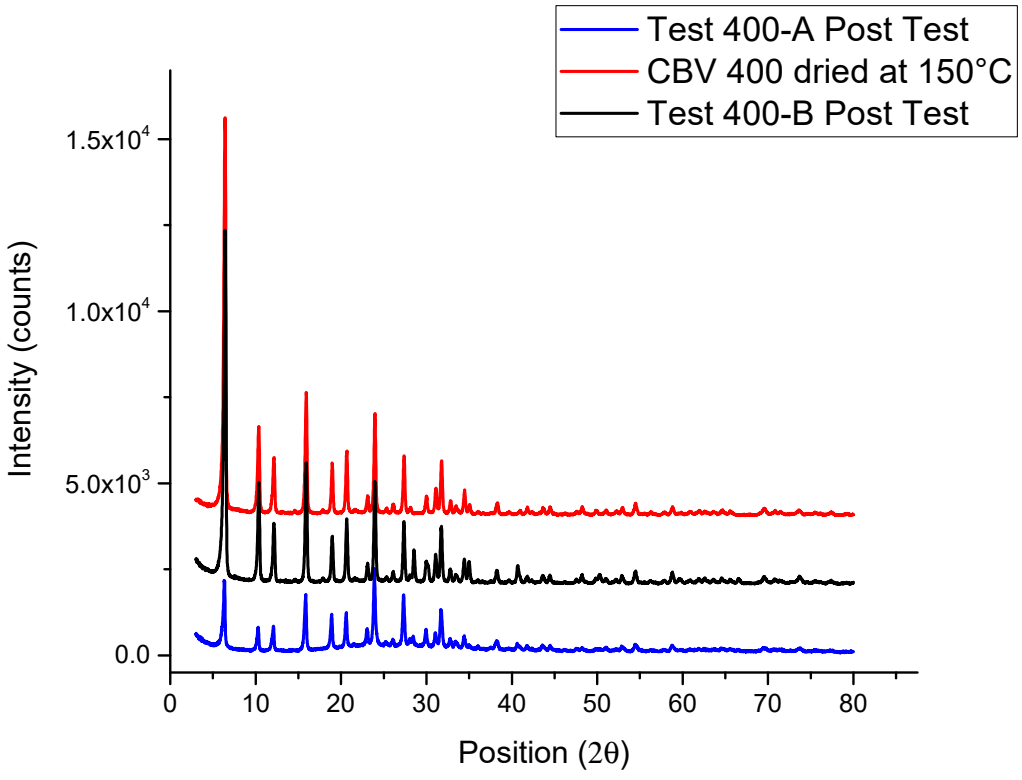

Figure 2.7. Comparison of x-ray diffraction pattern of zeolite dried at 150°C, zeolite heated to 300°C with salt and zeolite heated to 650°C with salt.

2.4 Summary

This preliminary study of an alternative to the baseline ceramic waste process has indicated that there is some promise for using H-Y zeolites to immobilize the waste ER salt. Up to half of the salt was converted to HCl in the experiments reported here using an autotitrator to capture and measure HCl evolution. However, neither extent of conversion to HCl or even extent of salt occlusion was as high as desired. This appears to be attributed to a number of factors or aspects of the process design. For one, further study is suggested to determine the optimal drying temperature for H-Y zeolite. Zeolites heated to 375°C and higher were thermally decomposed, while heating to 150°C left a significant amount of residual moisture. Also, the temperature at which the chloride salt is occluded into the dry zeolite needs to be carefully determined. In theory, occlusion precedes reaction. It is still believed that the process can be separated into occlusion followed by HCl evolution, a sequence that could be ideal of short-term management of ER salt waste. But certainly more investigation into the behavior of the salt-zeolite materials in the 300°C to 650°C temperature range is needed.

CHAPTER 3

THERMODYNAMICS OF MOLTEN SALT SOLUTIONS

In the first part of this chapter, some of the basic concepts, definitions relating to the thermodynamics of solutions, will be discussed. Subsequently, in the second part of this chapter, the theoretical work and the equations that were derived as a part of this work to support the experimental work will be presented.

3.1 Basic Concepts and Definitions

The total Gibbs free energy, G, of a fixed quantity of electrolyte solution of a given composition is a function only of the temperature and pressure irrespective of the convention adopted for expressing partial molar quantities such as activities of the constituents of the solution.

Let the solvent and solute be denoted by the subscripts A and B, respectively. The partial molar Gibbs free energies or chemical potentials of the solvent and solute is given by Equations 3.1 and 3.2, respectively.

$$\mu_A = \bar{G}_A = \left(\frac{\partial G}{\partial n_A}\right)_{n_B,T,P} \tag{3.1}$$

$$\mu_B = \bar{G}_B = \left(\frac{\partial G}{\partial n_B}\right)_{n_A,T,P} \tag{3.2}$$

where n_A and n_B are the number of moles of solvent and solute present in the system, respectively. For this work, two symbol for chemical potential μ_A and $\bar{G}_A$ have been used interchangeable. Both of the symbols represent the same thermodynamic quantity and must not be assumed to represent distinct quantities otherwise.

Generally, more interest is garnered by the change in the chemical potential with composition rather than its absolute value. Hence, it is more useful to express chemical potentials as a difference between the absolute value and a specific standard state. The standard state values are generally indicated with a superscript zero, $\bar{G}_A^0$ and $\bar{G}_B^0$. The choice of a standard state is discretionary. The standard state can be a pure substance, a saturated solution or an appropriate hypothetical solution. Generally for electrolyte solutions, the standard state almost always is the pure solvent at the same temperature and pressure as the solution of interest. Hence it is now possible to define the activity of a solvent, a_A, is defined by Equation 3.3.

$$\bar{G}_A - \bar{G}_A^0 = RT \ln a_A \tag{3.3}$$

For many aqueous solutions, the pure solute is not a very practical choice as a standard state, since it can often be a solid or liquid with properties very different from those of the solutions. Instead, for electrolytes the standard state is a hypothetical solution at unit concentrations on some chosen scale and at temperature and pressure of the solution. The chemical potential ascribed to this standard state depends on the choice of the concentration scale. The most common concentration scales used are:

(a) molar scale (c = moles of solute per liter of solution)

(b) molal scale (m = moles of solute per kilogram of solvent)

(c) mole fraction scale (X_B = moles of solute divided by the total number of moles in the system)

On each one of these concentration scales, an activity can be defined for the solute as shown in Equations 3.4, 3.5 and 3.6. In these equations, the parenthesized letters emphasize the concentration scale chosen to define the activity and the standard free energy of the solute.

$$\bar{G}_B = \bar{G}_B^0(c) + RT \ln a_B(c) \tag{3.4}$$

$$\bar{G}_B = \bar{G}_B^0 + RT \ln a_B(m) \tag{3.5}$$

$$\bar{G}_B = \bar{G}_B^0(X) + RT \ln a_B(X) \tag{3.6}$$

It is important to note here that the quantity $\bar{G}_B$ is unique for a given solution, temperature and pressure. Equations 3.4, 3.5 and 3.6 are currently simply definitions and the respective standard states have not yet been defined. Before doing that, it is useful to separate activity of the solute a_B into factors referring to the separate ions and their concentrations on the appropriate scales. It is logical that the chemical potential of the solute treated as a whole must be equal to the sum of the values of its separate constituent ions. The chemical potential of an ion is defines in Equation 3.7

$$\bar{G}_i = \left(\frac{\partial G}{\partial n_i}\right)_{n_A, n_j, T, P} \tag{3.7}$$

where i is the subscript for an ion, A and j refer to the solvent and the other ion, respectively. The quantity $\bar{G}_i$ cannot really be determined since it would entail adding to a solution some quantity of one kind of ion only. This is of course not possible experimentally. However a theoretical discussion of the free energy change due to the addition of one species of ion only can be entertained, neglecting self-energy effects due to electric charge involved,[44] provided the final equations involving electrically equivalent amounts of cations and anions.

For each ionic species, Equation 3.8 can be written

$$\bar{G}_i = \bar{G}_i^0 + RT \ln a_i \tag{3.8}$$

Let us assume for discussion that one mole of electrolyte in the ionized state gives v_+ moles of cations of valence z_+ and v_- moles of anions of valence z_-. Since the electrolyte must be electrically neutral the following three Equations 3.9, 3.10 and 3.11 can be derived.

$$v_+ \mid z_+ \mid = v_- \mid z_- \mid = -v_- z_- \tag{3.9}$$

$$\bar{G_B} = v_+\bar{G_+} + v_-\bar{G_-} \tag{3.10}$$

$$\bar{G_B^0} = v_+\bar{G_+^0} + v_-\bar{G_-^0} \tag{3.11}$$

Then it follows for a given concentration scale (from Equations 3.4, 3.5, 3.6) and the relationship shown in Equations 3.8 and conditions of neutrality presented in Equations 3.9, 3.10 and 3.11, the relationship shown in Equation 3.12 can be derived.

$$a_B = a_+^{v_+} a_-^{v_-} \tag{3.12}$$

Equation 3.12 is applicable at different values of activities, for each of the three concentration scales as discussed previously. For each of the ionic species, an activity coefficient can be defined. This value of activity coefficient can be obtained by dividing the ionic activity a_+ or a_- by the concentration of the ions on the chosen concentration scale. This is shown in Equations 3.13, 3.14 and 3.15. In these equations, f_+, y_+ and γ_+ are the molal, molar and rational activity coefficients, respectively.

$$molal\ \ scale : a_+(m) = f_+ m_+ \tag{3.13}$$

$$molar\ \ scale : a_+(c) = y_+ c_+ \tag{3.14}$$

$$mole\ \ fraction\ \ scale : a_+(\mathrm{X}) = \gamma_+ \mathrm{X}_+ \tag{3.15}$$

3.2 Activity Coefficient of Single Ionic Species

In the preceding discussion, Equations 3.13, 3.14 and 3.15 were derived to describe the relationship between the activity and activity coefficient of ionic species for a given concentration scale. These ionic activities are related to the activity of the solute as shown

in Equation 3.12. It is important to consider what these single ion activity coefficients represent and how they are measured experimentally. For discussion, let us consider the desired quantity γ_+, the rational activity coefficient that needs to be determined. While the subsequent discussion pertains to only the rational activity coefficient of an ion, the same holds true for the other activity coefficients on the molal and molar concentration scales. The activity coefficient γ_+ depends on the $\bar{G}_i - \bar{G}_i^0$ from Equation 3.8. This means that the need to determine the free energy change of an ionic solution per mole of ions of a single species i. Such a measurement of an individual ionic species cannot be performed because such measurements entail the transfer of ions of only one species into a solvent instead of two ionic species of equal and opposite charge. Even if such a transfer were physically possible, it would result in a charged solution. Even if the solution is not initially charged, it would become charged once an ionic species is added into it.

This change in the free energy associated with the addition of ionic species only would also include an unwanted work term which would represent the electrical work of interaction between the ionic species being added and the charged solution. The free energy change attributed to this interaction can be avoided if the change in concentration of the ionic species is accomplished such that the electrolyte solution ends up unchanged and electroneutral. This can be easily accomplished by addition of an electroneutral species containing the ion i to the electrolyte.

Thus if the concentration of lanthanum ions can be altered by the addition of an electrically neutral species like lanthanum chloride to an electrolyte, then the solvent, in this case LiCl-KCl eutectic salt, remains electrically neutral. When salts are dissolved instead of individual ionic species, the problem of a charged solution is eliminated. However another problem emerges. If one increased the concentration of lanthanum ions by the addition of lanthanum chloride, inevitably the concentration of chloride ions in the electrolyte also increases simultaneously. This implies that thermodynamically there are two contributions to the change in the free energy associated with the change in the salt concentrations namely the contributions from positive ions and the contributions from negative ions.

Since neither the positive ions nor the negative ions can be added independently of the other, the individual contributions of the ionic species to the free energy of the system cannot be readily determined. Experimentally, one can measure the activity coefficient

of the net electrolyte, i.e., at least two ionic species together. It is necessary therefore to establish a theoretical link between activity coefficient of an electrolyte solution (accessible experimentally) and that of only one of its ionic species (not accessible to experiments) but can be calculated theoretically from models presented in the literature like the Debye-Hückel equations and its derivative models.

This concept of an experimentally indeterminable single ion activity coefficient has its origins in the works on Guggenheim[45] from the late 1920s. In the ensuing nine decades, there has been vigorous debate in the literature about the possibility of experimentally determining single ion activity coefficients and its physical meaning. At present, the consensus view is that single ion activity coefficients are not accessible experimentally. There are some contrarian views in the literature. Most recently, Rockwood[46] presented a definition of single ion activity coefficients in terms of fundamental thermodynamic quantities and proposed their measurements in terms of purely thermodynamic quantities. This however remains the contrarian view and further validation of this hypothesis is needed before the idea of single ion activity coefficients can be widely adopted within the scientific community.

3.3 The Mean Ion Activity Coefficient

The above discussion makes clear that single ion activity coefficients cannot be experimentally determined. Here the concept of *mean ion activity coefficient* is introduced. Equation 3.12 can be rewritten in terms of ionic activity coefficients using Equation 3.15 for the mole fraction scale as shown in Equation 3.16.

$$a_B(X) = (v_+^{v_+} v_-^{v_-}) X^v \gamma_+^{v_+} \gamma_-^{v_-} \tag{3.16}$$

The symbol $v(= v_+ + v_-)$ denotes the total number of moles of ions given by one mole of an electrolyte. The individual ionic activity coefficients shown in Equation 3.16 are present as a product, each raised to the powers which satisfy the condition of electrical neutrality. To simplify Equation 3.16, the mean ion activity coefficient is introduced as defined in Equation 3.17.

$$\gamma_{\pm}^{v} = \gamma_{+}^{v_+}\gamma_{-}^{v_-} \tag{3.17}$$

Further mean ion mole fraction ($X_{\pm}$) can also be defined as shown in Equations 3.18.

$$X_{\pm}^{v} = (v_{+}^{v_+}v_{-}^{v_-})X^{v} \tag{3.18}$$

Further mean chemical potential ($\mu_{\pm}$), mean standard chemical potential ($\mu_{\pm}^{0}$) can also be defined as simply the arithmetic mean of the chemical potentials (or standard chemical potentials) of the individual ions. All of the discussion relating to mean ion activity coefficients can be summed into one simple relationship shown in Equation 3.19.

$$\mu_{\pm} = \mu_{\pm}^{0} + RT\ln X_{\pm} + RT\ln\gamma_{\pm} \tag{3.19}$$

The quantity $\mu_{\pm}$ and thus the activity coefficient $\gamma_{\pm}$ are the ones that can be experimentally determined. The theoretical approach must be to calculate the activity coefficients γ_{+} and γ_{-} for the positive and the negative ions and combine them through Equation 3.17 into the mean ion activity coefficient $\gamma_{\pm}$ which can then be compared to the experimentally derived mean ion activity coefficient. Similar relationships as described here can be derived for the molal and mole fraction scale. Frequently, the subscript, $\pm$, is not used when there is no danger of confusion or misrepresentation.

3.4 Excess Functions

Excess functions are thermodynamic properties of solutions that are in excess of those of an ideal solution. The ideal solution must be at the same conditions of temperature, pressure, and composition as those of a real solution. For an ideal solution, all of the excess functions are equal to zero. G^{E} is the excess Gibbs energy is defined as shown in Equation 3.20

$$G^{E} = G_{real\ \ solution\ \ at\ \ T,P,X} - G_{ideal\ \ solution\ \ at\ \ T,P,X} \tag{3.20}$$

Similar definitions are true for other thermodynamic properties like excess volume(V^E), excess entropy(S^E), excess enthalpy(H^E), excess Helmholtz energy(A^E), excess internal energy(U^E). Standard thermodynamic relations hold true for excess functions.

Excess functions may be positive or negative depending on the behavior of the solution. When excess Gibbs energy of a solution is greater than zero the solution is said to exhibit a positive deviation from ideal behavior. It follows that if the Gibbs energy of a solution is less than zero, the deviation from ideal behavior is said to be negative. Partial molar excess functions are defined similar to standard partial molar properties. For the purpose of this study, the most useful partial excess property is the partial molar excess Gibbs energy which is directly related to the activity coefficient. The relationship between partial molar excess Gibbs energy and activity coefficient is shown in Equation 3.21. This quantity, $\bar{G_i^E}$, can also be described as the excess chemical potential of the species i.

$$\bar{G_i^E} = RT \ln \gamma_i \tag{3.21}$$

3.5 Gibbs-Duhem Equation

In a mixture, the partial molar properties (chemical potential) of the components are related to one another by the Gibbs-Duhem equation as shown in Equation 3.22.

$$SdT - VdP + \sum_i N_i d\mu_i = 0 \tag{3.22}$$

In Equation 3.22, N_i are the moles of species i. Equation 3.22 can be easily be modified for constant pressure (isobaric) and constant temperature (isothermal) conditions to the Equation 3.23.

$$\sum_i N_i d\mu_i = 0 \tag{3.23}$$

As mentioned in the previous section, any thermodynamic equation can be modified to be written in terms of excess functions. Hence Equation 3.22 can be rewritten in terms of excess function as shown in Equation 3.24, for one mole of mixture.

$$s^E dT - v^E dP + \sum_i x_i d\mu_i^E = 0 \tag{3.24}$$

The excess chemical potential, $d\mu_i^E$, of a component i is related to activity coefficient γ_i by Equation 3.25.

$$\mu_i^E = RT \ln \gamma_i \tag{3.25}$$

At constant temperature and pressure, Equation 3.26 is valid.

$$\sum_i X_i d \ln \gamma_i = 0 \tag{3.26}$$

Using Equation 3.26, for any mixture, if experimental data over a range of concentrations yield activity coefficients of only $m-1$ component, the activity coefficient of the mth component can be computed for the same concentration range. Another important application of this Equation 3.26 is that if experimental data are available for the activity coefficient of each component of the system, then it is possible to check the thermodynamic consistency of the data using Equation 3.26. To illustrate, consider a binary system of two components 1 and 2. If the pressure is low enough to neglect the effect of pressure on the liquid phase activity coefficient, then Equation 3.27 can be written as follows:

$$x_1 \frac{d \ln \gamma_1}{dx_1} = x_2 \frac{d \ln \gamma_2}{dx_2} \tag{3.27}$$

For the purposes of discussion, let us assume that the data for γ_1 at various concentrations of x_1 have been obtained. Then to determine the activity coefficient of γ_2, the data for γ_1 would have to be curve fit to an algebraic expressing using x_1 (or x_2) as the independent variable. Once such an expressing has been obtained, it is possible to integrate Equation 3.27 analytically to calculate the values of γ_2. The Gibbs-Duhem equation provides a relationship for the activity coefficient of all of the components of a given mixture and can be effectively used for reducing the experimental work and checking experimental data for thermodynamic consistency.

3.6 Interpretation of Activity Coefficients/Chemical Potentials

In this section a brief discussion about the physical interpretation of activity coefficients will be presents. Some of discussion related to nonelectrolyte solutions is not really applicable for the experimental work presented in the subsequent chapters, but it serves to paint a physical image of activity coefficients in terms of ion-ion and ion-solvent interactions. If the natural log of the activity coefficient of a salt MY_n ($\ln \gamma_{MY_n}$) is plotted as a function of mole fraction of the salt MY_n (X_{MY_n}), it is observed that $\ln \gamma_{MY_n}$ approaches zero as a linear function i.e. the slope of the line at low concentrations approaches $-\infty$ as X_{MY_n} approaches zero. Robinson and Stokes[47] represented this as the mathematical relationship shown in Equation 3.28 for electrolyte solutions.

As $X_{MY_n} \rightarrow 0$:

$$\frac{\partial \ln X_{MY_n}}{\partial X_{MY_n}} \rightarrow -\infty \tag{3.28}$$

Guggenheim[44] noted that for electrolyte solutions, if Equation 3.28 holds true Guggenheim[44] noted that statistical theory required that long range forces between the solute particles must operate if the second case is found to be true. However, nonelectrolytes are characterized by short range forces between the solute particles and the first case is true for nonelectrolyte solutions. However, if long range forces are acting, as is expected in electrolyte solutions, then long range electrostatic attractions and repulsion obeying the inverse square law would be found to be active in addition to short range Van der Waals forces, ion-dipole interactions etc. If $\ln \gamma_B$ is represented by a series:

$$\ln \gamma_B = aX_B^n + bX_B + cX_B^2 + dX_B^3 + ... \tag{3.29}$$

where n is a fraction between zero and unity, $\partial \ln \gamma_B / \partial X_B$ must approach infinity as $X_B \rightarrow 0$ which has been observed in the literature. For electrolyte solutions a graph of $\log \gamma_{\pm}$ versus concentration for the solute show an infinite negative gradient at zero concentration is approached, which is a result of long range forces. At higher concentrations, the curves may flatten out and then rise again generally linearly or may even continue to fall. In this

region, the effects of short range interactions become important and finally dominate the behavior of ions of interest in the solution.

For many simple binary solutions, the excess thermodynamic properties of the solution phase can be represented in terms of a polynomial expression in terms of mole fractions of the constituents as shown in Equation 3.29. Other equivalent expressions such as orthogonal Legendre series have also been demonstrated to adequately describe the excess thermodynamic properties.[48]

For complete theoretical treatment of the thermodynamic properties of electrolyte solutions, both long range interionic forces and short range interactions between solute and solvent molecules must be taken into account. This is very challenging task. The net effect of interionic attractive and repulsive forces will be to decrease the free energy of the solute as compared with uncharged particles and hence decrease the activity coefficient. The interaction between ions and solvent molecules dipoles will tend to hold the solvent in solution with a consequent decrease in the solvent vapor pressure from ideal solution. This results in a corresponding increase in the activity coefficient of the solute. The short range effects are approximately a linear function of the concentration whereas the interionic effects approach linearity with the square root of the concentration.

3.7 Debye-Hückel Theory

The Debye-Hückel theory proposed by Peter Debye and Erich Hückel[49] in 1923 to explain the nonideality of solutions was a landmark hypothesis. It is the foundation on which all subsequent attempts to explain the nonideality of solutions is based. Equation 3.30 shows the main equation for mean ion activity coefficient ($\gamma_{\pm}$) as predicted by the Debye-Hückel theory.

$$\log_{10} \gamma_{\pm} = -\frac{A|z_1 z_2|\sqrt{I}}{1 + B\text{å}\sqrt{I}} \tag{3.30}$$

In Equation 3.30,

A is a constant that involves the absolute temperature

B is a constant that involves dielectric constant of the solvent

z_1 and z_2 are the valence of the cations and anions respectively

I is the ionic strength of the solution

α is the ion size parameter (Distance of closest approach of ions)

Equation 3.30 can be used to determine the activity coefficient of species. Debye-Hückel theory in its original form is applicable for dilute solutions. Since the theory was initially proposed, many researchers have extended and improved the Debye-Hückel theory to incorporate effects of salvation, applicability at higher concentrations, etc. The Debye-Hückel equation in its simplified form can be written as shows in Equation 3.31.

$$\log_{10} \gamma_{\pm} = -A|z_1 z_2|\sqrt{I} \tag{3.31}$$

Equation 3.31 is valid at high dilutions since the term $B\sqrt{I}$ is found to be a fundamental quantity, κ of interionic attraction theory. A simple ionic strength calculation for the base molten salt used here, the LiCl-KCl eutectic salt shows that it has an ionic strength of 17.9 molal. When trivalent rare earth chlorides are included up to a concentration of about 10 wt.%, the ionic strength increases for $LaCl_3$ to 20.5 molal. Such high ionic strength environments are well outside the concentration window to the Debye-Hückel equations to be valid. Similarly high ionic strengths values are obtained for the other rare earth chlorides used in this work. By comparison, a 0.1 molal concentration in water has an ionic strength of 0.01 molal, a fraction of the amount calculated for the molten salts.

Hence the reason to invoke the Debye-Hückel equations in not necessarily to demonstrate its applicability to molten salts systems but to draw attention to an important parameter, α, embedded in the Debye-Hückel equation that has implications in the latter part of this dissertation.

3.8 Ion Size Parameter α

In the Debye-Hückel equation, the ionic size is clearly an important parameter to consider when deducing the activity/activity coefficient of a species. It is one of the terms in the original Debye-Hückel Theory and has been a key parameter in all of the subsequent modifications/improvements to this theory. The ion size parameter does not necessarily represent the ionic radii of the species of interest but in fact it represents the effective size of the species in solution. Any species in solution is always solvated, i.e., it is surrounded

by oppositely charged ions of the solution. Hence its effective size in solution would not be the same as its ionic radii. However, the ionic size parameter is an important consideration to account for when thinking about activity coefficients.

3.9 Parameters Affecting μ^E

In this section, the major atomic interactions and forces that affect the excess chemical potential, μ^E in molten salt systems will be discussed. There are five major effects to consider: (1) Coulombic Effects, (2) Polarization Effects, (3) Van der Waals' Interactions, (4) Liquid Field Effects, (5) Packing and Steric Effects. Each of these effects has been briefly discussed below.

3.9.1 Coulombic Effects

It has been established in the molten salt literature that Coulombic interactions in mixtures of salts containing monovalent ions lead to negative values of μ^E (i.e. excess chemical potential). This effect also appears to be present in molten salt systems that have polyvalent cations. Additionally, long range interactions are very significant in this effect.

3.9.2 Polarization Effects

The electric field intensity at a given ion position, in general is non-zero because of ion motion and different sizes and changes of cations present. Consider an anion having two cations of the same size but different charges as its near neighbor. This anion will tend to have Coulombic fields acting on it. As a result, the electrons on the anion and the thermal motion of the anions will be *polarized* such that the negative ions reside near the cation with higher charge a greater fraction of the time. In pure molten salts, its effect will be more subdued than in mixtures and its net contribution will result in the stabilization of the mixture. Polarization effects have a negative contribution to the deviation from ideal solution behavior.

3.9.3 Van der Waals' Interactions

In molten salt mixtures that contain monovalent cations, Van der Waals' interactions usually make a positive contribution to the deviation from ideal solution behavior for mixtures with polarizable cations. Quantitative estimates of this effect are not very accurate.

3.9.4 Ligand Field Effects

Ligand field effects[50] will generally tend to stabilize the pure salts of transition metal ions. Particular configurations of near-neighbor anions will tend to be more probable.

3.9.5 Packing and Steric Effects

To satisfy the need to maintain local electroneutrality, it is likely that a highly charged cation will tend to have a large number of anions as its near neighbor rather than lower charge cations. Any energy changes, i.e., stabilization related to this effect will have to be limited by steric effects and the values of the cation-anion radii ratios.

3.10 Theoretical Work

In this section, the basic theoretical framework derived to support the experimental work reported in this work is present in detail. This is specifically applicable to the electrochemical testing that was conducted as a part of this work.

Consider a metal M and its dissolved species M^{n+} and its salt $\mathrm{MY_n}$, where Y is the anionic species. An elementary reversible reaction can be written as shown in Equation 3.32

$$M^{n+} + ne^{-} \rightleftharpoons M^{0} \tag{3.32}$$

For Equation 3.32, the Nernst equation can be written as shown in Equation 3.33

$$E^{eq} = E^{0} - \frac{RT}{nF} \ln\left(\frac{a_{M^0}}{a_{MY_n}}\right) \tag{3.33}$$

In Equation 3.33, R is the universal gas constant, T is the temperature in Kelvin, n is the number of electrons transferred in Equation 3.32 and F is Faraday's constant. a_{M^0} and a_{MY_n} are the activities of M^0 and MY_n. The activity is defined as the activity of the salt a_{MY_n} and not the activity of the ion $a_{M^{n+}}$ since experimentally measured activity coefficients are defined as mean ion activity coefficient as discussed earlier in this chapter. E^{eq} is the equilibrium potential and E^0 is the standard reduction potential. In general, E^0 is defined as the potential when a pure metal M is in equilibrium with its pure molten salt MY_n at the

temperature of interest. From thermodynamics it is known that $a_{M^0} = 1$, since it is a pure solid. Hence Equation 3.33 can be rewritten as follows:

$$E^{eq} = E^0 + \frac{RT}{nF} \ln \left(a_{MY_n} \right) \tag{3.34}$$

but,

$$a_{MY_n} = \gamma_{MY_n} X_{MY_n} \tag{3.35}$$

where γ_{MY_n} and X_{MY_n} is the activity coefficient and mole fraction of species MY_n respectively. Substitute Equation 3.35 in Equation 3.34,

$$E^{eq} = E^0 + \frac{RT}{nF} \ln \left(\gamma_{MY_n} X_{MY_n} \right) \tag{3.36}$$

Rearranging the terms,

$$E^{eq} = E^0 + \frac{RT}{nF} \ln \left(X_{MY_n} \right) + \frac{RT}{nF} \ln \left(\gamma_{MY_n} \right) \tag{3.37}$$

Equation 3.37 can be rewritten as follows:

$$E^{eq} - \frac{RT}{nF} \ln \left(X_{MY_n} \right) = E^0 + \frac{RT}{nF} \ln \left(\gamma_{MY_n} \right) \tag{3.38}$$

In deriving Equation 3.38, Equation 3.35 is used which defines the activity of the solute as a product of activity coefficient and mole fraction. The Nernst equation can be written correctly for any of the three concentration scales of molarity, molality and mole fraction.[51,52] Depending on the concentration scale used, the standard states for each of these concentration scales must be defined adequately. Hence for each of the concentration scales there will be unique values of standard reduction potential (E^0) designated as E^0_M, E^0_m and E^0_X for molarity, molality, and mole fraction, respectively.[51,52] The mole fraction scale is more convenient to use for molten salt systems than the molarity scale as it is independent of density and temperature. This is also the scale most widely used in the molten salt literature and hence comparable thermodynamic data are more easily available.

Density of salts is extremely hard to measure accurately due to solute effects. Hence, the Nernst equation is derived on the mole fraction scale.

All of the terms on the left hand side (LHS) of Equation 3.38 are known. E^{eq} would be measured in an electrochemical cell (as the OCP). Knowing the concentration of the species present, X_{MY_n} can be calculated. Thus, using Equation 3.38 the Apparent Potential ($E^{0'}$) can be calculated. $E^{0'}$ is defined as shown in Equation 3.39. Bard and Faulkner[53] call the term $E^{0'}$ as the *Formal Potential.*

$$E^{0'} = E^0 + \frac{RT}{nF} \ln \left(\gamma_{MY_n} \right) \tag{3.39}$$

The right hand sides (RHS) of both Equations 3.38 and 3.39 are the same. Hence the left hand sides of the aforementioned equations can be equated to obtain the value of $E^{0'}$. Knowing $E^{0'}$, the value of γ_{MY_n} can be determined from Equation 3.39 if the value of the only other unknown quantity; E^0 is known. As mentioned earlier, in the purist sense, E^0 for the $M|MY_n$ system, will be the equilibrium potential when pure metal M is in equilibrium with pure salt MY_n at the temperature of interest. The pyrochemical reprocessing of the spent fuel in eutectic LiCl-KCl salt is performed out at 773 K. Pure rare earth chlorides and actinide chloride salts melt at temperatures above 773 K.[54] Hence it is not possible to obtain a true value of E^0 for these lanthanides and actinide chloride salts for molten eutectic salt mixtures. Due to this conundrum, there is clearly a need to define the activity of MY_n versus a different standard state. For that the most basic definition of activities for real solutions is invoked. In general, activity of any species 'i' can be defined as shown in Equation 3.40.

$$\bar{G}_i = \bar{G}_i^0 + RT \ln a_i \tag{3.40}$$

In Equation 3.40, $\bar{G}_i$ is the partial molar Gibbs free energy (chemical potential) of the species i and $\bar{G}_i^0$ is the partial molar Gibbs free energy of the species i at the standard state (equivalent to the molar Gibbs free energy of the pure species). The standard state can be chosen to define the most appropriate conditions of extensive thermodynamic properties. For molten salt systems, if the deviation from ideal behavior has to be measured, $\bar{G}_i^0$ must be defined as the chemical potential of the *pure supercooled liquid salt.*[55] This is the

reference that has been used by various authors that have experimentally determined the activity coefficient of actinides and lanthanides for molten eutectic mixtures. Some authors have mistakenly used the value of Gibbs free energy of formation of pure crystal as the reference/standard state. Such a standard state has no physical meaning and is inherently inaccurate.

Converting potential to Gibbs free energies using the relationship $\Delta G = -nFE$ and replacing the value of ΔG^0 with ΔG^{SC}, the Gibbs free energy of pure supercooled liquid. Now, Equation 3.39 can be rewritten as follows:

$$\Delta G^{SC} - \Delta G^{0'} = RT \ln \left(\gamma_{MY_n}\right) \tag{3.41}$$

The term $\Delta G^{SC} - \Delta G^{0'}$ is also known as the Gibbs Excess Free Energy (ΔG^{Excess}). The term ΔG^{Excess} captures the deviation from ideal behavior of a liquid mixture.[56] For ideal solutions, ΔG^{Excess} is zero. Equation 3.41 can be rewritten as follows:

$$\boxed{\Delta G^{Excess} = \Delta G^{SC} - \Delta G^{0'} = RT \ln \left(\gamma_{MY_n}\right)} \tag{3.42}$$

Using Equation 3.42, the activity coefficient (and by extension the activity) of a species can be calculated. The only unknown in this equation is the value of ΔG^{SC}. A detailed discussion on how to determine this value is provided in the next subsection.

3.10.1 Determination of ΔG^{SC}

In general, the change in Gibbs free energy of fusion (ΔG_{Fusion}) is defined as shown in Equation 3.43, where $G_{PureLiquid}$ and $G_{PureSolid}$ are the chemical potentials of pure liquid and pure solid, respectively.

$$\Delta G_{Fusion} = G_{PureLiquid} - G_{PureSolid} \tag{3.43}$$

At temperatures below the melting point of the species, as is the case for the chloride salts of actinides and lanthanides at 773 K , then ΔG_{Fusion} is the hypothetical free energy of fusion, $G_{PureLiquid}$ is equal to the chemical potential of the pure supercooled liquid (G^{SC}), the desired standard state for determination of activity coefficients, and $G_{PureSolid}$ is equal

the Gibbs free energy of formation of pure crystal ($G_{Formation}$) at the temperature of interest (T_i). Hence Equation 3.43 can be rewritten as follows:

$$\Delta G_{Fusion}^{Hypothetical}(T_i) = G^{SC}(T_i) - G_{Formation}(T_i) \tag{3.44}$$

In Equation 3.44, 'T_i' represents the temperature (in Kelvin) for which the calculations are performed. For Equation 3.44 to be true as written, $T_i < T_M$, where T_M is the melting point of the pure solid (For $LaCl_3$, T_M = 1131 K). In Equation 3.44, the value of $G_{Formation}$ can be found in thermodynamic databases. G^{SC} is the unknown value of the "Pure Supercooled Standard State" that needs to be determined. In the next subsection, the method to determine the value of $\Delta G_{Fusion}^{Hypothetical}$ will be discussed.

3.10.1.1 Determination of $G_{Fusion}^{Hypothetical}$

In this section, the general method to calculate the value of $G_{Fusion}^{Hypothetical}$ will be briefly discussed. Figure 3.1 shows a schematic of the H vs. T diagram. T_i and T_M denote the temperature of interest for which the value of $G_{Fusion}^{Hypothetical}$ (hereafter denoted as G_{Fusion}) needs to be calculated and the melting temperature of the substance respectively. On an H vs. T diagram, the slope of the lines is the $C_{p(S)}$ and $C_{p(L)}$, which denote the specific heat capacity of solid and liquid at temperatures lower and higher than T_M, respectively. The value of ΔG_{Fusion}, can be determined as follows:

At $T = T_M$,

$$\Delta G_{Fusion} = \Delta H_{Fusion} - T_M \Delta S_{Fusion} = 0 \tag{3.45}$$

The values of ΔH_{Fusion} and ΔS_{Fusion} at $T = T_M$ can be found in thermodynamic databases. At any other temperature of interest (T_i), the values of $\Delta H_{Fusion}(T_i)$ and $\Delta S_{Fusion}(T_i)$ which are needed to calculate the value of $\Delta G_{Fusion}(T_i)$ can be calculated as shown in Equation 3.46 and 3.47, respectively.

$$\Delta H_{Fusion}(T_i) = \Delta H_{Fusion}(T_M) + \int_{T_M}^{T_i} (C_{p(Liquid)} - C_{p(Solid)})\, dT \tag{3.46}$$

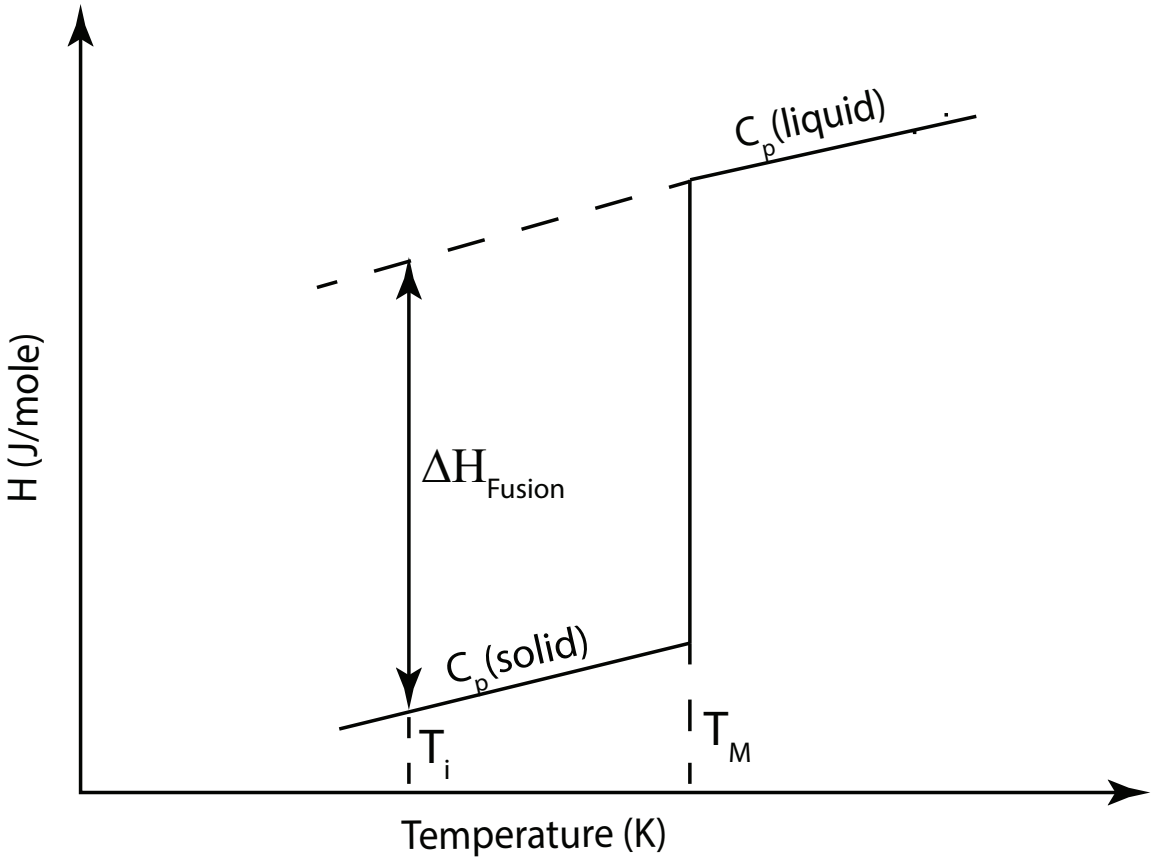

Figure 3.1. Schematic representation of an H vs. T diagram

$$\Delta S_{Fusion}(T_i) = \Delta S_{Fusion}(T_M) + \int_{T_M}^{T_i} \frac{C_{p(Liquid)} - C_{p(Solid)}}{T}\, dT \qquad (3.47)$$

For the above calculations, the value of $C_{p(L)}$ is extrapolated below the melting point to the temperature of interest. Using Equations 3.46 and 3.47, the values of $\Delta H_{Fusion}(T_i)$ and $\Delta S_{Fusion}(T_i)$ can be calculated. The value of $\Delta G_{Fusion}(T_i)$ can then be calculated simply by using the standard thermodynamic relationship $\Delta G_{Fusion}(T_i) = \Delta H_{Fusion}(T_i) - T\Delta S_{Fusion}(T_i)$. After having calculated the values of $\Delta G_{Fusion}(T_i)$, the value of $\Delta G^{SC}(T_i)$ can be calculated using Equation 3.44. If $T_i < T_M$, then the value calculated using the above described method will be equal to ΔG^{SC}. The value of ΔG^{SC} can now be used to calculate the activity coefficient from Equation 3.42.

In Equation 3.44, the value of $G_{Formation}$ at any desired temperature can be obtained readily from thermodynamic databases, software or from previously published literature.

The accuracy with which the value of $G_{Formation}$ can be calculated in generally $\pm 10\ kJ/mole$. This large variation in the value of $G_{Formation}$ can be a big source of error for the final calculations. Depending on the value of $G_{Formation}$ that is employed in the calculations, the final value of the activity coefficient can vary by over two orders of magnitude. There is a more sophisticated way to remove this source of potential error using a different reference electrode.

3.10.2 Determination of Standard Potentials

Using the above methods, the standard reduction potential (E^0) for supercooled chlorides versus the Cl^-/Cl_2 reference electrode was calculated as a function of temperature. To perform these calculations, publicly available literature[54] was used as the source for the values of heat capacity, melting points and ΔG values. The final calculations are presented in Table 3.1 and were published by this author in the literature.[57]

3.10.3 Saturated Analyte Reference Electrode

As stated above, it is desirable to eliminate the need to use the value of $G_{Formation}$ in the activity coefficient calculations due to the error associated with these values. In this section, the experimental techniques to eliminate the need for the $G_{Formation}$ values will be examined and derive the theoretical equations of such systems. Instead of using the more commonly used Ag/AgCl reference electrode, a specialized reference electrode can be used for this case. Of course a Cl^-/Cl_2 reference electrode could be used. However such Cl^-/Cl_2 electrodes are extremely tedious to make and operate along with the additional safety concerns of using chlorine gas. Hence a Ag/AgCl reference electrode is preferable. Here it is proposed to use a rare earth reference electrode. Let the metal M be the working electrode in equilibrium with its salt MY_n in a eutectic LiCl-KCl electrolyte. Then a $M^0/(MY_n)_{Saturated}$-LiCl-KCl reference electrode must be used. In other words, MY_n must be present at saturation concentration in the reference electrode such that, excess solid MY_n is present in the reference electrode. Such a cell would be represented as shown in Equation 3.48.

$$M|MY_{n(l)}||MY_{n(s)}|M \tag{3.48}$$

Table 3.1. Standard potentials (E^0) for supercooled chlorides versus the standard Cl^-/Cl_2 reference electrode reported as a function of temperature (K) within the temperature range of 673 to 873 K.

Chloride Salt	Melting Point of Pure Chloride (K)	Standard Potential (E^0) (V vs. Cl^-/Cl_2)
$CeCl_3(Ce^{3+}/Ce)$	1080	$7 \times 10^{-4}T(K) - 3.4723$
$CrCl_2(Cr^{2+}/Cr)$	1088	$5 \times 10^{-4}T(K) - 1.8863$
$FeCl_2(Fe^{2+}/Fe)$	950	$4 \times 10^{-4}T(K) - 1.5438$
$GdCl_3(Gd^{3+}/Gd)$	875	$7 \times 10^{-4}T(K) - 3.3478$
$LaCl_3(La^{3+}/La)$	1131	$7 \times 10^{-4}T(K) - 3.5301$
$MgCl_2(Mg^{2+}/Mg)$	987	$6 \times 10^{-4}T(K) - 3.0935$
$MnCl_2(Mn^{2+}/Mn)$	923	$5 \times 10^{-4}T(K) - 2.2892$
$NdCl_3(Nd^{3+}/Nd)$	1032	$7 \times 10^{-4}T(K) - 3.4220$
$NiCl_2(Ni^{2+}/Ni)$	1304	$5 \times 10^{-4}T(K) - 1.1974$
$PrCl_3(Pr^{3+}/Pr)$	1059	$7 \times 10^{-4}T(K) - 3.4559$
$PuCl_3(Pu^{3+}/Pu)$	1033	$6 \times 10^{-4}T(K) - 3.1112$
$ThCl_4(Th^{4+}/Th)$	1042	$6 \times 10^{-4}T(K) - 2.8827$
$UCl_3(U^{3+}/U)$	1110	$6 \times 10^{-4}T(K) - 2.8125$
$UCl_4(U^{4+}/U)$	863	$6 \times 10^{-4}T(K) - 2.5119$

The Nernst equation for such an electrochemical cell can be written as follows as shown in Equation 3.49. In Equation 3.49, E_{Cell} is the electrochemical potential of the cell, E_{WE} is the electrochemical potential of the working electrode and E_{RE} is the electrochemical potential of the reference electrode.

$$E_{Cell} = E_{WE} - E_{RE} \tag{3.49}$$

Equation 3.49 can be further expanded as shown in Equation 3.50

$$E_{Cell} = \left(E^0_{M^0/MY_n} - \frac{RT}{nF} \ln\left(\frac{a_{M^0}}{a_{MY_n}}\right) \right)_{WE} - \left(E^0_{M^0/MY_n} - \frac{RT}{nF} \ln\left(\frac{a_{M^0}}{a_{MY_n}}\right) \right)_{RE} \tag{3.50}$$

In Equation 3.50, E_{Cell} is the electrochemical potential of the cell, $E^0_{M^0/MY_n}$ is the standard reduction potential of the M/MY_n couple, a_{M^0} is the activity of the metal M, a_{MY_n} is the activity of the dissolved MY_n species in the working electrolyte. In Equation 3.50, the $E^0_{M^0/MY_n}$ in both the WE and RE brackets represent the standard reduction potential of M/MY_n species. Hence the $E^0_{M^0/MY_n}$ terms are identical and will get canceled from the Equation 3.50. The a_{M^0} term within both the RE and WE brackets represent the activity of solid metal M, which by definition is equal to 1. Hence Equation 3.50 can be rewritten as follows.

$$E_{Cell} = \frac{RT}{nF} \ln\left(a_{MY_n}\right)_{WE} - \frac{RT}{nF} \ln\left(a_{MY_n}\right)_{RE} \tag{3.51}$$

In Equation 3.51, $\left(a_{MY_n}\right)_{WE}$ is activity of the species MY_n in the working electrolyte, the desired unknown quantity. The value of the activity coefficient can be obtained by defining the activity as a product of mole fraction and activity coefficient. $\left(a_{MY_n}\right)_{RE}$ is the activity of the species MY_n in the reference electrolyte. Recall that the reference electrode is a saturated solution of the MY_n in LiCl-KCl. Thermodynamically, saturation is defined as the concentration at which for a given solute in a solution, the chemical potential of the liquid phase of the solute is equal to the chemical potential of the solid phase of the solute i.e. $\mu_{solid} = \mu_{liquid}$ for the solute MY_n. Hence, in the saturated reference electrode,

$\mu_{\mathrm{MY_n(s)}} = \mu_{\mathrm{MY_n(l)}}$. Therefore the activity of the species $\mathrm{MY_n}$ in reference electrolyte, i.e., $\left(a_{MY_n}\right)_{RE}$ is defined to be equal of 1 since chemical potential of all of the $\mathrm{MY_n}$ species in the reference electrode is equal to the chemical potential of solid $\mathrm{MY_n}$ and the activity of all solids is equal to unity. This implies that the activity of the species $\mathrm{MY_n}$ in the working electrolyte is being measured versus a solid standard state (SSS) reference electrode. Thus Equation 3.51 can be rewritten as follows.

$$E_{Cell} = \frac{RT}{nF} \ln \left(a_{MY_n}\right)_{SSS} \tag{3.52}$$

In Equation 3.52, SSS implies that the activity of the working electrolyte was measured versus a solid standard state. In order to measure the deviation from ideal solution behavior in a molten salt solution, the activity must be defined versus a 'Liquid Standard State' (LSS). Thus, the measured activity needs to be converted from a solid standard state to a liquid standard state to have a tangible physical meaning. To enable the conversion from a solid standard state to a liquid standard state the most elementary definition of activity of a species can be invoked. The activity of any species can be defined in terms of chemical potentials by Equation 3.53.

$$\mu_i = \mu_i^0 + RT \ln(a_i) \tag{3.53}$$

In Equation 3.53, μ_i is the chemical potential of a species, μ_i^0 is the chemical potential of the species at standard state and a_i is the activity of the species. Using Equation 3.53, an analogous relationship for the activities at solid standard state and liquid standard state can be written for the species $\mathrm{MY_n}$ as shown in Equations 3.54 and 3.55.

$$\frac{\mu_{MY_n} - \mu^0_{Pure\ Solid}}{nF} = \frac{RT}{nF} \ln(a)_{SSS} \tag{3.54}$$

$$\frac{\mu_{MY_n} - \mu^0_{Pure\ Liquid}}{nF} = \frac{RT}{nF} \ln(a)_{LSS} \tag{3.55}$$

In Equation 3.54 and 3.55, the activity of the MY_n in the working electrolyte is defined versus two different standard states: pure solid MY_n and pure liquid MY_n. It is important to remember that thermodynamically there is no correct standard state. The choice of a standard state is generally discretionary, with the constraint that they must represent the most meaningful condition physically under which activity of the species under consideration is equal to 1. Equation 3.54 and 3.55 have a common term on their LHS; μ_{MY_n}, i.e., the chemical potential of the species MY_n in the working electrolyte. Hence the two equations can be rearranged and rewritten to yield Equation 3.56.

$$\frac{RT}{nF}\ln(a_{SSS}) = \frac{RT}{nF}\ln(a_{LSS}) + \frac{\mu^0_{PureLiquid} - \mu^0_{PureSolid}}{nF} \tag{3.56}$$

In Equation 3.56, the LHS of the equation is the same as the measurements made using the saturated analyte reference electrode (see Equation 3.52). Additionally, in Equation 3.56, the term $(\mu^0_{PureLiquid} - \mu^0_{PureSolid})$ represents the difference in the chemical potential between a pure liquid MY_n species and pure solid MY_n species. This difference is equal to the Gibbs free energy of fusion (ΔG_{Fusion}) by definition. Inserting that definition and combining Equations 3.52 and 3.56 yields a very meaningful relationship as shown in Equation 3.57.

$$\boxed{E_{Cell} = \frac{RT}{nF}\ln\left(a_{MY_n}\right)_{SSS} = \frac{RT}{nF}\ln\left(a_{MY_n}\right)_{LSS} + \frac{\Delta G_{Fusion}}{nF}} \tag{3.57}$$

Using Equation 3.57, the measured activity versus a solid standard state can be converted to meaningful value of activity versus a liquid standard state by the addition of the ΔG_{Fusion}. Hence, using the analyte reference electrodes, there is no need to calculate the value of the standard potential or the hypothetical Gibbs free energy of pure supercooled liquid. The activity of the species can be directly measured. Only the value of ΔG_{Fusion} at the temperature of measurements needs to be calculated. This can be done by calculating the values of the enthalpy (ΔH_{Fusion}) and entropy (ΔS_{Fusion}) of fusion. These two values can be calculated using the previously stated Equations 3.46 and 3.47, respectively.[57,58] Once these two values have been calculated, the value of ΔG_{Fusion} can be easily calculated ($\Delta G = \Delta H - T\Delta S$).

There are a few advantages of using an analyte reference electrode that are believed to yield better experimental measurements. Firstly, the need to calculate the values of $\Delta G_{Formation}$ for both the analyte and the reference electrode (Ag/AgCl) is eliminated. If a Ag/AgCl reference electrode is used, $\Delta G_{Formation}$ values of both the analyte and the reference system contribute to errors. Secondly, the conversions of potentials from the Ag/AgCl scale to the Cl^-/Cl_2 scale need not be performed. There are quite a few conversion equations available in the literature.[22,59,60] For the determination of the activity of the analyte using an analyte reference electrode, this conversion is not necessary. Additionally the error contributions due to lack of knowledge of the activity coefficient of AgCl in the reference electrode are also eliminated. Thirdly, the errors associated with the membrane potential are eliminated. Though they have not proved to be really significant source of error for a 5 mole % Ag/AgCl reference electrode,[59] they will nevertheless be eliminated. Further, it is a well-established basis of classical thermodynamics that the heat capacity has a temperature dependent relationship, for all species: elements, compounds and mixtures. Hence the error associated with the linear extrapolation of the heat capacity (C_p) to the supercooled region, a few hundred degrees kelvin, most definitely has a much smaller error associated with it than the ± 10 kJ/mole error with the need to determine the value $\Delta G_{Formation}$ values. This extrapolation of the heat capacity is needed to determine the value of ΔG_{Fusion} value as previously discussed. One final advantage of the use of an analyte reference electrode is the ability to incorporate a real, tangible standard state into the experimental set-up. Although this is a solid standard state, it still represents a universally accepted standard state for a species and eliminates the necessity to rely on an esoteric hypothetical standard state concept.

The use of an analyte reference electrode is not the only experimental method to eliminate the $\Delta G_{Formation}$ value from the calculations. One can use a conventional Ag/AgCl reference electrode if desired and make the open circuit measurements, called E for this discussion. After such measurements have been completed, another experiment can be performed in which the same Ag/AgCl reference electrode is used. The working electrode should be the analyte metal and the working electrolyte is a saturated solution of analyte (MY_n) in LiCl-KCl with excess solids present. The open circuit potential of such a cell is measured, called E_{Sat}. Then $E - E_{Sat}$ will give the same measurement that can be achieved

with an analyte reference electrode. In effect, $E - E_{Sat}$ will give the same measurement as shown in Equation 3.52. From that point, all of the subsequent derivation will hold true, and the activity versus a liquid standard state can be calculated as previously described. Equations from the above presented derivation were used for the determination of the activity coefficient of $GdCl_3$ and $CeCl_3$ in molten LiCl-KCl eutectic salt at the temperature of interest 773 K.

3.11 Summary

In this chapter, the fundamentals of solution thermodynamics and activity coefficients were discussed. Additionally important concepts like excess functions were introduced and discussed along with the parameters that affect them. Finally, physical interpretation of activity coefficients and the intermolecular forces that affect the activity coefficients was presented and discussed.

The theoretical work that was performed to support the experimental measurements has been presented in this chapter. In this chapter, equations to help determine activity coefficient for two sets of experimental systems were presented. First when a Ag/AgCl reference electrode is used, equations are presented to help determine the value of $G_{Formation}$ that are necessary to calculate the value of the hypothetical pure supercooled liquid standard state. The activity coefficient in such a case can be calculated according to Equation 3.58. Additionally, the standard reduction potential for 14 redox systems was calculated using the equations presented in this chapter.

$$\Delta G^{Excess} = \Delta G^{SC} - \Delta G^{0'} = RT \ln \left(\gamma_{MY_n}\right) \tag{3.58}$$

Theoretical equations for an experimental system in which a saturated analyte reference electrode is used were also present in this chapter. For such an experimental system, it was deduced that the activity of the analyte can be directly measured. This measured activity needs to be converted from a solid standard state to a liquid standard state using Equation 3.59. The use of such an experimental set-up has been shown to have several advantages over a conventional Ag/AgCl reference electrode.

$$E_{Cell} = \frac{RT}{nF} \ln \left(a_{MY_n} \right)_{SSS} = \frac{RT}{nF} \ln \left(a_{MY_n} \right)_{LSS} + \frac{\Delta G_{Fusion}}{nF} \tag{3.59}$$

CHAPTER 4

EXPERIMENTAL SECTION

In this chapter, the general experimental set-up for each category of experiments will be documented.

4.1 General Equipment and Design

4.1.1 Inert Atmosphere Glovebox

Rare earth chlorides including the base salt (LiCl-KCl eutectic) are extremely hygroscopic and will pick up moisture very quickly when exposed to air. The salts then form hydroxide species in the presence of moisture. Hence all of the experiments were performed in an inert atmosphere (Ar) glovebox. The oxygen and moisture levels in the glovebox were below 0.1 ppm. Inert atmosphere gloveboxes (Innovative Technologies) are available at the University of Utah in which all of the electrochemical experiments were performed. All the salts and samples were always stored in the glovebox. The gloveboxes are equipped with a heat exchanger, which was connected to a chiller (Polyscience WisperCool^{TM}) to prevent the glovebox atmosphere from heating up during high temperature molten salt experiments. The coolant in the chiller was a 50:50 ethylene glycol : distilled water mixture. An image of the glovebox stet-up is shown in Figure 4.1

4.1.2 Potentiostat

To perform the electrochemical experiments an Autolab PGSTAT302N (Metrohm) was available at the University of Utah. The potentiostat was placed outside of the glovebox as shown in Figure 4.1. The leads of the potentiostat were connected to copper posts at the back of the glovebox. Inside the glovebox, copper wires with alligator clips were attached to the corresponding posts to complete the electrical connections for performing electrochemical experiments inside the glovebox.

Figure 4.1. Photo of the inert (argon) atmosphere glovebox, potentiostat and chiller set-up available at the University of Utah.

4.1.3 Furnace

A Kerr furnace was used for heating the salt mixture for the experiments. The Kerr furnaces are permanently stored inside the aforementioned glovebox and used during the experiments. Kerr furnaces are programmable and the heating rate (°C/hour) and the set point can be effectively controlled using this furnace. The Kerr furnaces used for all of the experiments are top loading, hence a 50 mm hole was drilled on the top face of the Kerr furnace insulation. This now allowed for a custom made alumina lid (Advalue Technology) to be used for supporting the working and reference electrodes in place. The alumina lid, shown in Figure 4.2, was designed to have three holes. The largest hole was used to insert the reference electrode into the working electrolyte, and the intermediate hole was used to insert the working electrode into the molten salt. The smallest hole was generally left

Figure 4.2. The custom alumina lid used for all of the electrochemical experiments.

unused. It was used intermittently to insert a thermocouple to record the temperature of the working electrolyte.

4.1.4 Electrochemical Cell

A two-electrode electrochemical cell was used for all open circuit potential measurements. For a two-electrode set-up, both the counter electrode (CE) and reference electrode (RE) leads of the potentiostat are connected to the reference electrode. The working electrode (WE) lead of the potentiostat is connected to the working electrode. For open circuit potential measurements, the potentiostat was operated under the *cell off* instrument setting. This means that the potentiostat is simply measuring the potential difference between the working and reference electrode as the system reached equilibrium independently, applying no external perturbation to the system. If the potentiostat is operated under the *cell on* condition then the potentiostat is actively forcing the system to zero current. Hence the measurements under the *cell on* condition are not equilibrium measurements since an external perturbation is being applied to the electrochemical cell. Since open circuit potential measurements are performed when the externally applied current is zero, there are no concerns of uncompensated iR drop due to solution resistance.

4.1.5 Reference Electrode

An adequate reference electrode is necessary for completion of the electrical circuit and to perform open circuit potential measurements. For the molten chloride salt systems, the

Cl^-/Cl_2 is analogous to the H_2/H^+ scale for aqueous systems. The potential of the Cl^-/Cl_2 half cell is defined to be zero by convention. In practice, building and using a Cl^-/Cl_2 reference electrode for experimental measurements is extremely tedious and poses many safety risks. Hence most often an alternative, easy to build reference electrode is used in experiments to measure potentials. The most commonly used reference electrode is a Ag/AgCl reference electrode. In the literature, many varying concentrations of Ag/AgCl have been used, from 1 mol % AgCl to 100 mol % AgCl. The balance is generally LiCl-KCl eutectic salt (working electrolyte). For this work, broad reference electrode systems were used; 5 mole % Ag/AgCl reference electrode (for $LaCl_3$, $NdCl_3$) and a saturated rare earth reference electrode for all other systems.

4.1.5.1 Ag/AgCl Reference Electrode

All of the measured potentials need to be converted from the Ag/AgCl scale to the Cl^-/Cl_2 scale. For such conversions, there have been a number of studies[59,60] in the literature that have determined the conversion from the Ag/AgCl to Cl^-/Cl_2 scale at various concentrations of AgCl in LiCl-KCl eutectic salt. The results published by Yang and Hudson[59] are the most frequently cited in the literature for conversion from the Ag/AgCl scale the Cl^-/Cl_2 scale. For a 5 mol % Ag/AgCl reference electrode (used for this work), Yang and Hudson[59] report a conversion factor of -1.071 V (at 773 K) whereas Shirai et al.[60] report a conversion factor of -0.921 V. If the work by Shirai et al.[60] is corrected for a sharp increase in density near 100 mol % AgCl, the conversion factor becomes -1.012 V. Clearly there is some discrepancy in the reported conversion values. Experimental data of a number of students at the University of Utah agree well with the literature values when the conversion reported by Yang and Hudson[59] is used. Hence for this work, the conversion factors reported by Yang and Hudson[59] will be used. Even though the difference in the various conversions reported in the literature is only a tens of millivolts, they can cause quite large errors in the activity coefficient of a given species.

4.1.5.2 Saturated Rare Earth Reference Electrodes

For some of the rare earth chloride systems studies in this work ($GdCl_3$, $CeCl_3$), saturated rare earth chloride reference electrodes were used for the electrochemical experiments.

The identity of the rare earth chloride was the same as the analyte used. Use of this rare earth chloride reference negates the need for the use of any conversion factors for conversion to the chloride scale for the determination of the activity coefficients. These electrodes have been discussed in detail in Chapter 3.

4.2 Electrochemical Testing

In this section, the details of the experimental apparatus and set-up for each section will be presented. In general, for each analyte system, the experimental apparatus was not altered once testing for that particular system was commenced. Any meaningful alterations/changes/improvements were made for the subsequent system. If any changes were made to the experimental set-up within one analyte system, they will be specifically mentioned.

4.2.1 Electrochemical Cell Design

Electrochemical testing was performed for four rare earth chlorides as a part of this work: $LaCl_3$, $NdCl_3$, $GdCl_3$ and $CeCl_3$. A schematic of the electrochemical cell used for the experiments is shown in Figure 4.3. All of the experiments were performed with a similar set-up. Only things that changed between the various systems were either the working crucible material (glassy carbon, quartz, and alumina), the reference electrode housing material (quartz, mullite) or the construction of the reference electrode. Details on specific experimental set-up will be described in detail in the individual chapters. A Kerr furnace was used to heat the salt and maintain a temperature of 773 K. An alumina lid with three holes was used to hold the electrodes in place. The largest hole was used to insert the stainless steel basket, shown in Figure 4.4, into which the rare earth metal was placed to function as the working electrode.

The intermediate hole was used to insert a reference electrode into the working electrolyte. The quartz tube used for the $LaCl_3$ system was of the exact size of the intermediate hole. The mullite tube (3mm ID x 5mm OD) used for the $NdCl_3$,$GdCl_3$ and $CeCl_3$ systems was supported with the help of alumina tubes, Teflon tape and a Viton O-rings to ensure its snug fitting into the intermediate hole. An image of the mullite reference electrode is shown in Figure 4.5. The smallest hole was used to insert thermocouples into the molten salt bath

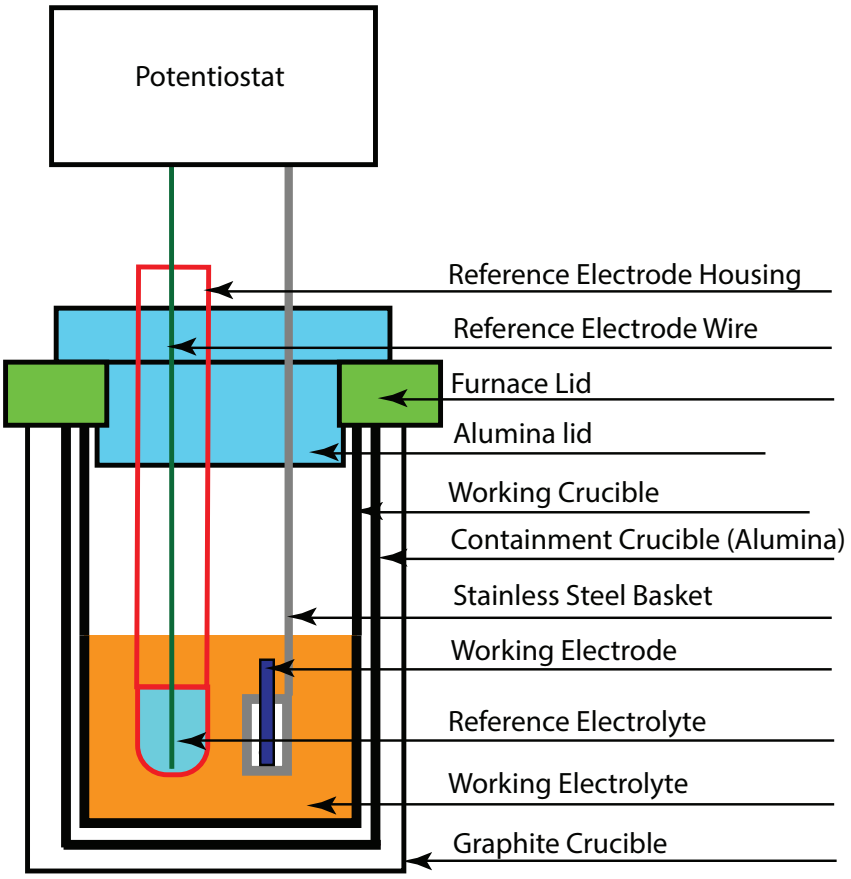

Figure 4.3. Schematic of the general experimental set-up used for all of the electrochemical experiments performed for this work.

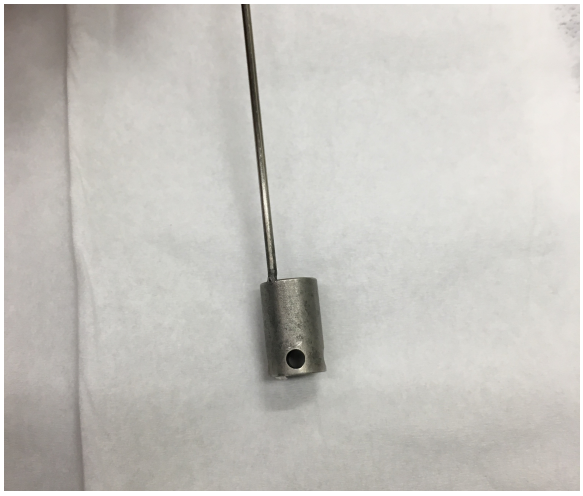

Figure 4.4. The custom stainless steel basket used to hold the rare earth metal rod in the working electrode.

Figure 4.5. Image of the mullite tube used as a reference electrode.

during the test to monitor the temperature of the working electrolyte. A custom built off center quartz funnel was used to introduce additional reagents into the working electrolyte as required during the test.

During the test, a stainless steel all-thread was used to take samples of the working electrolyte for ICP and TGA/DTA analysis. When inserted, the molten working electrolyte will freeze onto the metal all-thread. This frozen molten salt can be easily separated from the all-thread by simply using metal pliers. These samples were labeled and stored in the glovebox for both ICP analysis for analyte concentration and TGA/DTA analysis.

4.2.2 Experimental Methodology

During the electrochemical testing, preweighed quantity of pure LiCl-KCl salt was heated to the desired temperature (773 K). Subsequently, preweighed quantities of the rare earth chlorides were added to this molten salt progressively. After every addition of rare earth chlorides, the solution was allowed to stand and equilibrate. The stainless steel basket with the rare earth metal rod was then inserted into the molten salt mixture and open circuit potential was recorded using a computer. After such a measurement, rare earth chlorides were again added and the process was repeated. After every OCP measurement, a sample was taken using the stainless steel all-thread rod. For tests with CsCl present, the initial melt consisted of LiCl-KCl-CsCl. During the life of the tests, small quantities of CsCl were added to prevent dilution of CsCl concentration due to the addition of the rare earth chlorides. The remaining experimental methodology was similar to the one described

above.

The sample retrieved using the all-thread is isolated from the stainless all-thread using pliers. This sample is labeled and stored in a scintillation vial for further analysis. At the end of the test, the salt is generally discarded. The alumina crucible removed from the glovebox and cleaned using nitric acid and a mixture of acetone and isopropyl alcohol. This is then dried in an oven at 150°C before being reused. At the end of a test, the rare earth metal rod used as the working electrode had substantial salt deposits on it that could potentially contaminate the next texts using the same rod. Hence this also needs to be cleaned. Since the rare earth metals used for this work cannot be contacted with moisture and air without being oxidized, washing it with water is not an option. These rods are cleaned by heating (773 K) fresh batches of fresh LiCl-KCl eutectic in a small crucible. The rare earth metal rod is completely submerged in this fresh salt for about 30 minutes. This causes the previously adhered salt on the rod to melt in the pool of fresh eutectic salt. The rod is then withdrawn from the molten pool and allowed to cool. This process is again repeated twice more with fresh batches of eutectic salt each time. After the third rinse in fresh eutectic salt, this rod is now ready for use in the next test.

4.3 Experimental Challenges

One of the most commonly used methods to determine the activity and activity coefficient of species in a molten salt solution is electromotive force measurements of M/MX_n electrochemical cell versus a selected reference electrode. In this section, some of the experimental challenges associated with such measurements will be briefly discussed.

4.3.1 Definition of Standard States

One of the most important concepts to understand during the empirical determination of the activity and activity coefficients for any system is to rigorously understand the concept of ‘Standard State.’ The classical definition of the standard state is the condition under which the activity of the species is equal to one, at the temperature of interest. Within the field of classical thermodynamics, the two most commonly used standard states for mixtures are governed by Henry’s law and Raoult’s law. Henry’s law defines the standard state to be ‘infinitely dilute solution’. Raoult’s law defines the standard state to be a ‘pure substance’.

In the pyrochemical treatment of spent nuclear fuel, electrorefining is generally operated at conditions under which the mole fraction of most of dissolved species present is less than 5 mol %. However, for the molten salt system associated with the pyroprocessing of spent nuclear fuel, wherein eutectic mixtures are used and at temperatures well below the melting point of most pure actinide and rare earth chlorides, it is most convenient to use the Raoultian definition of the standard state of a pure substance. The use of either of the standard states is acceptable practice. But consistency must be maintained with how the properties are reported and used in process models/calculations. The activity calculated relative to any one standard state can be converted to the other using the relationship presented by Näfe.[61]

4.3.2 Selection of Reference Electrode

The selection of an appropriate reference electrode is critical to reliable and reproducible cell EMF measurements. While potentials are usually calculated (as in Table 3.1) relative to the standard Cl^-/Cl_2 reference electrode, using these electrodes for measurements is difficult and impractical. The most commonly used experimental reference electrode is the Ag/AgCl reference electrode with concentrations of silver chloride fixed at a value ranging from 1 to 5 mole % AgCl with the balance being the electrolyte (LiCl-KCl). If higher concentrations of AgCl are used, the liquid junction potential can become significant and cause meaningful errors in physical measurements.[59,62]

4.3.3 Working Electrode

The working electrode can be an inert rod (Mo or W). When using an inert working electrode, a reducing current is run to deposit some of the analyte metal onto this rod. After the current is stopped, the OCP can be measured for a short period of time (few seconds) as the deposited metal corrodes off. Such measurements are not necessarily 'equilibrium' measurements. Better measurements can be obtained by using a source of the metal analyte (a small rod of analyte metal) as the working electrode. This gives more stable and reproducible measurements.

4.3.4 Oxidation State of Analytes

One of the major challenges for using electrochemical cells during such measurements can be the presence of multiple oxidation state of the elements present. U(+3, +4), Am(+2,

+3), and Nd(+2, +3) are some of the many elements, frequently encountered in spent nuclear fuel, that can be present in molten LiCl-KCl eutectic salt in multiple oxidation states. The presence of these oxidation states inherently means that any salt added into the molten electrolyte will speciate into more than one oxidation state. In such a case, it is important to know the relative amounts of the two oxidation states present to be able to make meaningful conclusions from that data. Ideally, the molten salts should be analyzed to determine the oxidation state using methods like XANES, Raman spectroscopy or UV-Vis spectroscopy. Access to instrumentation capable of performing these measurements for molten salt systems can be limited and/or expensive.

4.4 Phase Diagram Studies

Phase diagram development to determine the solidus and liquidus temperatures of quaternary chloride systems was performed as a part of this work. The samples for these studies were generated in the glovebox as a part of the electrochemical testing and final concentrations were determined using ICP analysis. The samples for the LiCl-KCl-CsCl-$NdCl_3$ system were generated independently in a MTI muffle furnace in a 10 ml quartz crucible. This was done since no electrochemical testing was performed for the LiCl-KCl-CsCl-$NdCl_3$ system. A TA Instruments Q600 TGA/DTA instrument shown in Figure 4.6 was available at the University of Utah to determine the melting temperature of the salts. This instrument was always calibrated prior to every set of experiments as per the manufacturer's recommendation. The calibration protocol included four parts: DTA baseline calibration, TGA weight calibration (using two standard weights), DSC heat flow calibration (using sapphire standard) and cell constant calibration (using zinc metal). Additionally, a one point temperature calibration was performed using zinc metal. The calibration was always performed under the same conditions (heating ramp rate, argon flow rate) under which the experiments were to be performed. If the experimental conditions were altered, the calibration was also always updated. All of the samples were run under ultra high purity argon purge gas. Disposable aluminum pans were used in all of the experiments performed as part of the phase diagram development work.

The thermograms generated using a DTA/DSC is most sensitive to the heating ramp rate.[63] Faster scan rates are known to result in increased sensitivity and improvement in the

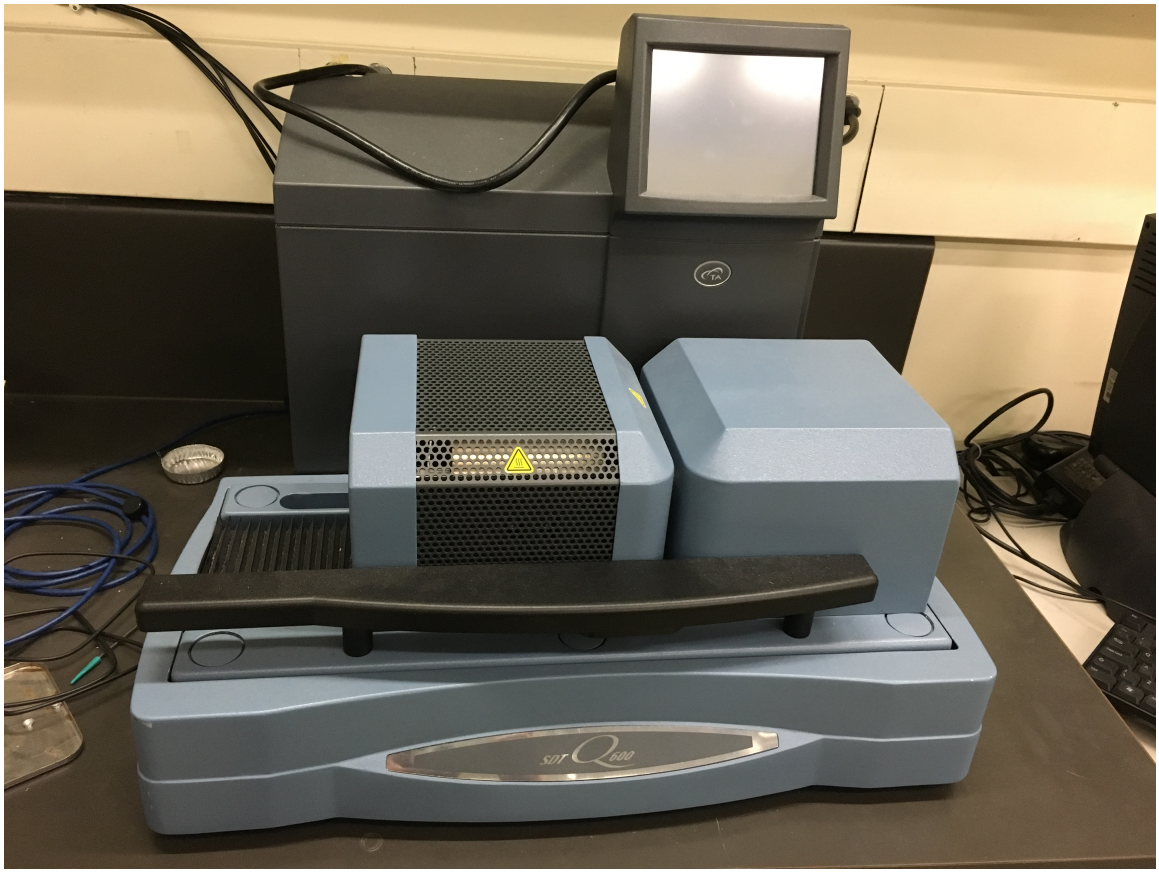

Figure 4.6. Photo of the TA Instruments Q600 TGA/DSC instrument available at the University of Utah.

quality of the data generated. At higher scan rates increased sensitivity is a result of the fact that energy flows more quickly, i.e., the amount of energy involved remains the same but the time during which it flows is reduced as the scan rate increases. For the experiments reported here, two scan rates were used for the experiments; 5°C/min (for $LaCl_3$ system) and 20°C/min for all other rare earth systems. The highest heating rate that the Q600 is capable of heating without loss of accuracy is 20°C/min. The other parameters that were fine-tuned were merely cosmetic and are not expected to have any significant impact on the quality of the data.

4.4.1 Experimental Methodology

The samples used for thermal analysis were generated in the argon atmosphere glove-box. A few milligrams of the salt sample was isolated into a clean scintillation vial, closed

tightly and transferred outside to load into the aluminum pan. During the life of the test, the sample was continuously being purged with a stream of ultra high purity argon. No significant moisture gain was observed for the sample during the test. Any moisture gain would be observable as an increase in the weight of the sample during the life of the test. No such phenomenon was observed for any of the samples whose melting temperatures are reported in this work. The methods information for running the instrument is documented below.

4.5 Summary

In this chapter, the experimental methods employed for this work have been discussed and presented. For the electrochemical testing, a two-electrode cell was set up to measure the open circuit potential of the cell. Two types of reference electrodes were used, a 5 mol % Ag/AgCl electrode and a saturated rare earth reference electrode. Samples taken during the electrochemical testing using a steel all-thread. These samples were subsequently used for phase diagram studies using a TA Instrument TGA/DTA instrument and for ICP analysis.

CHAPTER 5

ACTIVITY OF RARE EARTH CHLORIDES

In this chapter, the activity and activity coefficient work for the four rare earth chlorides; $LaCl_3$, $GdCl_3$, $NdCl_3$, and $CeCl_3$ will be presented.

5.1 Introduction

A brief literature review for all of the rare earth chlorides studied in this work is presented here.

5.1.1 Literature Review for Activity of $LaCl_3$

For $LaCl_3$ in molten eutectic LiCl-KCl salt, the activity coefficient has been previously measured experimentally by a number of groups over the years.[21–24,64] Activity coefficient of lanthanides like Gd, Nd, Ce has been measured by a much larger group of authors. A good summary of the data was published by Zhang[65] recently. One of the common themes of the studies to date has been the inherent presumption that the activity coefficients are independent of concentration of analyte present in solution. The activity coefficient of lanthanum chloride has been studied only at single concentration in these studies. There is significant divergence in the data reported in literature. One of the contributing factors for such divergence may be the fact that every study was performed at a different concentration of $LaCl_3$.

Cesium is an important fission product that can accumulate in the electrolyte in the molten salt over time. Large amounts of accumulated cesium in the electrorefiner electrolyte can interfere with the separation process for the uranium and transuranics. This would require either the eventual replacement of the electrolyte or the selective extraction of cesium from the salt. One of the motivations of this chapter is to study the concentrations at which the presence of CsCl will begin to affect the properties of the lanthanides in the molten salts, to enable us to predict and anticipate the levels of CsCl concentrations would

be a cause of concern from a reprocessing standpoint.

In this chapter, activity coefficient of $LaCl_3$ in molten eutectic LiCl-KCl salt is experimentally determined. Further, the effects of concentration of $LaCl_3$ and the effect of cesium chloride on the activity coefficient of $LaCl_3$ will be examined.

5.1.2 Literature Review for Activity of $GdCl_3$

Gadolinium is an important fission product due to its very high ability to absorb neutrons. ^{157}Gd is known to have the highest thermal neutron capture cross-section of any known stable nuclide. This has important implications from the standpoint of reprocessing of spent nuclear fuel. A high degree of separation of gadolinium from the actinides is needed to support recycle of spent nuclear fuel. Knowledge of the activity of $GdCl_3$ in LiCl-KCl eutectic salt will aid in that process.

The activity coefficient of $GdCl_3$ in molten eutectic LiCl-KCl has been reported by three main studies in the literature.[22,25,26] Tang and Pesic[25] also reported the activity coefficient of $GdCl_3$ at a concentration of 2.0 wt. % $GdCl_3$. Caravaca et al.[26] reported the activity coefficient of gadolinium chloride in LiCl-KCl eutectic salt at a single concentration of 0.166 mol % $GdCl_3$. Caravaca et al.[26] in calculating their activity coefficients use two different standard states for their calculations reporting two vastly different activity coefficient values for the same concentration of gadolinium chloride. Lantelme and Berghoute[22] determined the activity coefficient as a function of concentration up to 1.44 mol % $GdCl_3$. Lantelme and Berghoute[22] for their work used a definition of standard state with unit activity at infinite dilution and reported activity coefficients of $GdCl_3$ that are vastly different from the other two studies cited here.[25,26]

From the data reported in the three main studies cited here, two key areas remain with substantial knowledge gaps. First is expanding the concentration range and concentration dependence of the activity coefficient of $GdCl_3$ above and beyond the 1.44 mol % $GdCl_3$ reported in the single study by Lantelme and Berghoute.[22] A second and key area where knowledge gaps remain and further advancements can be made is the selection of an adequate standard state. The choice of two different standard states by Caravaca et al.[26] in a single study and a completely unique standard state by Lantelme and Berghoute[22] to report activity coefficients of $GdCl_3$ greater than unity shows that clearly there is room

to develop a better experimental and theoretical framework to define standard states and activity coefficients of rare earth chlorides in general and $GdCl_3$ in particular. Further the influence that other salts like CsCl will have on the thermodynamic properties of $GdCl_3$ also needs to be examined. In this chapter, the activity coefficient of $GdCl_3$ in LiCl-KCl eutectic molten salt has been measured up to 4.29 mol % $GdCl_3$ using an analyte reference electrode and further examined the influence of CsCl on the activity coefficient of $GdCl_3$ at 773 K.

5.1.3 Literature Review for Activity of $CeCl_3$

For cerium chloride, the only studies in the literature for the activity coefficient of cerium chloride in have been reported by Marsden and Pesic,[27] Castrillejo et al.,[24] and Zhang et al.[28] Marsden and Pesic[27] report the activity coefficient of cerium chloride as a function of temperature (673 K - 973 K). In their work, the concentration of cerium chloride at which these measurements were made is not reported. At 773 K, Marsden and Pesic[27] reported the activity coefficient of $CeCl_3$ to be 1.18×10^{-2}. Apart from the work by Marsden and Pesic,[27] there is one additional study in the literature on the activity coefficient cerium chloride. Castrillejo et al.[24] reported the activity coefficient ($\log \gamma$) of cerium chloride at two temperatures of 723 and 823 K to be 2.87×10^{-3} and 7.87×10^{-3} respectively (on the mole fraction scale). Again the concentration of $CeCl_3$ at which such measurements were made is not clear from the paper.

Zhang et al.[28] also studied the activity coefficient of $CeCl_3$ in a temperature range of 823 to 923 K at a concentration of 0.125 mol L^{-1} $CeCl_3$. For their calculations of the activity coefficient of cerium chloride, Zhang et al.[28] used data generated from cyclic voltammograms rather than equilibrium measurements. They reported values in the range of 9.14 x 10^{-3} at 823 K to 7.78 x 10^{-3} at 923 K. Another point to note in their data is the choice of standard state. They state in their paper that the standard state chosen for their calculations is the Gibbs free energy of formation of $CeCl_3$ at standard states. This value at the operating temperatures of 823 to 923 K would represent the Gibbs free energy of formation of solid cerium chloride. The appropriate standard states for such calculations would be represented by the Gibbs free energy of supercooled liquid $CeCl_3$.

5.1.4 Literature Review for Activity of $NdCl_3$

The $LiCl-KCl-NdCl_3$ neodymium chloride system was evaluated in an attempt to determine the activity coefficient of dissolved $NdCl_3$. This was the first system in which an attempt was made to use a saturated analyte reference electrode. This was not successful due the complicated chemistry of $NdCl_3$ in LiCl-KCl eutectic salt. The chemistry of $NdCl_3$ in molten LiCl-KCl eutectic salt is different from the other rare earth chlorides studied here. $NdCl_3$ is present in two stable oxidation states of +2 and +3 in the molten LiCl-KCl eutectic salts. Due to the existence of the two oxidation states of neodymium, the experimental determination of activity coefficient of $NdCl_3$ is more challenging than the other rare earths in this work.

Masset et al.[23] determined the activity coefficient of $NdCl_3$ at a concentration of 70 x 10^{-5} mol cm^{-3} at 733 K. For these measurements, Masset et al.[23] used cyclic voltammograms rather than equilibrium measurements. Further they derived a relationship between the two reduction peaks (Nd(III)/Nd(II) and Nd(II)/Nd(0)) that are observed. They reported an activity coefficient of $NdCl_3$ of 8×10^{-5}.

Castrillejo et al.[24] also studied the activity coefficient of the $NdCl_3$. They concede in their paper that due to the existence of Equation 1.2, potentiometric methods cannot be used to determine the standard potential (and by extension the activity coefficient) of Nd(III)/Nd(0) system. For such calculations, various assumptions need to be made as noted by Castrillejo et al.[24] as noted in Section 1.6.1.4.

5.1.4.1 Chemistry of $NdCl_3$ in LiCl-KCl

Neodymium chloride is present in two oxidation states of +2 and +3 in molten LiCl-KCl eutectic salt at 773 K. This fact has been well established in the literature and extensively documented. The reduction of dissolved neodymium is a two-step process, with Nd(III) reducing to Nd(II) and subsequently Nd(II) reducing to Nd(0). This has been observed in cyclic voltammograms published by various authors. This presence of two oxidation states of neodymium poses a particular challenge to the endeavor to determine the activity coefficient of $NdCl_3$. These challenges will be briefly explained here.

In a molten LiCl-KCl eutectic salt, when a known quantity of $NdCl_3$ is added, this $NdCl_3$ will disproportionate into Nd(III) and Nd(II) according to the chemical reaction shown in

Equation 5.1.

$$NdCl_3 + \frac{1}{2}Nd = \frac{3}{2}NdCl_2 \tag{5.1}$$

Hence even though a known quantity of $NdCl_3$ is added into the molten salt mixture, after addition, some of it will form $NdCl_2$. Hence, there is no way of knowing the real concentration of added $NdCl_3$ in the molten salt with the experimental techniques and apparatus currently available in the laboratory. Hence, it is not possible to determine the *real* mole fraction of $NdCl_3$ present in the salt mixture. Equation 5.2 shows the Nernst Equation is written in terms of activities.

$$E = E^0 + \frac{RT}{nF}\ln a \tag{5.2}$$

For the $NdCl_3-NdCl_2-Nd$ system that, if equilibrium measurements are performed, all of the three species must be in equilibrium with each other. Hence the measured E must be the same for the $NdCl_3-Nd$ and $NdCl_2-Nd$ system. This can be represented in terms of Equation 5.3

$$E = E^0_{NdCl_3} + \frac{RT}{nF}\ln a_{NdCl_3} = E^0_{NdCl_2} + \frac{RT}{nF}\ln a_{NdCl_2} \tag{5.3}$$

It is evident from Equation 5.3 that even if the mole fraction of $NdCl_3$ is an unknown quantity, the activity and not activity coefficient of $NdCl_3$ can be determined by choosing an appropriate standard state. Hence for the neodymium chloride system, only the experimentally determined activities are reported and not activity coefficients.

5.2 Experimental

5.2.1 Equipment and Reagents

All the experiments were performed inside an ultra-dry argon atmosphere ($\leq$ 0.1 ppm O_2 and $\leq$ 0.1 ppm H_2O) glovebox (Innovative Technologies). A Kerr Electro-Melt furnace was used to heat the salts to the desired temperature. The salts were heated in an alumina (AdValue Technology) or glassy carbon crucible. A two-electrode electrochemical cell

was set-up to perform open circuit potential (OCP) measurements. The temperature of the molten salt was measured using RTD thermocouples (Omega). The open circuit potential was measured using an Autolab PGSTAT302N potentiostat (MetrohmUSA). All samples were weighed on a precision balance (Mettler Toledo). Precision balances are susceptible to drift due to build-up of static charges which is aggravated with balances placed inside a dry atmosphere glovebox. A vial full of radioactive material (uranium oxide) was always kept inside the precision balance to neutralize the static charges.

For the electrochemical measurements, the working electrodes were always a rare earth metal rod placed in a perforated stainless steel basket. The only substantive difference in the experimental set-ups of the four rare earths was the choice of reference electrodes. For the $CeCl_3$ tests, the counter/reference electrode was a saturated Ce/$CeCl_3$-LiCl-KCl electrode encased in a mullite tube (Ceramic Solutions). For the $GdCl_3$ tests, the counter/reference electrode was a saturated Gd/$GdCl_3$-LiCl-KCl electrode encased in a mullite tube. For the $NdCl_3$ tests, the counter/reference electrode was a 5 mol % Ag/AgCl electrode encased in mullite tube. Finally for the $LaCl_3$ tests, the counter/reference electrode was a 5 mol% Ag/AgCl electrode encased in quartz tube. A schematic of a general experimental set-up is shown is Figure 5.1. A summary of the experimental set-ups used in this work has been tabulated in Table 5.1.

Reagents used for this study were as follows: Ultra dry 99.99 % LiCl-KCl (SAFC Hitech), 99.998 % cesium chloride salt (Sigma-Aldrich), 99.99 % cerium chloride salt (Sigma-Aldrich), 99.99 % gadolinium chloride salt (Sigma-Aldrich) 99.9 % lanthanum chloride salt (Alfa Aesar), 99.9 % neodymium chloride salt (Alfa Aesar), cerium metal rod (6.35 mm x 25 mm; 99.9 % ESPI Metals), gadolinium metal rod (6.35 mm x 25 mm; 99.9 % ESPI Metals), lanthanum metal rod (6.35 mm x 25 mm; 99.9 % ESPI Metals), neodymium metal rod (6.35 mm x 25 mm; 99.9 % ESPI Metals), cerium metal sheet (0.050” Thick x 3mm Wide x 8” Long, 99.9 %; ESPI Metals), and gadolinium metal sheet (0.050” Thick x 3mm Wide x 8” Long, 99.9 %; ESPI Metals),

5.2.2 Experimental Procedure

For studying the activity coefficient of a given species as a function of concentration, a preweighed quantity of pure LiCl-KCl salt was heated to the desired temperature (773

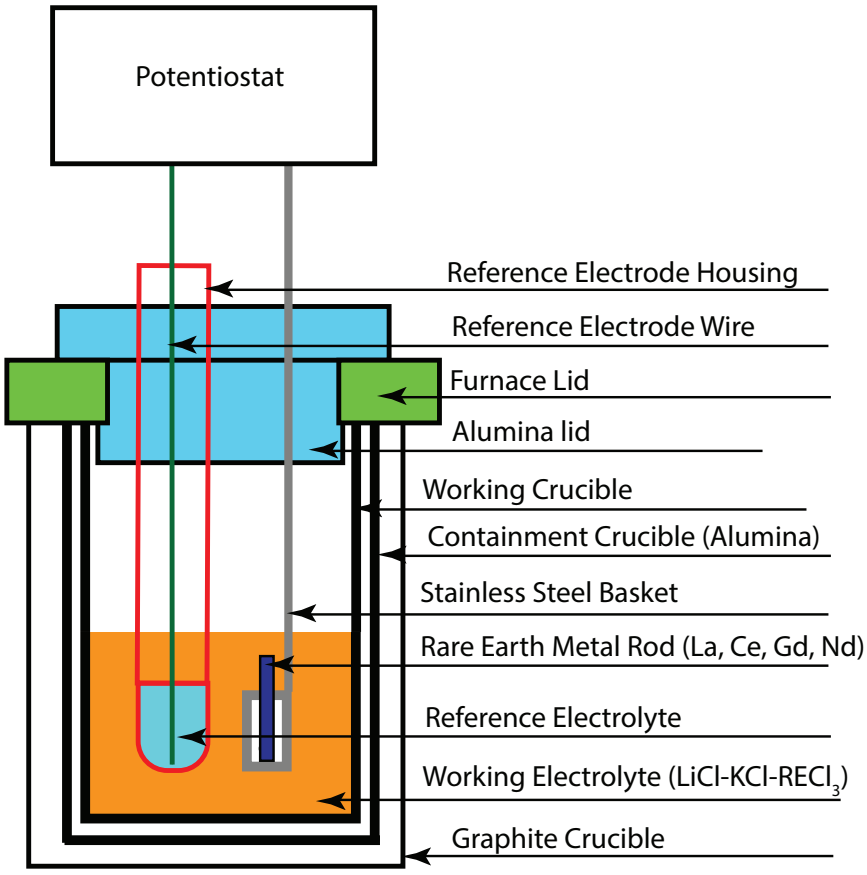

Figure 5.1. Schematic of the experimental set-up used for this work

Table 5.1. Summary of the electrochemical set-ups used for this work.

Salt System	Working Electrode	Reference Electrode	Working Electrolyte
$CeCl_3$	Ce metal rod	Saturated $Ce/CeCl_3$-LiCl-KCl[a]	LiCl-KCl-$CeCl_3$
$GdCl_3$	Gd metal rod	Saturated $Gd/GdCl_3$-LiCl-KCl[a]	LiCl-KCl-$GdCl_3$
$NdCl_3$	Nd metal rod	5 mol % Ag/AgCl in LiCl-KCl[a]	LiCl-KCl-$NdCl_3$
$LaCl_3$	La metal rod	5 mol % Ag/AgCl in LiCl-KCl[b]	LiCl-KCl-$LaCl_3$

[a] Encased in mullite tube
[b] Encased in quartz tube

K) overnight with the reference electrode submerged in the molten salt for wetting of the reference electrode. Subsequently, preweighed quantities of the rare earth chloride salts were added to this molten salt progressively. After every addition of analyte salt, the solution was allowed to stand and equilibrate. The stainless steel basket with the gadolinium metal rod was then inserted into the molten salt mixture and open circuit potential (OCP) measurements were made. After such a measurement, rare earth chloride salt was again added and the process was repeated. After every OCP measurement, a sample was taken using a stainless steel all-thread rod. For tests with CsCl present, the initial melt consisted of LiCl-KCl-CsCl. For the duration of the tests, small quantities of CsCl were added to prevent dilution of the cesium chloride in the molten salt mixture. The remaining experimental methodology was similar to the one described above.

5.3 Results

5.3.1 Activity of $LaCl_3$

In general, it was observed that the OCP values recorded using the potentiostat were very stable to the third decimal place (which is the limit for the instrument) with fluctuations nonexistent. Statistical analysis performed on a random sample of 17 independent OCP measurements yielded an average standard deviation of 0.120 mV in the measurements. Using that data set, within a 95% confidence interval the average margin of error for the OCP measurement was calculated to be 0.04 mV. These statistical calculations help us perform error propagation analysis through the entire calculations. All the potentials reported in this paper are reported versus a Cl^-/Cl_2 reference electrode unless otherwise stated. Data reported by Yang and Hudson[59] were used to convert the potentials from the 5 mol % Ag/AgCl reference electrode that was used here to a standard Cl^-/Cl_2 reference electrode scale. In this section, results will now be presented from the experiments for activity coefficient of $LaCl_3$ first as a function of $LaCl_3$ concentration. Next data will be presented on the effect of CsCl on the activity coefficient of $LaCl_3$.

Figure 5.2 shows a cyclic voltammogram (CV) of lanthanum chloride present in molten eutectic salt. The CV was performed at four scan rates of 200, 300, 400, and 500 mV/s. The La(III)/La(0) peak can be observed clearly in the CV and has been labeled. As expected, it is observed that the current increases with the scan rate. The main takeaway from the

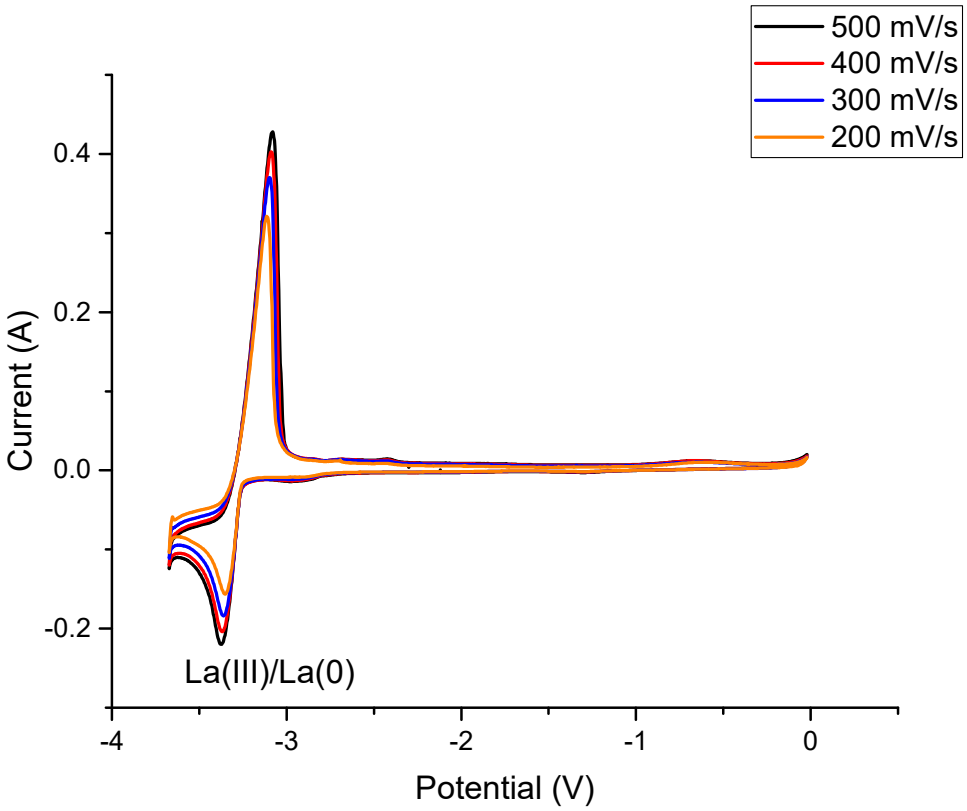

Figure 5.2. Cyclic voltammogram at four scan rates of 200, 300, 400 and 500 mV/s for $LaCl_3$ (0.46 mol %) in molten LiCl-KCl eutectic salt performed at 773 K. Working Electrode: Glassy carbon rod (ϕ = 2 mm), Counter Electrode: La metal rod, Reference Electrode: 5 mol % Ag/AgCl. Potentials reported vs. a standard Cl^-/Cl_2 reference electrode.

CV is that there is no other analyte species present in the molten salt electrolyte. Any Cs(I) present introduced in the form of CsCl will reduce at a potential more negative than the reduction potential of Li^+/Li peak.[20] Hence Cs^+/Cs reduction cannot readily be observed in the cyclic voltammetry scans.

5.3.1.1 Effect of $LaCl_3$ Concentration

The calculation of activity coefficients from OCP measurements is an exponential mathematical relationship as described earlier. Even small errors in the measurements of the open circuit potentials will not only propagate through the calculations but indeed get magnified. Hence it was decided to smooth the open circuit potential measurements at this initial

stage using a suitable mathematical function to prevent the further propagation and magnification of errors. Matlab was used to generate this function, of the form $y = ae^{bx} + ce^{dx}$, from the experimental data.

The average difference between the measured and modeled values is observed to be about 2 mV with a standard deviation of 1.4 mV. Such small errors are well within the realm of experimental error associated with physical measurements. Figure 5.3 shows the experimental values of OCP plotted along with the model fit. The coefficient of determination for the fit to function was greater than 0.99. For all further calculations, the values obtained from the best-fit functions were used rather than discrete measured data points.

Using the values obtained, the apparent potential and activity coefficient of $LaCl_3$ in the

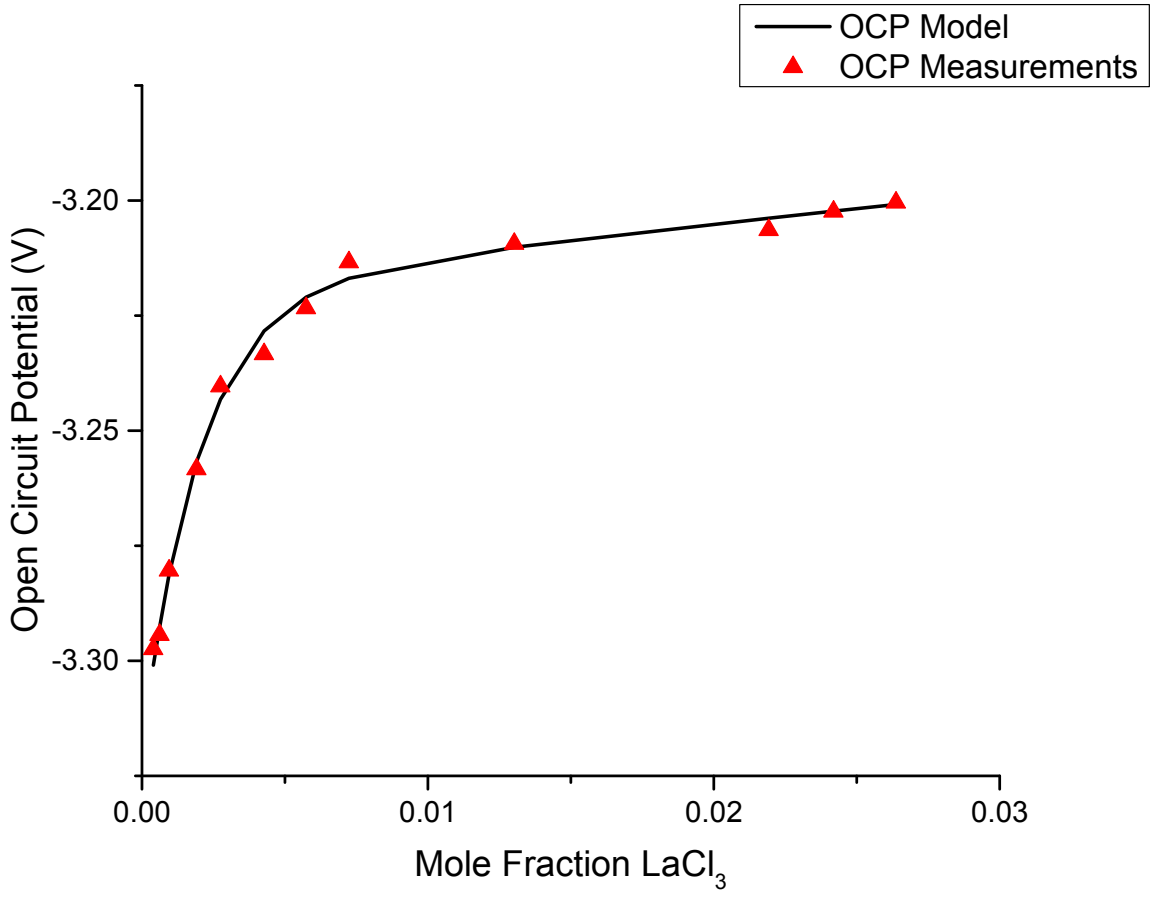

Figure 5.3. Experimental and modeled values of open circuit potential (vs. standard Cl^-/Cl_2 electrode) for $La/LaCl_3$ couple, plotted as a function of $LaCl_3$ concentration at 773 K.

molten salt can be calculated. Figure 5.4 shows a plot of the apparent potential ($E^{0'}$) plotted as a function of concentration. It can be observed that the value of the apparent potential is not a constant value as previously assumed and is indeed a function of concentration. The value of $E^{0'}$ initially increases (becomes more positive) reaching its most positive value at about 0.55 mol % La. It then proceeds to decrease (becomes more negative) and beginning to taper off at higher concentrations of $LaCl_3$ towards a constant value. Within the concentration range tested, the electrochemical potential for the reduction of La(III) to La(0) varies by about 25 mV.

Previously, Shirai et al.,[66] Kuznetsov et al.,[67] and Tang and Pesic[21] independently reported the apparent potential of the La(III)|La(0) couple at 773 K to be -3.137 V, -3.079 V, and -3.072 respectively. These values are of course outside of the potential window reported

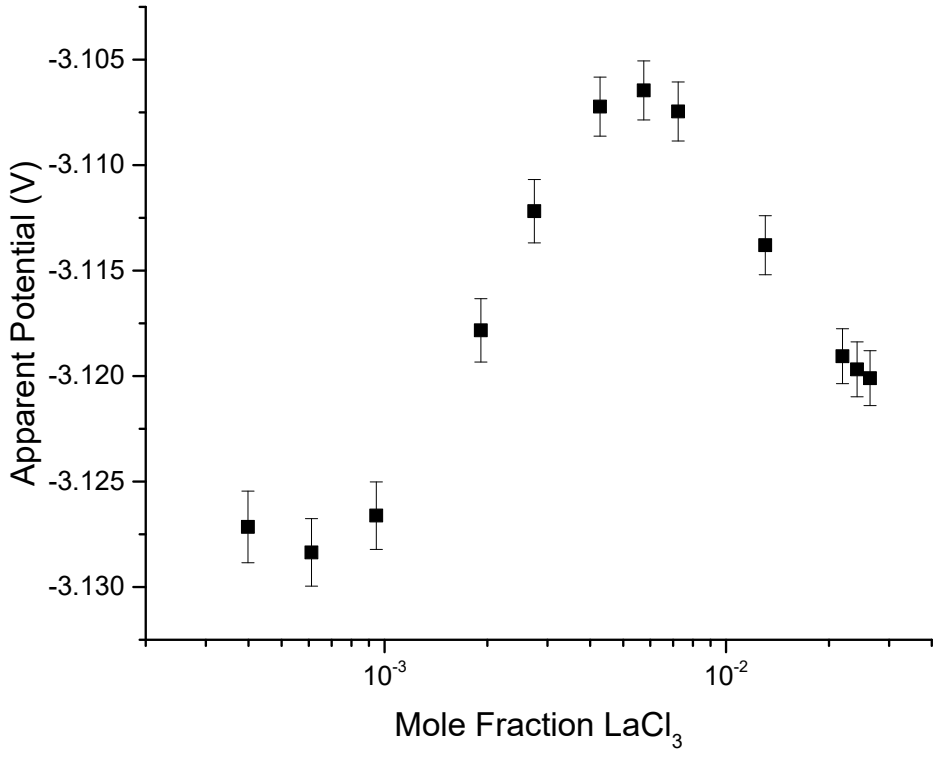

Figure 5.4. Apparent potential (vs. standard Cl^-/Cl_2 electrode) for $La/LaCl_3$ couple plotted as a function of $LaCl_3$ concentration at 773 K.

in this paper. However, a closer look at the experimental methods employed by each of these authors likely explains why that is the case. Shirai et al.[66] used cyclic voltammetry (CV) to determine the reduction potentials of the La(III)|La(0) couple. The use of CV's is not necessarily an optimal technique to determine equilibrium reduction potentials since the potentials measured during CV include overpotentials associated with nucleation and growth of the metal crystals on the cathode.[68,69] Kuznetsov et al.[67] performed their experiments in a mixture of LiCl-KCl-UCl_3-$LaCl_3$ mixture. In such a scenario, there are likely to be other effects at play between the two analytes present. Tang and Pesic[21] meanwhile used equilibrium measurements. The only difference was that they used a molybdenum working electrode. They deposited some La metal on to the working Mo electrode and measured the OCP. This allowed for a very short time to study the open circuit potentials.

The activity coefficient of $LaCl_3$ (γ_{LaCl_3}), can now be calculated for each concentration of lanthanum chloride for which the open circuit potential measurements were performed using Equation 5.4. The standard state used for such calculations was the *Pure Supercooled Liquid Standard State*, the calculations for which have been shown in the Table 5.2. Figure 5.5 shows a plot of activity coefficient as a function of $LaCl_3$ concentration. It is observed that the activity coefficient of $LaCl_3$ varies with concentration, initially increasing and subsequently decreasing, a function that is similar to the variation of apparent potential.

$$\boxed{\Delta G^{Excess} = \Delta G^{SC} - \Delta G^{0'} = RT \ln\left(\gamma_{M^{n+}}\right)} \tag{5.4}$$

Previously from reports in the literature, the value of γ_{LaCl_3} has been assumed to be independent of concentration, presumably based on an assumptions regarding pseudo ideal behavior of dilute solutions. Results reported here clearly show that the activity coefficient

Table 5.2. Calculated values of Gibbs free energy of pure supercooled $LaCl_3$.

Temperature	ΔH_{Fusion}	ΔS_{Fusion}	ΔG_{Fusion}	$\Delta G_{Formation}$	ΔG^{SC}
(Kelvin)	(kJ/mol)	(J/K-mol)	(kJ/mol)	(kJ/mol)	(kJ/mol)
773	41.813	34.507	15.139	-882.767	-867.628

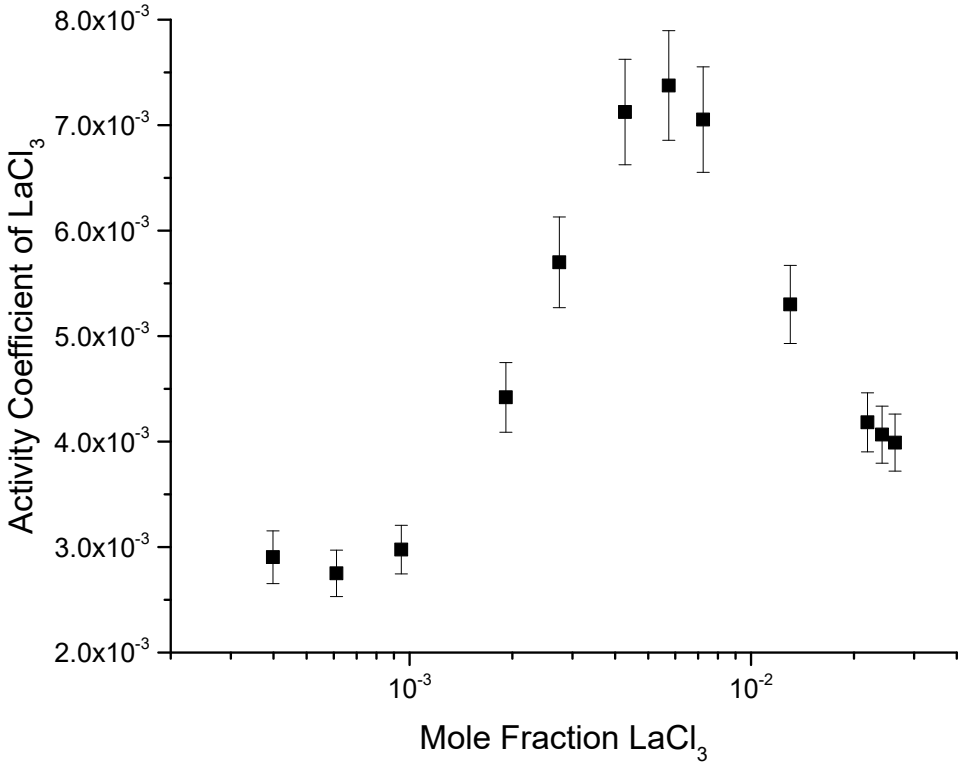

Figure 5.5. Activity coefficient (γ_{LaCl_3}) of $LaCl_3$ plotted as a function of $LaCl_3$ concentration at 773 K.

is a function of concentration of $LaCl_3$ even at low concentrations of $LaCl_3$. Previously various authors[21–24] have calculated the activity coefficients of $LaCl_3$ from experimental measurements. From the above studies, Tang and Pesic[21] used values of ΔG^{SC} that are different from the ones used in this paper. They used HSC Chemistry software to perform these calculations. They report values which are three orders of magnitude greater than the ones reported here. Masset et al.[23] reported the value of γ_{LaCl_3} as 0.0057 at a concentration of 20×10^{-5} mol/cm^3. That value is within the range of data reported here. Without knowledge of the density of the salt, it would be hard to convert that concentration to mole fraction accurately, for comparison. Castrillejo et al.[24] reported values at 723K and 823 K, not at 773 K as reported here. At 723 K, they reported a value of 0.0053 for the activity coefficient of $LaCl_3$.

5.3.1.2 Effect of Cesium Chloride

The behavior of lanthanum chloride in the presence of Group I element Cs was also studied since it is a major fission product that accumulates in electrorefiner salt. For this study, CsCl was added to the salt at two concentrations– 0.69 mol % (Standard Deviation: 0.04 mol %) and 1.40 mol % (Standard Deviation: 0.04 mol %). The same methodology for analysis as reported in the previous section including the fitting of OCP data to an interpolating function. The average difference between the experimentally measured values and modeled values was again found to be less than 2 mV. Figure 5.6 shows a plot of open circuit potentials for tests with three concentrations of CsCl; 0, 0.69 and 1.40 mol % CsCl as a function of $LaCl_3$ concentration. It can be observed that there is not much difference between the open circuit potentials for La/La(III) for the tests with the two lowest concentrations of CsCl i.e. 0 and 0.69 mol %. However, the equilibrium potentials for the La/La(III) couple show a notable positive shift in the presence of 1.40 mol % CsCl. This is only true at higher concentrations of $LaCl_3$. At low concentrations of $LaCl_3$, the equilibrium potentials for all of the three tests are fairly similar.

Figure 5.7 shows the plot of apparent potential ($E^{0'}$) as a function of $LaCl_3$ concentrations, for three distinct concentrations of 0, 0.69 and 1.40 mol % CsCl. From the figure, it can be observed that the nature of the graphs for all of the three tests is similar. All the three tests demonstrate that the apparent potential does indeed follow a pseudo Gaussian function, with a maximum at some concentration followed by a decline. Lower concentration (0.69 mol %) of Cs does not seem to have a substantial impact on the apparent potential. However the presence of 1.40 mol % Cs does seem to move the curve to the right and make the apparent potential of $LaCl_3$ more positive. An additional observation is that, both without any CsCl and with the presence of 0.69 mol % CsCl, the apparent potential for $LaCl_3$ reaches its most positive value at about 0.55 mol % $LaCl_3$.

Figure 5.8 shows the graph of activity coefficient of lanthanum chloride for the three concentrations of CsCl. It is observed that the activity coefficient of $LaCl_3$ increases in the presence of 1.40 mol % CsCl. The interaction of the lanthanum and cesium ions in the molten slat changes the activity coefficients of the ions. It is presumed that this is caused by the influence Cs ions have on the complexation and coordination chemistry of lanthanum ions dissolved in the molten salt.

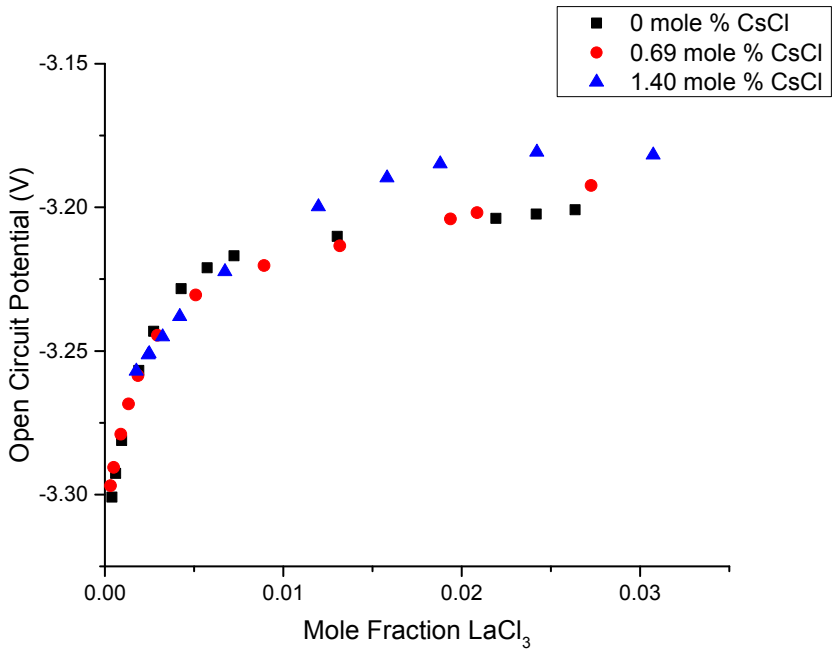

Figure 5.6. Open circuit potential (vs. standard Cl^-/Cl_2 electrode) for $La/LaCl_3$ couple plotted as a function of $LaCl_3$ concentration for three independent concentrations of CsCl; 0, 0.69 and 1.40 mol % CsCl at 773 K.

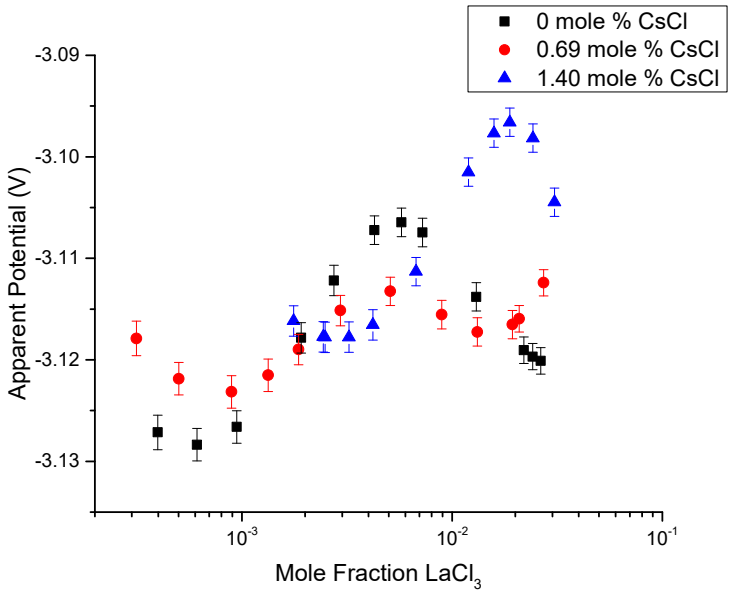

Figure 5.7. Apparent potentials (vs. standard Cl^-/Cl_2 electrode) for $La/LaCl_3$ couple plotted as a function of $LaCl_3$ concentration for three independent concentrations of CsCl; 0, 0.69 and 1.40 mol % CsCl at 773 K.

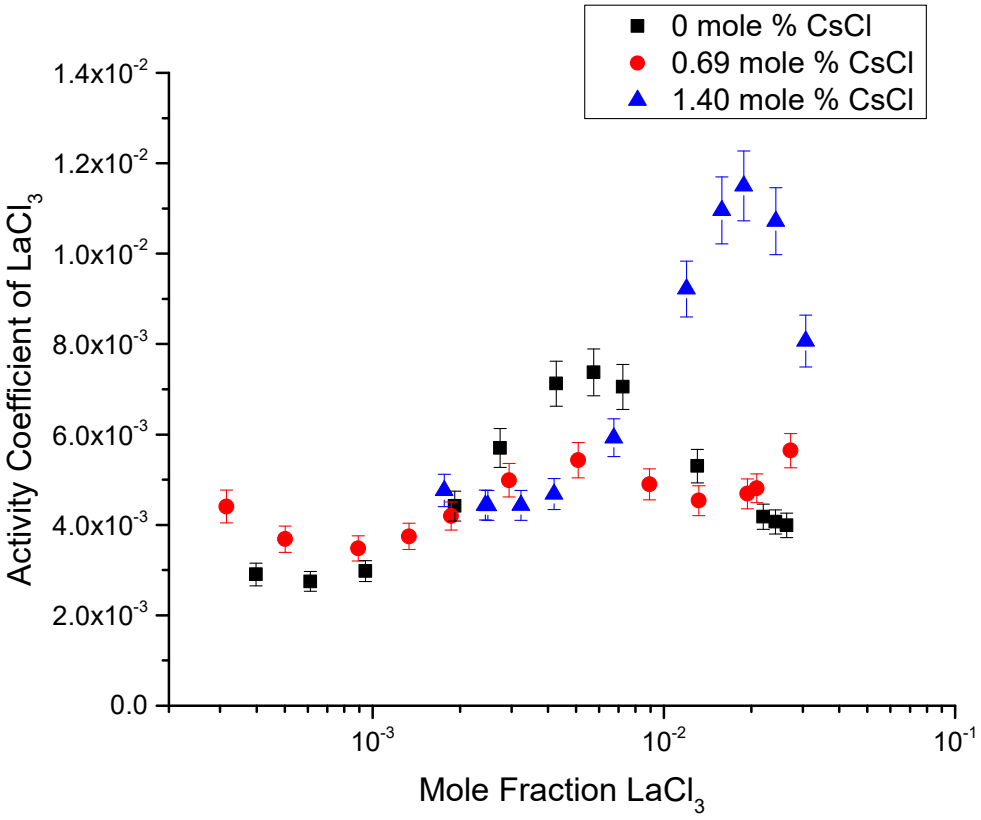

Figure 5.8. Activity coefficient of $LaCl_3$ (γ_{LaCl_3}) plotted as a function of $LaCl_3$ concentration for three independent concentrations of CsCl; 0, 0.69 and 1.40 mol % CsCl at 773 K.

It is important to consider if the effects of CsCl observed and reported here are statistically significant. For this purpose, the Student's t-test was employed. Analyzing the apparent potential data using the t-test indicates that with at least 95% confidence it can be concluded that the difference in the apparent potentials of the tests with 0 & 0.69 mol % CsCl are statistically insignificant. Further, the difference in the apparent potentials of the tests with 0.69 & 1.40 mol % CsCl is statistically significant (within a 95% confidence interval). A similar conclusion can be made about the activity coefficients of the three data sets where there is observed to be a statistical difference between the activity coefficients of the tests with 1.40 mol % CsCl and the other two tests.

5.3.1.3 Discussion

From the data presented above, it is evident that the activity coefficient of $LaCl_3$ dissolved in molten eutectic LiCl-KCl salt is dependent on the concentration of $LaCl_3$ dissolved in solution and not just a single value as previously reported. Recently Wang et al.[70] published a very detailed study looking into the activity coefficient and apparent potentials of $LaCl_3$ as a function of concentration of $LaCl_3$ using Molecular Dynamic Simulations (MDS). The results presented here differ only meaningfully from the ones presented by Wang et al.[70] at the higher concentrations of $LaCl_3$ wherein a decline in both the apparent potential and activity coefficient are reported here wheres they report a linear dependence throughout the concentration range of up to 3 mol % $LaCl_3$. Additionally, there is extensive documentation of such concentration dependence of activity coefficient within the more vigorously researched field of aqueous chemistry which necessitated the need to develop sophisticated models like the ones developed by Kenneth Pitzer.[71–75]

The concentration dependence of activity coefficients is most likely dependent on the local complexation structure of $LaCl_3$ in the molten eutectic electrolyte. Quite a few studies using various experimental techniques like Raman Spectroscopy,[76,77] neutron diffraction,[78–81] and x-ray diffraction[82–84] have demonstrated that for $LaCl_3$, there exist a multitude of complexes that can be formed by $LaCl_3$ with lanthanum ions capable of having variable coordination numbers. In 2010, Okamoto et al.[85] conducted XAFS tests and MDS studies of a LiCl-KCl-$LaCl_3$ molten salt mixture. They studied mixtures containing from 1 to 100 mol % $LaCl_3$. They demonstrated that the coordination number and interionic distance increase with increasing concentration of $LaCl_3$. This and other data available in that paper clearly demonstrate that the coordination chemistry of the dissolved La species is dependent on the concentration of the total La present in the mixture. This concentration dependence of complexation reactions of $LaCl_3$ and ability of $LaCl_3$ to have a multitude of coordination numbers likely explain the observed trends for apparent potentials and activity coefficients reported here.

A graph of OCP vs. $\mathrm{Ln}(X_{LaCl_3})$ for the three main tests reported here is shown in Figure 5.9. As expected, a linear relationship is observed between the two plotted quantities. The slope of the line is equal to RT/nF. Equating the slope to the expected value of RT/nF and calculating 'n', the following values are obtained; n = 2.70, 2.80 and 2.21 for tests with

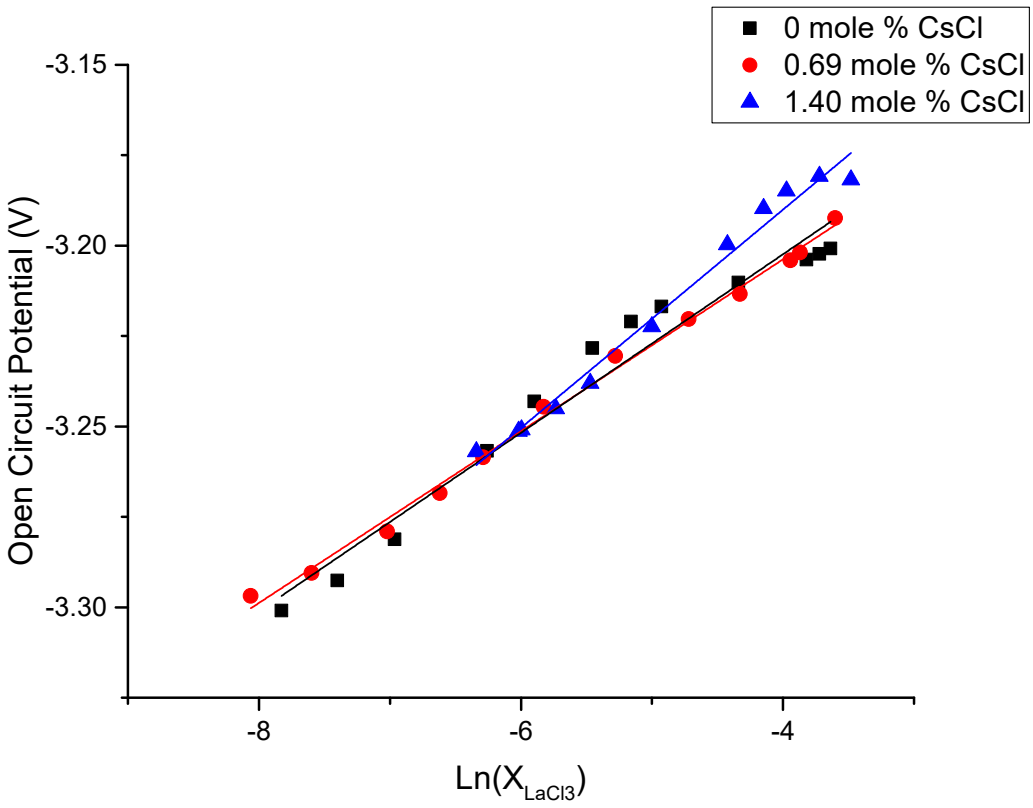

Figure 5.9. Open circuit potential (vs. standard Cl^{-}/Cl_2 electrode) plotted as a function of $Ln(X_{LaCl_3})$ for three independent concentrations of CsCl; 0, 0.69 and 1.40 mol % CsCl at 773 K respectively.

0, 0.69 and 1.40 mol % CsCl respectively. Now for the first two cases, the value of n = 2.70 and n = 2.80 is relatively close to the expected value of the expected value of n = 3. In the presence of 1.40 mol % CsCl, the value of n = 2.21 is significantly lower than the value expected. This perceived trend broadly reflects the trends observed in the measured properties. Properties of $LaCl_3$, tests with 0 and 0.69 mol % CsCl are fairly similar. However the case with 1.40 mol % CsCl shows much lower value of n, which implies that n = 2. This evidence indicates that the presence of higher concentrations of CsCl does indeed seem to affect the local coordination structure of $LaCl_3$.

The effect of CsCl on the coordination chemistry of $LaCl_3$ is much harder to determine theoretically based on previously published open literature. While there has been no study to date of the LiCl-KCl-CsCl-$LaCl_3$ systems. There is some evidence in the literature that

alkali metals play a role in altering the local coordination structure in molten salts with an increased efficiency going from Li to Cs.[86] These perturbations in the local coordination chemistry of molten salt most likely translate into the effects of CsCl reported in this paper.

In molten salt systems, for $LaCl_3$, an initial increase in the activity coefficient in the species can be attributed to the increase in the concentration of the lanthanum. It is likely that at these low concentrations, the concentration of lanthanum is not high enough to engender the formation of higher order complexes as the coordination number of lanthanum is very low. The reduction in the activity coefficient can certainly be attributed to the formation of higher order complexes as reported in literature. It is known from thermodynamic literature for both aqueous and molten salt chemistry, the existence of *interaction parameters* that heavily influence the activity coefficients. The presence of other lanthanum ions and Cs ions most certainly influence the coordination chemistry of $LaCl_3$, manifesting itself as a systematic variation in the activity coefficients and apparent potentials.

5.3.2 Activity of $GdCl_3$

5.3.2.1 Effect of $GdCl_3$ Concentration

The first test performed was to measure the activity and activity coefficient of gadolinium chloride as a function of total gadolinium chloride concentration present in the salt. Figure 5.10 shows the measured open circuit potential (OCP_{LSS}) as a function of $GdCl_3$ concentration. OCP_{LSS} represents the measured open circuit potential corrected for the Gibbs free energy of fusion ($\Delta G_{Fusion}/nF$) for gadolinium chloride (at 773 K) to convert the measurement from a solid standard state to a liquid standard state as required in Equation 3.57. OCP_{LSS} can be defined as shown in Equation 5.5. For the purposes of calculating ($\Delta G_{Fusion}/nF$), the value of n is assumed to be equal to 3. This value of ΔG_{Fusion} was calculated to be 4.532 kJ/mol for gadolinium chloride at 773 K. The Barin[54] data source was used for these calculations. In electrochemistry, potentials are generally reported on a chosen scale versus an established reference electrode. The open circuit potential measurements made experimentally are versus a $Gd/GdCl_{3(s)}$ reference electrode. These potentials were converted to liquid standard state potentials. Thus the values of OCP_{LSS} reported versus a $Gd/GdCl_{3(l)}$ reference electrode.

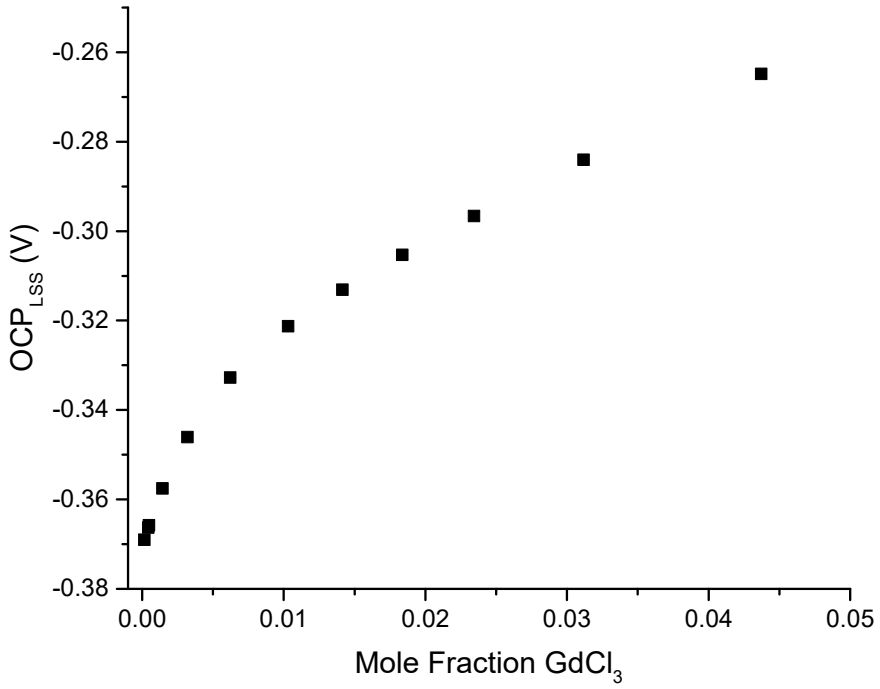

Figure 5.10. Open circuit potential (OCP_{LSS}) (vs. $Gd/GdCl_{3(l)}$) for the $Gd/GdCl_3$ system in LiCl-KCl eutectic salt plotted as a function of mole fraction of $GdCl_3$ at 773 K.

$$OCP_{LSS} = E_{Cell} - \frac{\Delta G_{Fusion}}{nF} \tag{5.5}$$

The measured OCP_{LSS} was fitted to a best fit function using Matlab of the form $y = ae^{bx} + ce^{dx}$. The coefficient of fit was greater than 0.99. This is important since according to Equation 3.57, activity coefficient and the open circuit potential have an exponential relationship. Even a small error in the measurement of the open circuit potential gets magnified when determining the activity coefficient. The average difference between the measured values and the modeled values was 1.6 mV. Such small errors are well within the realm of errors associated with experimental measurements. For all of the subsequent calculations, the values of open circuit potential obtained from the best fit function were used as opposed to the actual measured values. This allows for the noise in the data to be eliminated.

From Figure 5.10 it can be observed that as the concentration of $GdCl_3$ increases, the

potential becomes more positive. From the OCP_{LSS} values, the activity of $GdCl_3$ in molten LiCl-KCl eutectic salt can be determined easily according to Equation 3.57, where OCP_{LSS} is equal to $(E_{Cell} - \Delta G_{Fusion}/nF)$. The activity of $GdCl_3$ versus both a solid standard state and liquid standard state has been shown in Figure 5.11. As expected, the $GdCl_3$ activity increases with increasing mole fraction in LiCl-KCl eutectic salt. Note that the slope also increases with increasing mole fraction of $GdCl_3$.

From the activity and knowing the mole fraction of $GdCl_3$, the activity coefficient of the gadolinium chloride, γ_{GdCl_3}, was determined and has been shown in Figure 5.12 versus both a solid standard state and liquid standard state. It can be observed from Figure 5.12 that the activity coefficient initially decreases with concentration, remaining unchanged for some concentration range and subsequently increases starting at about 2 mol % $GdCl_3$.

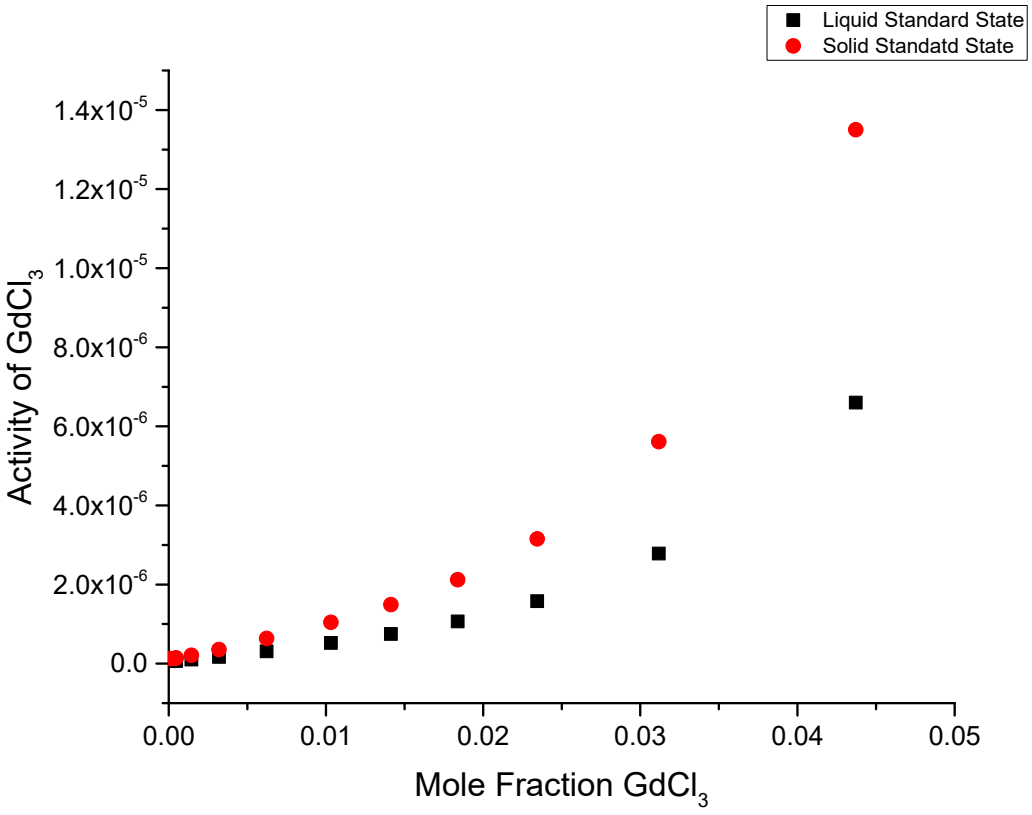

Figure 5.11. Activity of $GdCl_3$ in LiCl-KCl eutectic salt plotted as a function of mole fraction of $GdCl_3$ at 773 K, versus both a solid standard state and liquid standard state.

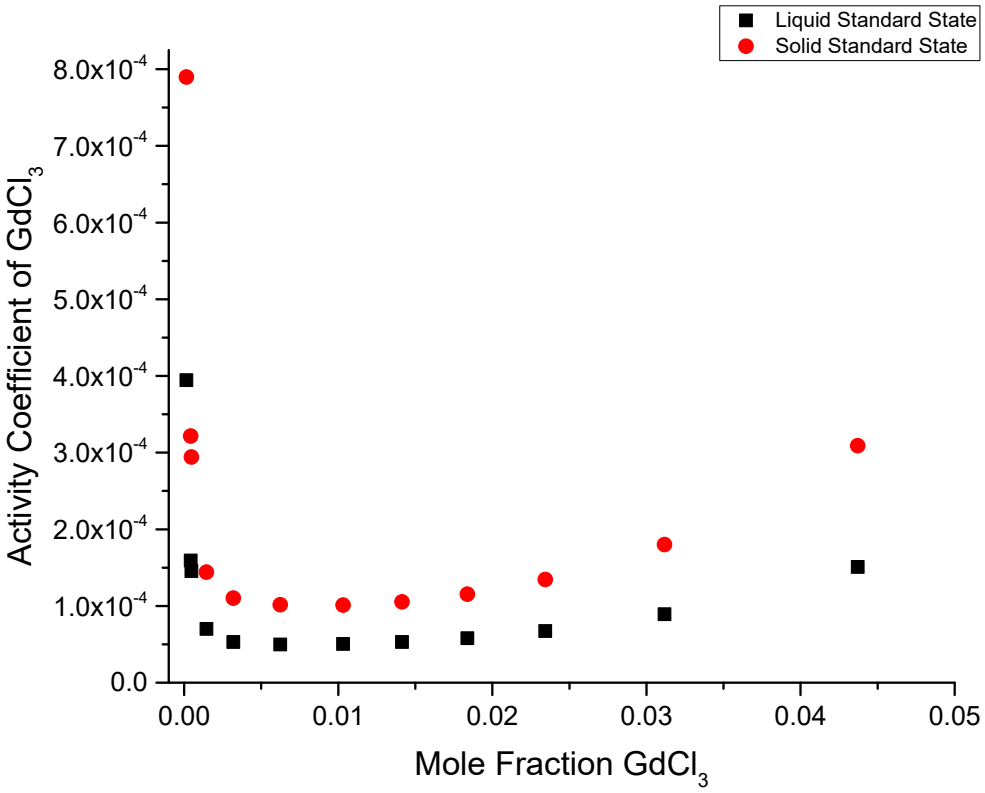

Figure 5.12. Activity coefficient of $GdCl_3$ in LiCl-KCl eutectic salt plotted as a function of mole fraction of $GdCl_3$ at 773 K, versus both a solid standard state and liquid standard state.

From Figures 5.11 and 5.12, it can be seen that there is a distinct difference between the liquid standard state and solid standard state values of activity and activity coefficients of $GdCl_3$. This is despite the fact that the value of ΔG_{Fusion} value of gadolinium chloride was calculated to be a modest 4.532 kJ/mol. For some rare earths and actinides that have a melting temperature much higher than the operating temperature of 773 K, the value of ΔG_{Fusion} is likely to be much larger. This would lead to much larger disagreements between the solid standard state and liquid standard state values of activity and activity coefficients, making such corrections very necessary. The ΔG_{Fusion} values at 773 K for some other salts of interest were calculated to be as follows: $CeCl_3$: 13.478 kJ/mol, $LaCl_3$: 15.093 kJ/mol, $NdCl_3$: 11.950 kJ/mol, $PrCl_3$: 13.567 kJ/mol, $PuCl_3$: 15.499 kJ/mol, and UCl_3: 13.482 kJ/mol. As can be observed for all these salts, the value of ΔG_{Fusion} is much larger

than that of $GdCl_3$. This means that the difference between the solid standard state and liquid standard state values of the activities and activity coefficients will be much larger, underscoring the importance of converting from solid standard state to liquid standard state when using an analyte reference electrode as proposed in this paper for determination of activity and activity coefficients in molten salt systems.

In the literature, there are reports of studying the activity coefficient of $GdCl_3$.[22,25,26] It is important to note that all of these authors used different electrochemical cell set-up from the one presented here for their experimental measurements. Tang and Pesic[25] and Caravaca et al.[26] both used Ag/AgCl reference electrode for their measurements experimental measurements. Lantelme and Berghoute[22] used a Cl^-/Cl_2 reference electrode for their measurements. Hence the data must be compared with caution. A comparison of the activity coefficient data for this work and existing literature is given in Table 5.3.

Lantelme and Berghoute[22] studied the thermodynamic behavior of $GdCl_3$ for up to 1.44 mol % $GdCl_3$ for a series of temperatures. They modeled the activity coefficient as a second-order polynomial function of mole fraction of $GdCl_3$. If the activity coefficient is computed based on the model presented for 750 K, an activity coefficient value of 1.04 for 0.16 mol % $GdCl_3$ going up to 1.54 for 1.44 mol % $GdCl_3$. In a similar concentration range of 0.14 to 1.41 % $GdCl_3$ the activity coefficient reported here is almost unchanged with an average

Table 5.3. Activity coefficient of $GdCl_3$ in LiCl-KCl eutectic salt reported in the literature

Reference	T (K)	[$GdCl_3$]	γ_{GdCl_3}	γ_{GdCl_3} This Work
Tang and Pesic[25]	773	2.0 wt. %	1.749 x 10^{-4}	5.312 x 10^{-5}[a]
Caravaca et al.[26]	771	0.166 mol %	4.60 x 10^{-3}	6.99 x 10^{-5}[b]
Caravaca et al.[26]	771	0.166 mol %	1.50 x 10^{-4}	6.99 x 10^{-5}[b]
Lantelme and Berghoute[22]	750	0.16 to 1.44 mol %	1.04 to 1.54	5.52 x 10^{-5}[c]

[a] 1.49 wt. % $GdCl_3$ at 773 K
[b] 0.14 mol % $GdCl_3$ at 773 K
[c] Average value in a concentration range of 0.14 to 1.41 mol % $GdCl_3$ at 773 K

activity coefficient of 5.52 x 10^{-5} for $GdCl_3$. It is evident that Lantelme and Berghoute[22] used a different definition for standard state from the one used in this work. In the work by Lantelme and Berghoute[22] unit activity was assumed at infinite dilution and one in which the equilibrium potential is equal to the standard potential for infinite dilution.

Tang and Pesic[25] studied the activity coefficient of $GdCl_3$ at a concentration of 2.0 wt. % $GdCl_3$ and reported a $\log \gamma_{GdCl_3}$ value of -3.757 at 773 K. This value represents an activity coefficient value of 1.749 x 10^{-4}. At the closest comparable concentration of 1.49 wt. % $GdCl_3$ at 773 K, an activity coefficient value of 5.312 x 10^{-5} is reported in this work. Caravaca et al.[26] reported the activity coefficient of $GdCl_3$ at a single concentration of 1.66 x 10^{-3} mole fraction at 773 K. They reported two values of the activity coefficient; 4.60 x 10^{-3} and 1.50 x 10^{-4}. The reason for the two significantly different values reported by Caravaca et al.[26] was the use of two different standard states by them for their calculations. The two standard states were the pure compound in supercooled state and pure compound in liquid state.[26] At the closest comparable concentration of 0.14 mol % $GdCl_3$, an activity coefficient value of 6.99 x 10^{-5} for $GdCl_3$ at 773 in LiCl-KCl eutectic salt is reported for this work. The second value of 1.50 x 10^{-4} is within the concentration range reported in this work.

However the uncertainty manifest in the choice of the appropriate standard state serves to underscore the advantages of the use of an analyte reference electrode. When using a saturated analyte reference electrode, a standard state ($GdCl_{3(s)}$) is incorporated into the experimental set-up and measurements. From thence, the only change needed is from a solid standard state to liquid standard state for a more adequate physical interpretation of the activity coefficient. There is no ambiguity about the standard state for such measurements.

5.3.2.2 Effect of CsCl Concentration

The effect of the presence of CsCl on the activity coefficient of $GdCl_3$ was also investigated. For this, two distinct tests were performed. For the first test, a melt of LiCl-KCl-CsCl was prepared with 0.70 mol % CsCl present. A saturated Gd/$GdCl_3$-LiCl-KCl reference electrode was used. In this test, $GdCl_3$ was progressively added as the open circuit potential was measured while the CsCl concentration was held constant at 0.70 mol % . The open circuit potential results for the tests with 0 and 0.70 mol % CsCl are given in Figure 5.13. It

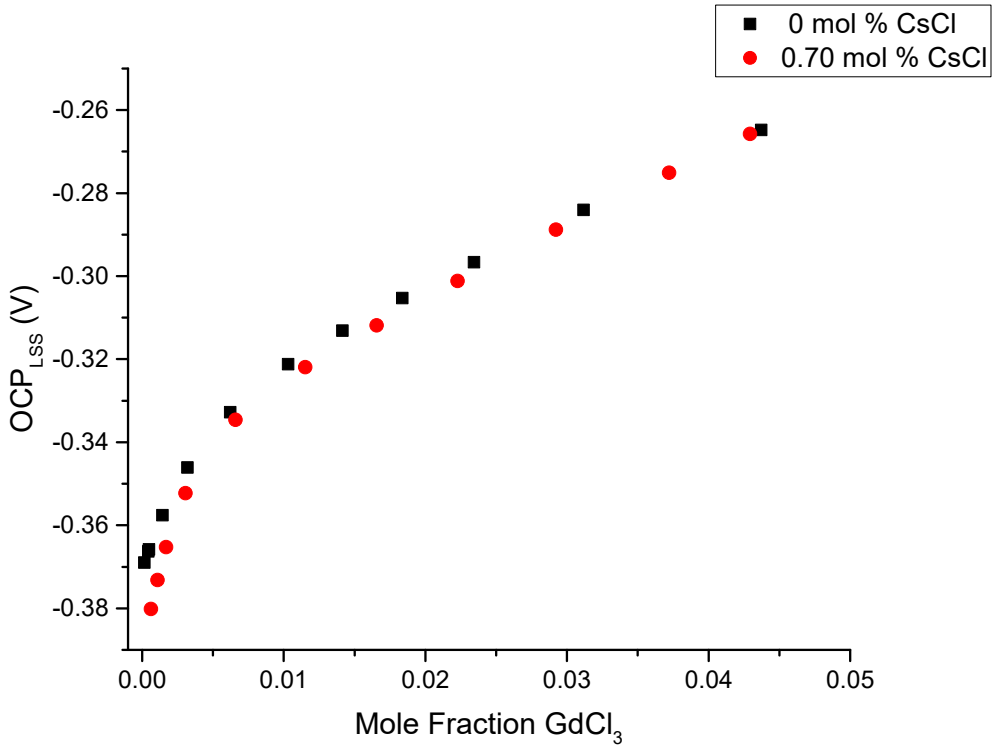

Figure 5.13. Open circuit potential (OCP_{LSS}) (vs. $Gd/GdCl_{3(l)}$) for the $Gd/GdCl_3$ system in LiCl-KCl eutectic salt plotted as a function of mole fraction of $GdCl_3$ for two concentrations of CsCl; 0 and 0.70 mol % CsCl at 773 K.

can be observed that the potentials for the two sets of data are very similar. Using Student's t-test, it was concluded with at least 95 % confidence that the two sets of data are statistically identical. If this were the only data available on the effect of CsCl, it would be concluded that it does not affect the thermodynamic properties of $GdCl_3$ in LiCl-KCl eutectic salt.

In a second set of tests, to examine the influence of CsCl on the activity coefficient of $GdCl_3$, the concentration of $GdCl_3$ was kept constant at 4.29 mol % $GdCl_3$ and the additional cesium chloride was introduced into the molten salt mixture. Then open circuit potential measurements were performed. From these open circuit potential measurements, the value of OCP_{LSS} was determined and is shown in Figure 5.14. It can be observed from Figure 5.14 that the value of OCP_{LSS} becomes more negative as a function of increasing cesium chloride concentration for a fixed $GdCl_3$ concentration. The activity of gadolinium chloride can also be calculated as previously discussed from the OCP_{LSS} values according

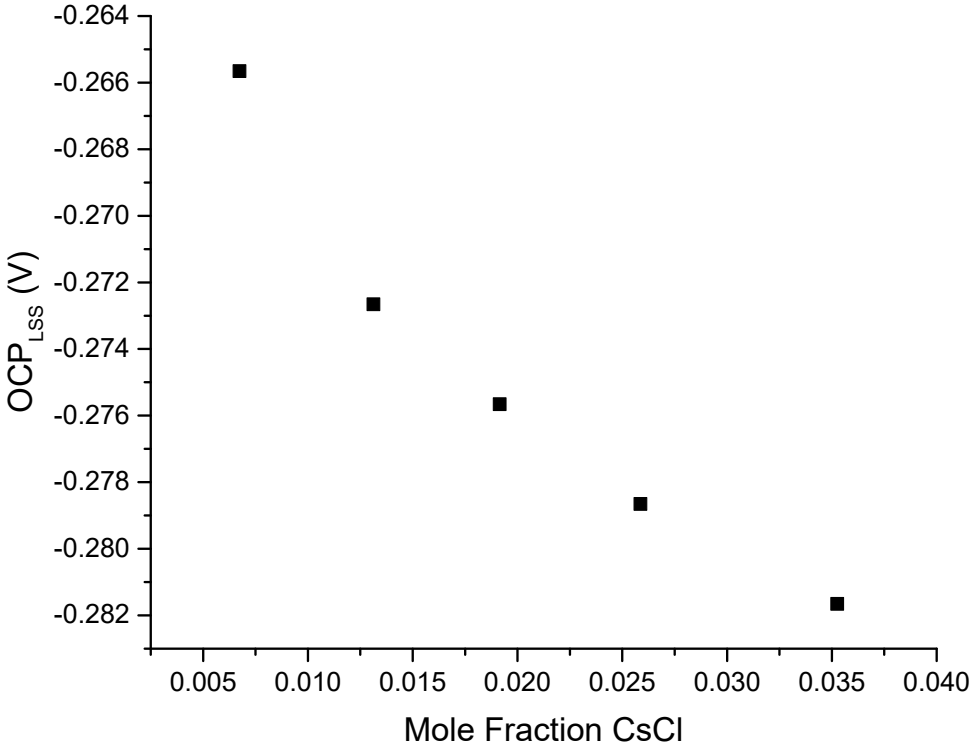

Figure 5.14. Open circuit potential (OCP_{LSS}) (vs. Gd/$GdCl_{3(l)}$) for the Gd/$GdCl_3$ system in LiCl-KCl eutectic salt plotted as a function of mole fraction of CsCl (X_{CsCl}) for a fixed $GdCl_3$ concentration of 4.29 mol % at 773 K.

to Equation 3.57. The results of these calculations have been shown in Figure 5.15. Figure 5.15 shows the activity of $GdCl_3$ as a function of increasing CsCl concentration for a fixed $GdCl_3$ concentration of 4.29 mol % $GdCl_3$. It can be observed from Figure 5.15 that the activity of $GdCl_3$ decreases with increasing CsCl concentration. Further the activity coefficient of $GdCl_3$ also shows a similar relationship to concentration of CsCl as shown in Figure 5.15. From the data presented above, it can be concluded that there is a definite inverse relationship between the amount of CsCl present and the activity coefficient of gadolinium chloride. This demonstrates that the presence of cesium chloride does indeed influence the activity of $GdCl_3$.

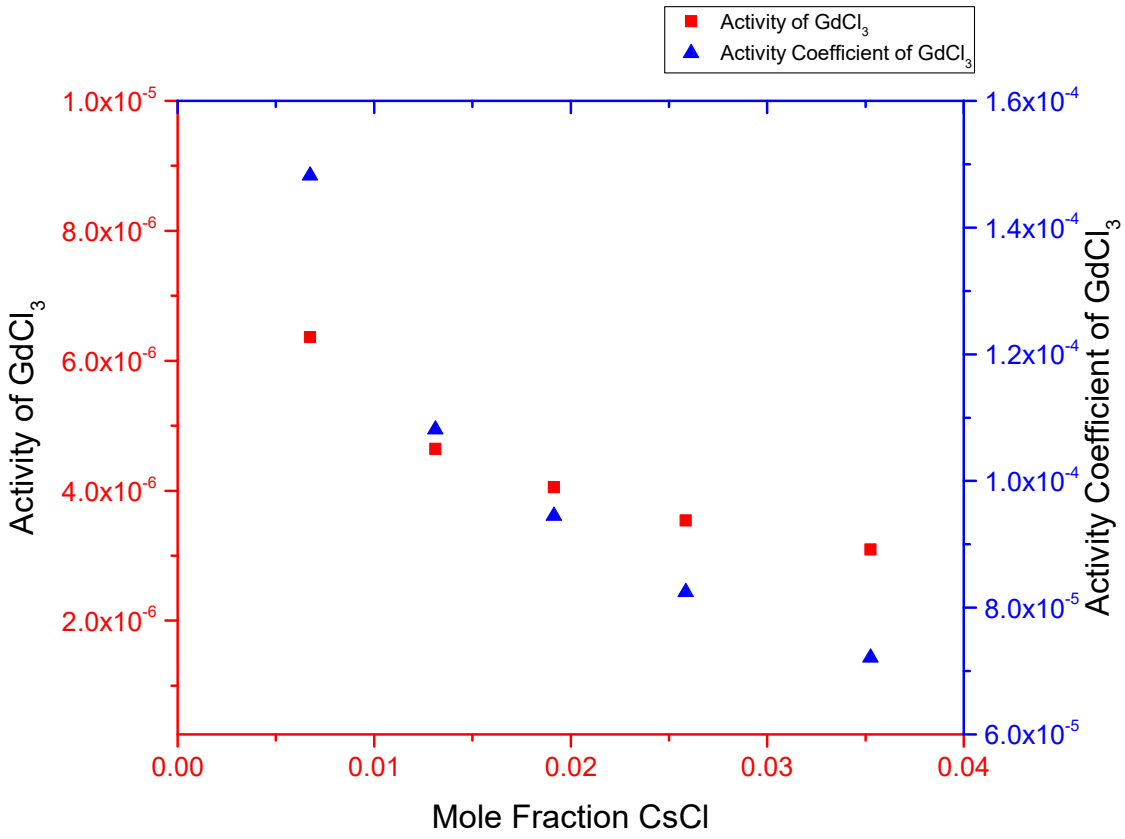

Figure 5.15. Activity of $GdCl_3$ in LiCl-KCl eutectic salt plotted as a function of mole fraction of CsCl (X_{CsCl}) for a fixed $GdCl_3$ concentration of 4.29 mol % at 773 K. On the second Y-axis, the activity coefficient of $GdCl_3$ also as a function of CsCl concentration for a fixed $GdCl_3$ concentration of 4.29 mol % at 773 K.

5.3.2.3 Calculation of Apparent Potentials

$ApparentPotentials$ ($E^{0'}$) also called $FormalPotentials$[87] can be calculated from the experimental data presented in this study. It is important to emphasize that these apparent potential values are calculated and not experimentally measured values. Apparent Potentials are defined as shown in Equation 5.6.[87]

$$E^{0'} = E^0 + \frac{RT}{nF} \ln\left(\gamma_{GdCl_3}\right) \tag{5.6}$$

According to Equation 5.6, for calculation of apparent potential values, the value of the standard reduction potential, E^0 and activity coefficients should be known quantities.

Strictly speaking, E^0 would be the equilibrium potential when pure liquid salt ($GdCl_3$) is in equilibrium with pure metal (Gd) at the temperature of interest (773 K). As previously mentioned, pure $GdCl_3$ melts at 875 K.[54] Hence it is not possible to make such measurements experimentally. The value of E^0 can also be calculated theoretically for such cases and has been discussed extensively in previous work.[57,58] Calculations for $GdCl_3$ yield a standard potential value of -2.806 V (vs. standard Cl^-/Cl_2 electrode) at 773 K.[57] Using this E^0 value and activity coefficient data presented above, the apparent potential ($E^{0'}$) for gadolinium reduction was calculated and is shown in Figure 5.16 as a function of $GdCl_3$ concentration. It can be observed from Figure 5.16 that the value of ($E^{0'}$) decreases and subsequently increases as the concentration of $GdCl_3$ increases in the molten salt within a 55 mV window. Since the value of the standard potential, E^0, is calculated versus a standard Cl^-/Cl_2 reference electrode, the value of the apparent potential, $E^{0'}$, is also reported versus a standard Cl^-/Cl_2 reference electrode and not a $Gd/GdCl_{3(l)}$ reference electrode.

In the literature, three important works have experimentally determined the apparent potentials for $GdCl_3$ in molten salt systems and have been summarized in Table 5.4. All three of these studies used a Ag/AgCl reference electrode. Tang and Pesic[25] reported the experimental measurement of apparent potential for the $Gd/GdCl_3$ for a concentration of 0.00422 mole fraction (0.42 mol %). At 773 K, they reported a value of -3.008 V (vs. standard Cl^-/Cl_2 electrode). At 0.32 mol % $GdCl_3$ at 773 K, a value of -3.023 V (vs. standard Cl^-/Cl_2 electrode) is reported here, a difference of 15 mV.

Lantelme and Berghoute[22] at 750 K for a concentration range of 0.2 to 1.4 mol % $GdCl_3$ reported an apparent potential within the range -3.015 V to -3.010 V (vs. standard Cl^-/Cl_2 electrode). In that concentration range, an apparent potential range of -3.025 to -3.020 V (vs. standard Cl^-/Cl_2 electrode) is reported in this work. Again the values reported by them and the ones reported here are extremely close. Caravaca et al.[26] experimentally measured the apparent potential at 0.166 mol % $GdCl_3$ at 723 K. They reported an apparent potential value of -3.0397 V (vs. standard Cl^-/Cl_2 electrode). For a similar concentration of 0.14 mol % at 773 K, an apparent potential of -3.016 V (vs. standard Cl^-/Cl_2 electrode) is reported here. That equates to a difference of 23 mV between the two values, though much of it may probably be attributed to the 50 K temperature difference between the measurements since it is known that apparent potentials become more positive with higher temperatures as the

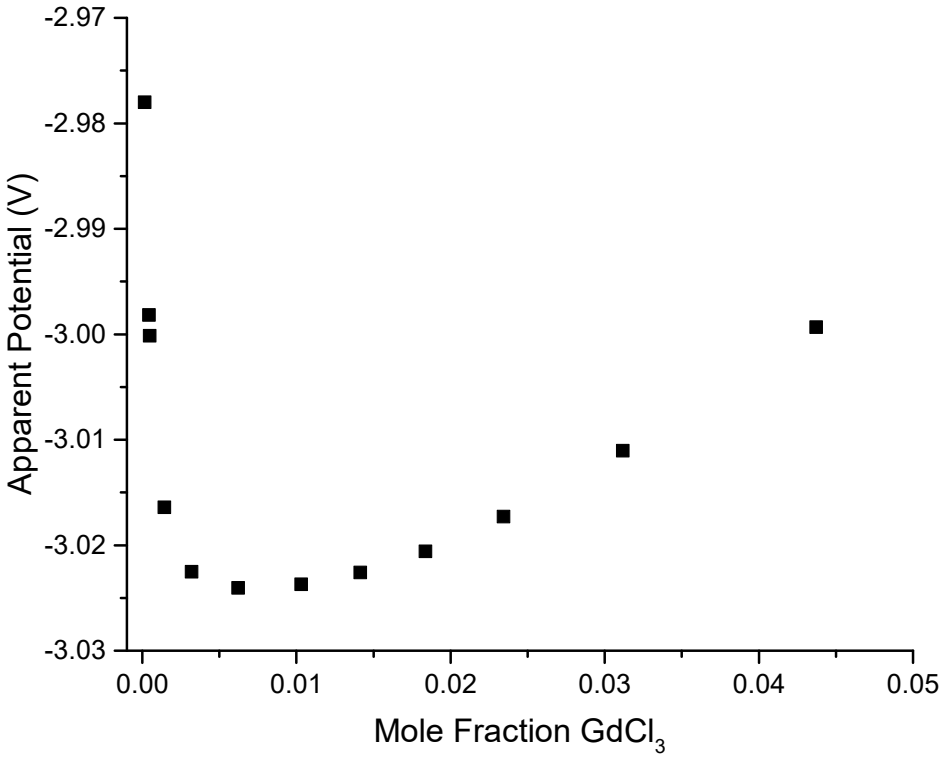

Figure 5.16. Apparent potential ($E^{0'}$) (vs. standard Cl^-/Cl_2 electrode) of $GdCl_3$ plotted as a function of mole fraction of $GdCl_3$ in a LiCl-KCl eutectic salt system at 773 K.

relationship developed by Zhang[65] demonstrates.

5.3.2.4 Discussion

At this point, it is appropriate to indulge in a discussion to deduce the physical interpretation of the activity coefficients of $GdCl_3$ and what this behavior implies in terms of the intermolecular forces present and acting on the molecules. If the natural log of the activity coefficient of $GdCl_3$ ($\ln \gamma_{GdCl_3}$) is plotted as a function of mole fraction of $GdCl_3$ (X_{GdCl_3}), as is shown in Figure 5.17, it is observed that $\ln \gamma_{GdCl_3}$ approaches zero as a linear function, i.e., the slope of the line at low concentrations approaches $-\infty$ as X_{GdCl_3} approaches zero. Robinson and Stokes[47] represented this as the mathematical relationship shown in Equation 5.7 for electrolyte solutions.

Table 5.4. Apparent potential of $GdCl_3$ in LiCl-KCl eutectic salt reported in the literature compared to the data reported in this work.

Reference	T (K)	[$GdCl_3$] (mol %)	$E^{0'}$ (V vs. Cl^-/Cl_2)	$E^{0'}$ This Work (V vs. Cl^-/Cl_2)
Tang and Pesic[25]	773	0.42	-3.008 V	-3.023 V[1]
Lantelme and Berghoute[22]	750	0.2 to 1.4	-3.015 V to -3.010 V	-3.025 to -3.020 V[2]
Caravaca et al.[26]	723	0.166	-3.0397 V	-3.016[3]

[1] 0.32 mol % $GdCl_3$ at 773 K
[2] 0.2 to 1.4 mol % $GdCl_3$ at 773 K
[3] 0.14 mol % $GdCl_3$ at 773 K

As $X_{GdCl_3} \rightarrow 0$:

$$\frac{\partial \ln X_{GdCl_3}}{\partial X_{GdCl_3}} \rightarrow -\infty \tag{5.7}$$

Equation 5.7 implies that as $X_{GdCl_3} \rightarrow 0$, the slope of the line on a $\ln X_{GdCl_3}$ vs. X_{GdCl_3} graph has a slope of $-\infty$ which is a result of dominant long range forces. This is exactly what is observed in Figure 5.17. Guggenheim[44] noted that for electrolyte solutions, if Equation 5.7 holds true, statistical theory required that long range forces between the solute particles (in this case $GdCl_3$) must be operative. These interactions include long range electrostatic attractions and repulsions in addition to short range Van der Waals forces and ion-dipole interactions.[47] Since Equation 5.7 holds for the LiCl-KCl-$GdCl_3$ system, Guggenheim[44] hypothesis must also hold true. Robinson and Stokes[47] noted that at higher concentrations in such systems, the curves may flatten out and then rise generally linearly or may even continue to fall in some cases. They note that in this region, the effects of short term interactions become important and dominate the solution behavior. This a readily applicable for the data reported here as demonstrated by Figure 5.17. This helps us better understand the intermolecular nature of the interactions present in the molten salt systems.

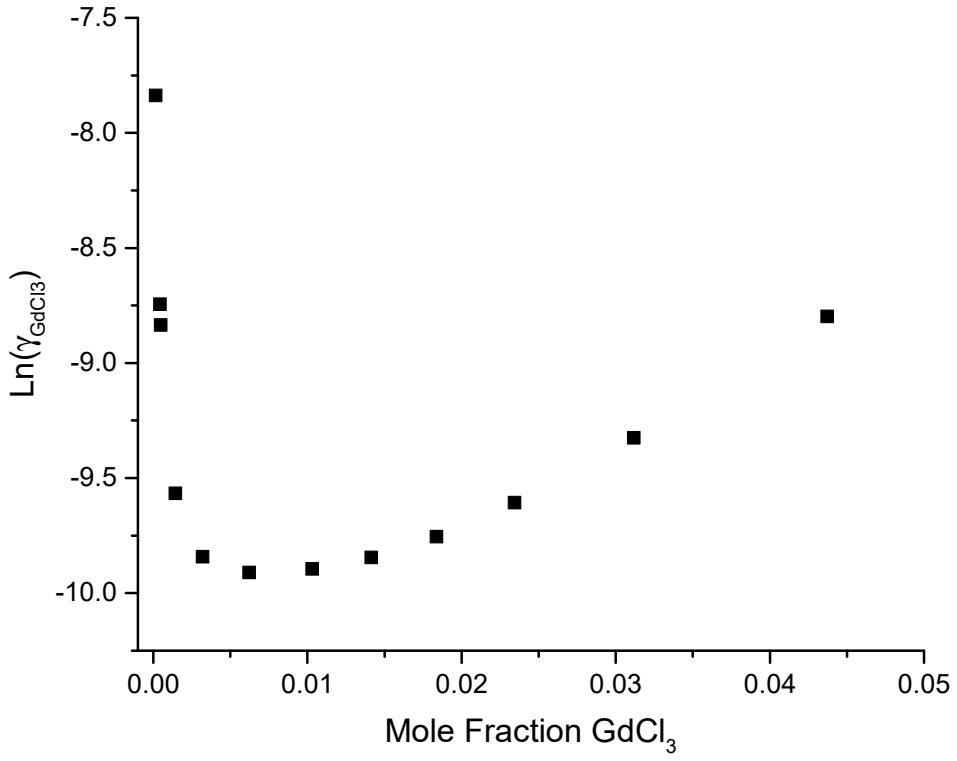

Figure 5.17. Natural log of activity coefficient of $GdCl_3$ ($\ln \gamma_{GdCl_3}$) plotted as a function of mole fraction of $GdCl_3$ in a LiCl-KCl eutectic salt system at 773 K.

5.3.3 Activity of $CeCl_3$

The first test examined the activity coefficient of $CeCl_3$ as a function of $CeCl_3$ concentration. Based on the theory presented earlier, the ΔG_{Fusion} of cerium chloride at 773 K was calculated to be 13.478 kJ/mol. After the open circuit measurement was made, the measurement was converted from the solid standard state to liquid standard state using ΔG_{Fusion} value according to Equation 3.57. This corrected open circuit potential (OCP_{LSS}) was plotted as a function of $CeCl_3$ concentration and shown in Figure 5.18. It can be observed that the open circuit potential shows a logarithmic relationship as has been observed previously. From this OCP_{LSS} value, the activity of $CeCl_3$ can be calculated. The activity of $CeCl_3$ has been shown in Figure 5.19. Again it is clearly visible from Figure 5.19 that the activity deviates significantly from ideal solution behavior.

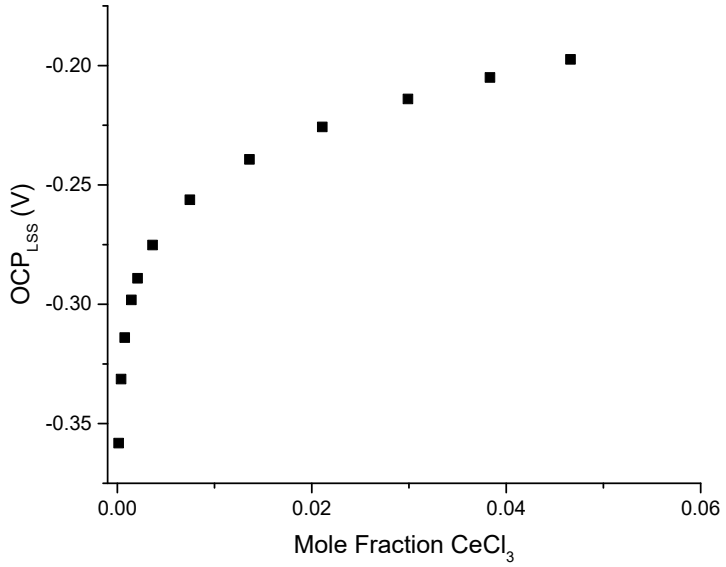

Figure 5.18. Open circuit potential (OCP_{LSS}) (vs. Ce/$CeCl_{3(l)}$) for the Ce/$CeCl_3$ system in LiCl-KCl eutectic salt plotted as a function of mole fraction of $CeCl_3$ at 773 K.

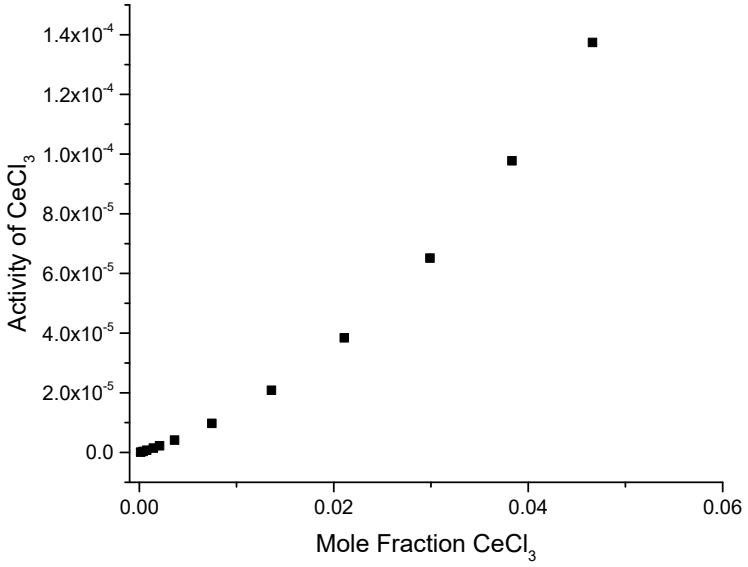

Figure 5.19. Activity of $CeCl_3$ in LiCl-KCl eutectic salt plotted as a function of mole fraction of $CeCl_3$ at 773 K.

Finally from the activity, it is possible to calculate the activity coefficient of $CeCl_3$ as previously discussed. Figure 5.20 shows the activity coefficient of $CeCl_3$ as a function of mole fraction of $CeCl_3$. From Figure 5.20, it can be observed that the nature of the activity coefficient is quite different from the previously reported rare earths. The activity coefficient linearly increases with concentration of $CeCl_3$ for most of the concentration range tested.

As was discussed in the Introduction (Chapter 1), the activity coefficient of cerium chloride has been reported by Marsden and Pesic,[27] Castrillejo et al.,[24] and Zhang et al.[28] Their findings have been previously discussed in Section 1.6.1.3 and have been summarized in Table 5.5. It can be observed from Table 5.5 that the previously recorded activity coefficients are in the 10^{-3} order of magnitude. A similar activity coefficient window is reported in this work.

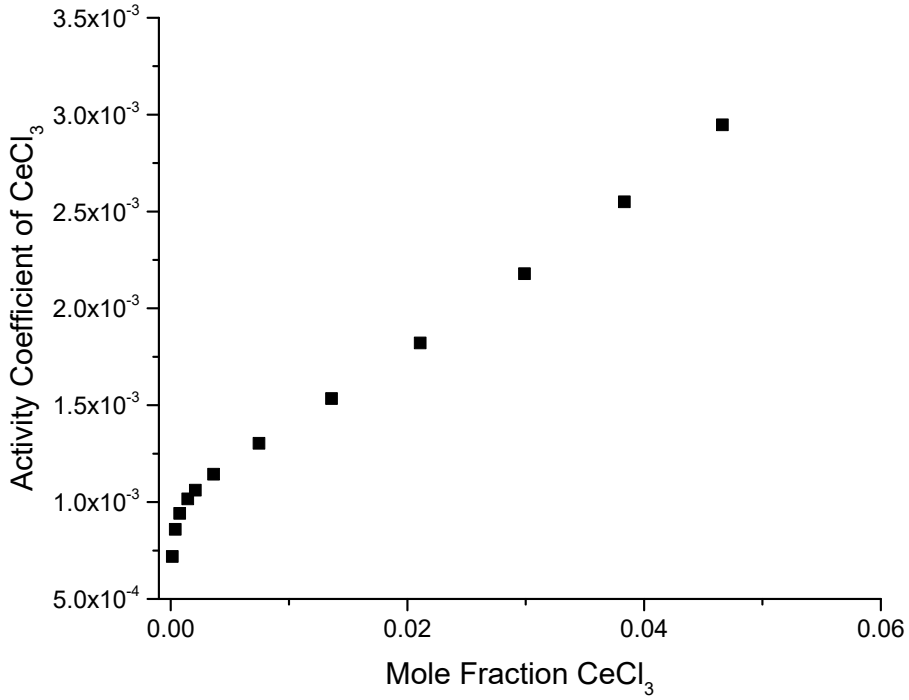

Figure 5.20. Activity coefficient of $CeCl_3$ in LiCl-KCl eutectic salt plotted as a function of mole fraction of $CeCl_3$ at 773 K.

Table 5.5. Activity coefficient of $CeCl_3$ in LiCl-KCl eutectic salt reported in the literature

Reference	T (K)	[$CeCl_3$]	γ_{CeCl_3}
Marsden and Pesic[27]	773	N/A	1.18×10^{-2}
Castrillejo et al.[24]	723	N/A	2.87×10^{-3}
Castrillejo et al.[24]	823	N/A	7.87×10^{-3}
Zhang et al.[28]	823	0.125 mol L^{-1}	9.14×10^{-3}
Zhang et al.[28]	923	0.125 mol L^{-1}	7.78×10^{-3}

5.3.3.1 Effect of Cesium Chloride

The effect of cesium chloride on the activity coefficient was also examined. For this, a salt with a fixed concentration of $CeCl_3$ (4.66 mol % $CeCl_3$) was prepared and CsCl was progressively added to the salt mixture whilst making open circuit potential measurements. It was observed that the open circuit potential remains almost unchanged with the addition of CsCl up to 1.92 mol % CsCl as shown in Figure 5.21. Tests at higher concentrations of CsCl were not performed.

5.3.3.2 Calculation of Apparent Potentials

The apparent potentials of the salt can be calculated similar to the $GdCl_3$ system. The standard reduction potential E^0 was calculated to be -2.941 V (vs. standard Cl^-/Cl_2 electrode).[57] The results from the calculations are shown in Figure 5.22. It can be observed from Figure 5.22 that like the previous rare earths, the apparent potentials vary with concentration as a function that is similar to the activity coefficient of the salt itself. The apparent potential becomes more positive with increasing concentration of $CeCl_3$ by about 30 mV.

Zhang[65] developed a temperature based correlation for the apparent potential of cerium chloride in LiCl-KCl eutectic salt. In the literature, Zhang[65] developed a temperature based correlation for apparent potentials for the $CeCl_3$ in LiCl-KCl eutectic salt. This correlation was developed based on the data presented by Fusselman et al.[88] and Castrillejo et al.[24] A

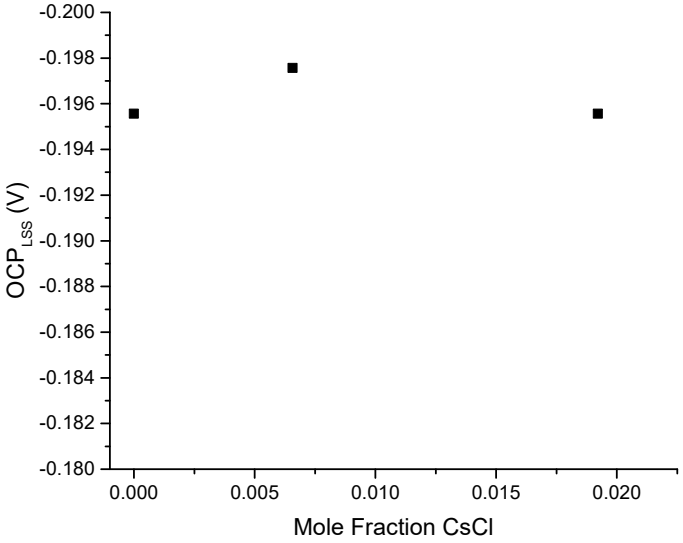

Figure 5.21. Open circuit potential of $Ce/CeCl_3$ couple in LiCl-KCl eutectic salt plotted as a function of mole fraction of CsCl at a fixed concentration of 4.66 mol % $CeCl_3$ at 773 K.

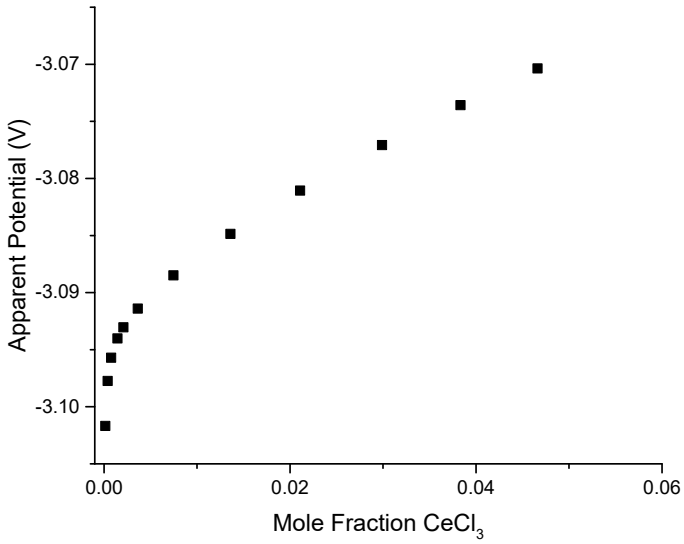

Figure 5.22. Apparent potential ($E^{0'}$) (vs. standard Cl^-/Cl_2 electrode) of $CeCl_3$ plotted as a function of mole fraction of $CeCl_3$ in a LiCl-KCl eutectic salt system at 773 K.

review of the works by Fusselman et al.[88] and Castrillejo et al.[24] shows that they both in fact report values of standard reduction potentials, E^0, and not apparent potentials as presumed by Zhang.[65] Hence a direct comparison of the values reported here and those reported by either Fusselman et al.,[88] Castrillejo et al.[24] or to the values obtained from the correlation presented by Zhang[65] is not entirely accurate.

5.3.4 Activity of $NdCl_3$

In general, it was observed that the OCP values recorded using the potentiostat were very stable to the third decimal place with fluctuations nonexistent. All the potentials reported in this section are reported versus a standard Cl^-/Cl_2 reference electrode unless otherwise stated. Data reported by Yang and Hudson[59] was used to convert the potentials from the 5 mol % Ag/AgCl reference electrode that was used to the standard Cl^-/Cl_2 electrode scale.

Using the above mentioned experimental methodology, the open circuit potentials for the system were determined as a function of concentration of $NdCl_3$. Note that for the purpose of this study, the neodymium(III) chloride is quantified as the *Added* $NdCl_3$ since as previously mentioned, it is not possible to quantify the real concentration of $NdCl_3$ present in the system. Figure 5.23 shows the open circuit potential measured as a function of mole fraction of *Added* $NdCl_3$. It can be observed that the open circuit potential shows an exponential relationship with added $NdCl_3$ concentration. Further E vs. $\ln X_{NdCl_3}$ shows a linear relationship as expected and is shown in Figure 5.24.

Using these measurements, the activity of $NdCl_3$ can be calculated as shown in Equation 5.3. To be able to use Equation 5.3 for the $NdCl_3$, the standard state potential ($E^0_{NdCl_3}$) needs to be known and use $n = 3$. Calculations to determine standard state potentials have been discussed earlier in this document. $E^0_{NdCl_3}$ was calculated to be -2.909 V (vs. standard Cl^-/Cl_2 electrode).

Now, using the experimentally determined value of E and calculated value of $E^0_{NdCl_3}$ and setting $n = 3$, the activity of $NdCl_3$ was calculated. Figure 5.25 shows the real and ideal activity of $NdCl_3$ as a function of added $NdCl_3$. It is obvious from Figure 5.25 that the real activity deviates significantly from ideal behavior. For ideal activity, the activity coefficient of $NdCl_3$ is assumed to be equal to 1. Using the same experimental measurements, the activity of $NdCl_2$ can also be calculated. However, these calculations were not performed

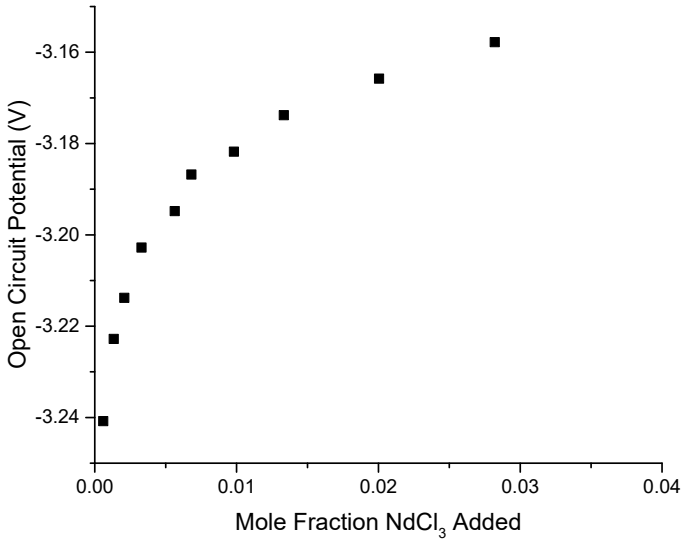

Figure 5.23. Open circuit potential (vs. standard Cl^-/Cl_2 electrode) plotted as a function of added $NdCl_3$. Experiment performed at T = 773 K

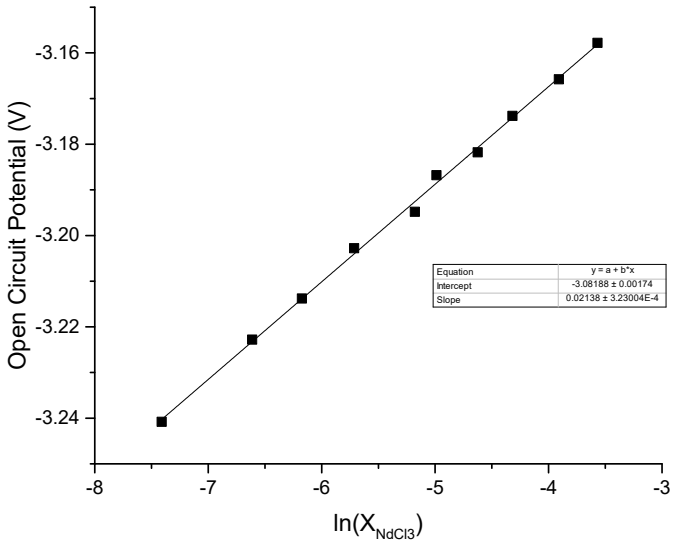

Figure 5.24. Open circuit potential (vs. standard Cl^-/Cl_2 electrode) plotted as a function of natural logarithm of added $NdCl_3$ Experiment performed at T = 773 K

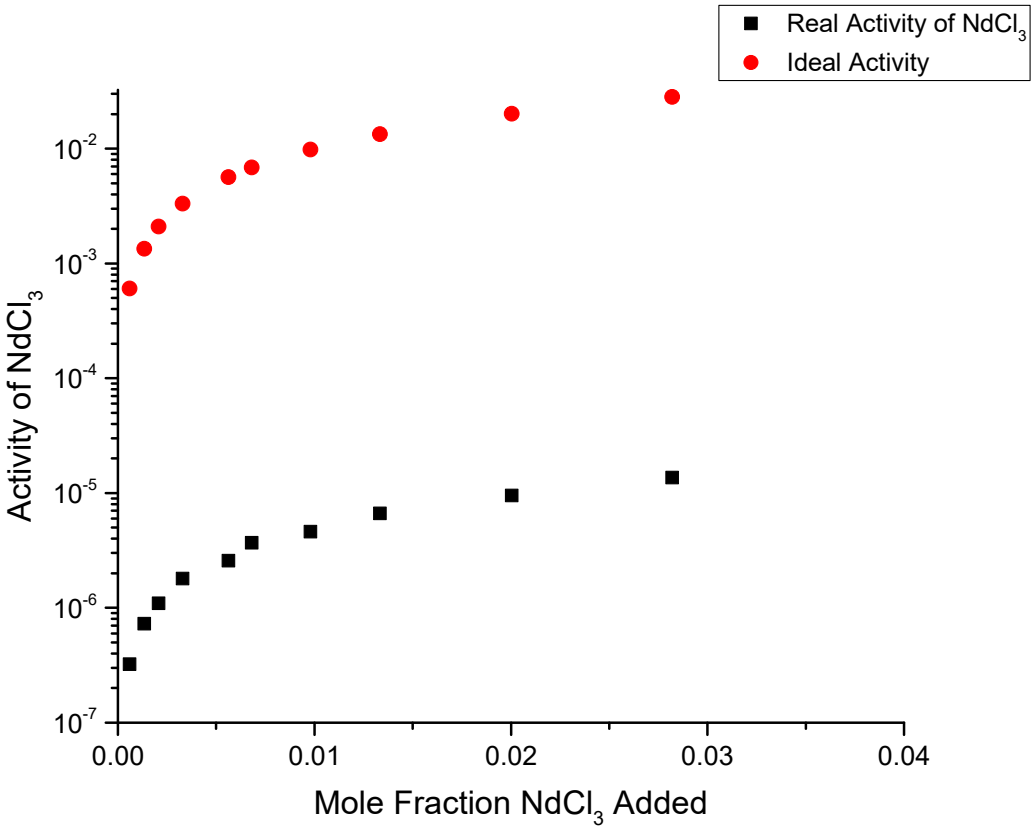

Figure 5.25. Ideal and real activity of $NdCl_3$ as a function of added $NdCl_3$ concentration. Experiment performed at T = 773 K

since high quality thermodynamic data for $NdCl_2$ are not readily available. Hence it is extremely hard to determine the standard state potential accurately.

5.4 Discussion

In this section, the activity of all of the four rare earth chlorides studied in this project will be reviewed. Details of the activity of all of the rare earths have been discussed in various chapters earlier in the dissertation. The activity of the three rare earths: $LaCl_3$, $GdCl_3$, and $CeCl_3$ can be determined simply as the arithmetic product of the activity coefficient and mole fraction. These data have now been plotted together along with the activity data of the $NdCl_3$ and are presented in Figure 5.26. Figure 5.26 shows the activity of $LaCl_3$, $CeCl_3$, $NdCl_3$, and $GdCl_3$ plotted as a function of mole fraction of the rare earth chloride.

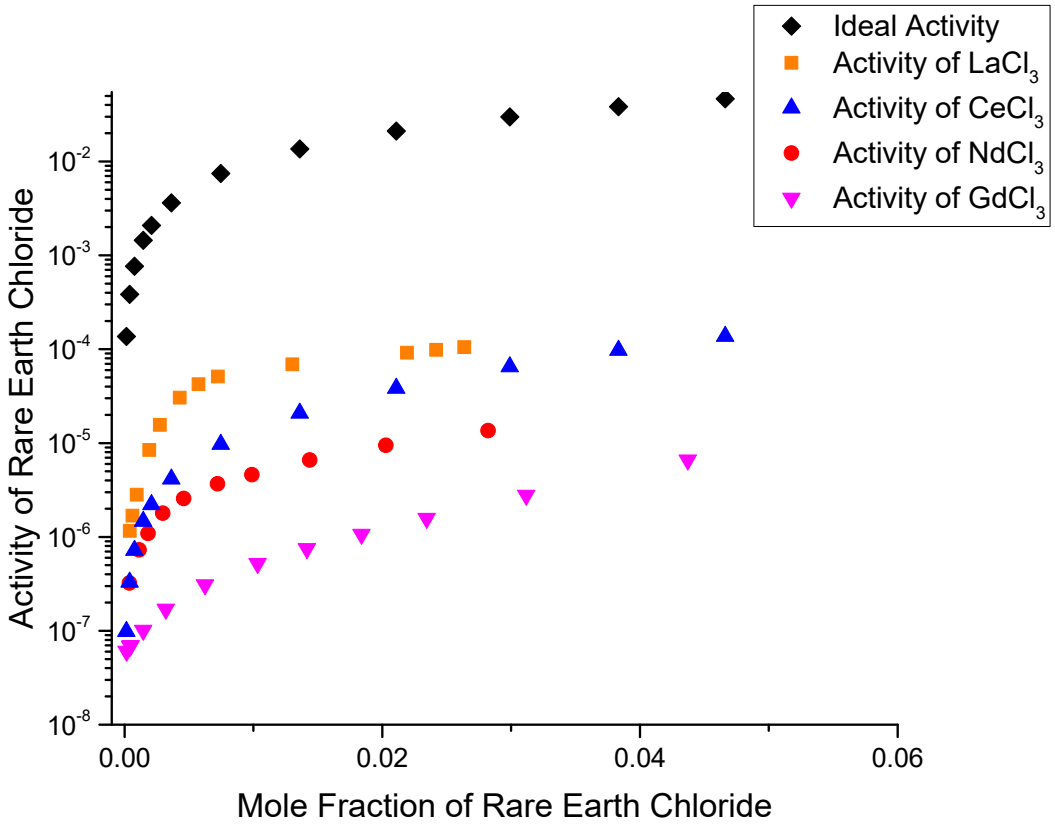

Figure 5.26. Activity of four rare earth chlorides, $LaCl_3$, $CeCl_3$, $NdCl_3$, and $GdCl_3$, as a function of mole fraction of chloride salt measured at 773 K compared to the activity of the rare earth chloride exhibiting ideal solution behavior.

Also plotted in Figure 5.26 is the ideal activity, which is based on an activity coefficient of one.

It is important to note that for the elements in the lanthanide series, there is a phenomenon known as lanthanide contraction. This means that as the atomic weights of the elements increase, their ionic sizes decrease. These properties for the four rare earth elements have been summarized in Table 5.6. The ionic radius and crystal radius were obtained from an online database hosted by the Imperial College, London.[2] Both ionic radius and crystal radius change with the coordination number and charge. In Table 5.6 the ionic radius and crystal radius have been reported for the +3 charge and coordination number of 6. It can be seen in Table 5.6 that as the atomic number increases, both the crystal radius and ionic radius decrease. This relationship is expected. A similar trend was observed for the

Table 5.6. Ionic properties of rare earths[2]

Element	Atomic Number	Charge	Coordination Number	Ionic Radius Å	Crystal Radius Å
Lanthanum	57	+3	VI	1.032	1.172
Cerium	58	+3	VI	1.01	1.15
Neodymium	60	+3	VI	0.983	1.123
Gadolinium	64	+3	VI	0.938	1.078

other coordination numbers and oxidation states from the data hosted at Imperial College.[2]

From Figure 5.26 and Table 5.6 it appears that one can draw the conclusion that as the ionic radius becomes smaller, a larger deviation from ideal solution behavior for the rare earth chlorides studied in this work is observed. Lantelme and Berghoute[22] studied the activity coefficient of both $LaCl_3$ and $GdCl_3$. In their summary, Lantelme and Berghoute[22] conclude that, *...gadolinium ions form stronger complexes with the ligand chloride ions coming from the solvent, which is coherent with the greater departure from ideality for the $GdCl_3$ solutions than for the $LaCl_3$ solutions.* The findings reported here support that conclusion and further expand on it.

In Figure 5.27, the activity of all of the four rare earth chlorides at a concentration of 1 mol % is plotted versus the ionic radii as documented in Table 5.6. It is clear from Figure 5.27 that the activity of rare earth chlorides seems to follow an exponential relationship with ionic size, increasing exponentially with increasing ionic radii. Though factors other than ionic size are definitely important, the evidence of Figure 5.27 definitely leads to the conclusion that the ionic size is a dominant factor in determining the activity of rare earth chlorides in molten salts.

In the discussion about the Debye-Hückel Theory in Sections 3.7 and 3.8, the importance of the ion size parameter, α, was stated based on the weight assigned to it by the many models predicting the activity coefficients of species. While the Debye-Hückel Theory is not directly applicable to molten salt systems, due to their high ionic strengths, its recognition of

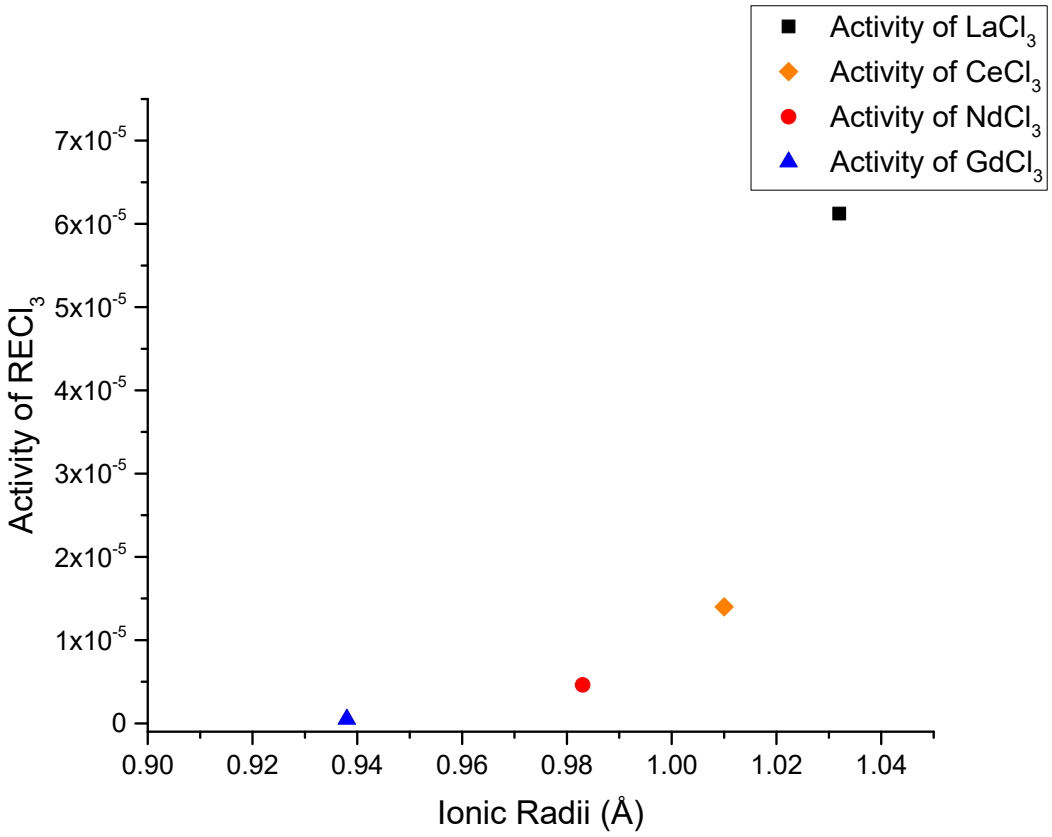

Figure 5.27. Activity at a concentration of 1 mol % for four rare earth chlorides, $LaCl_3$, $CeCl_3$, $NdCl_3$, and $GdCl_3$, in LiCl-KCl eutectic salt at 773 K plotted as a function of the respective ionic radius for each lanthanide.

the importance of the ion size parameter, α, adds credence to the observations reported here that for rare earth chlorides in molten salt systems, the ionic size plays an very important role in determining the activity of species in solution.

In the wider literature, Cantor[89] used cryoscopy methods to determine the freezing point depression of NaF by polyvalent salts. Cantor[89] further correlated the liquidus temperature to the activity of NaF and found that the smaller the radius of alkaline earth, the greater the deviations from ideal solution behavior. In discussing the data presented by Cantor,[89] Blander[90] concluded that the evidence indicated that the deviations from ideal behavior are related by a function which appears to be monotonic in charge of the solute cation z and in $1/d_2$ where d_2 us the sum of the cation and anion radii of the solute. However other effects such as Van der Waals' interactions and ligand field effects are also at play.

Yang and Hudson[91] performed e.m.f. measurements for Pb^{2+},Cd^{2+}, Zn^{2+}, Mg^{2+}, Be^{2+} ions over a range of concentrations in LiCl-KCl eutectic salt to calculate the activities. In all of the systems, the deviation from ideality was negative ($\gamma < 1$). It was observed that except for $ZnCl_2$, the value of the term (μ^E / X) is more negative the smaller the radius of the divalent ion. The term (μ^E / X) is of course closely related to the activity coefficient. There is quite a lot of literature that suggests that in polyvalent ions, the ionic size plays an important role in determining the deviation from ideal solution behavior.

The departure from ideality in molten salt systems has often been attributed to the phenomenon of *complexing* or *complex ion formation*. This terminology is often used widely to explain many different phenomenon observed in chemistry. In a discussion about the phenomena of complexing, Blander[90] broadly classified *complexing* into two categories. In the first case, Blander[90] defined a complex ion as being conceived as a microscopic grouping of at least one central cation and near-neighbor anions having a particular configuration. If such a grouping is isolated from others and shares no anions, then this grouping is a finite complex. If the groupings are all interconnected by shared anions, then infinite complexes are present. Hence, by definition all pure salts are infinite three-dimensional complexes and very dilute solutions of one salt in another contain finite.[90]

The second category of complexes is used to describe the propensity for stabilization of species in chemical environments. In a solution, the tendency to complexing for stabilization is characterized by a negative value of μ^E. The solution effects briefly discussed in Section 3.9 were Coulombic effects, polarization effects, van der Waals' interactions, ligand field effects and packing, and steric effects. All or any combination of these solution factors contribute to the complexing of ions in solutions.

Since there is no overarching theory for the determination of activities in molten salt systems, these properties need to be determined for every unique system with careful consideration for the various phenomena that would be present. If activity coefficient is plotted for all of the three rare earth chlorides as shown in Figure 5.28 it makes for some very interesting conclusions. Firstly, it is evident from Figure 5.28 that for every element the activity coefficient behaves uniquely with increasing concentration. In the case of $LaCl_3$, it increases and subsequently decreases. In the case of $CeCl_3$, the activity coefficient continues to increase almost linearly for most of the concentration range tested. Finally in the case

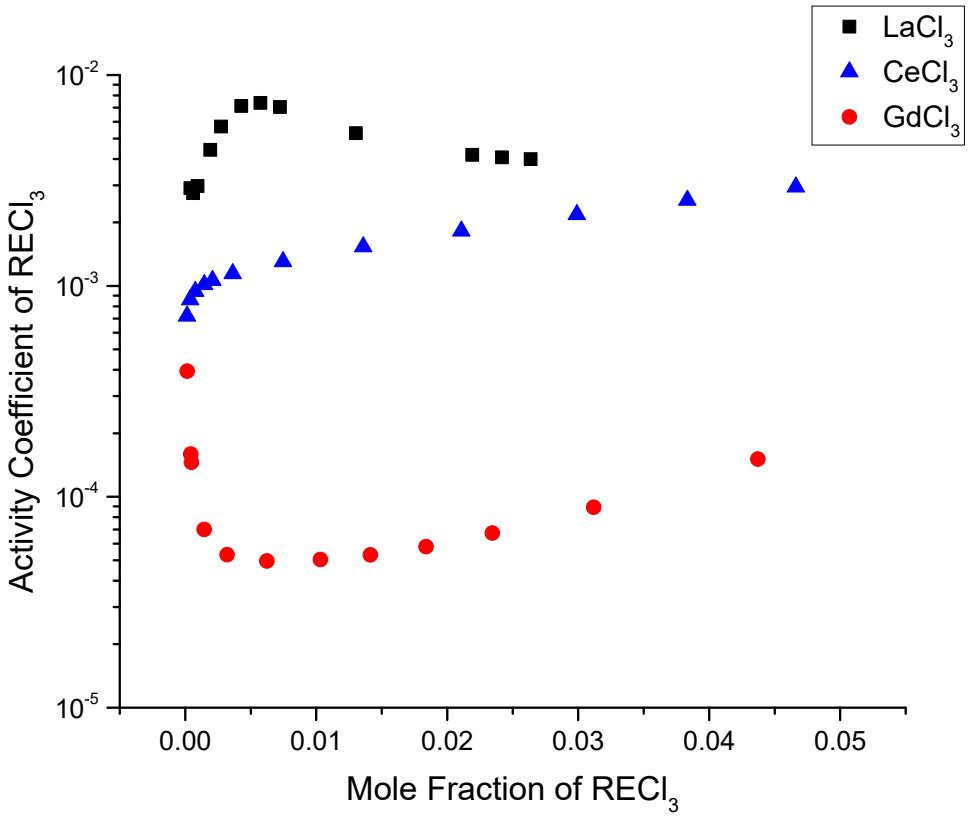

Figure 5.28. Activity coefficient of three rare earth chlorides, $LaCl_3$, $CeCl_3$ and $GdCl_3$, in LiCl-KCl eutectic salt plotted as a function of mole fraction of chloride salt 773 K.

of $GdCl_3$, the activity coefficient initially decreases precipitously, then remains unchanged before beginning to increase.

One underlying theme of the data presented in Figure 5.28 is the fact that the activity coefficient changes with concentration of the respective salt in question. The nature of such a change is unique to each chloride salt, but the change itself is constant. To understand this change, the answers are probably in the local coordination chemistry of the lanthanide halides in molten salt solutions. It is well established and widely accepted that trivalent lanthanide chlorides are present in molten salts as octahedral species of the form $LnCl_6^{3-}$.[86] These local complexation structure of trivalent rare earths have been determined experimentally using Raman Spectroscopy[76,77] and Neutron Diffraction[78–81] techniques in addition to molecular dynamic simulations.

For widely studied salts like $LaCl_3$, Okamoto et al.[85] conducted XAFS tests and MDS studies of a LiCl-KCl-$LaCl_3$ molten salt mixture. They studied mixtures containing from 1 to 100 mol % $LaCl_3$. They demonstrated that the coordination number and interionic distance increase with increasing concentration of $LaCl_3$. These and other data available in that paper clearly demonstrate that the coordination chemistry of the dissolved La species is dependent on the concentration of the total La present in the mixture. This concentration dependence of complexation reactions of $LaCl_3$ and ability of $LaCl_3$ to have a multitude of coordination numbers likely explains the concentration dependence of important properties like activity coefficients reported here not only for $LaCl_3$ but also the other lanthanides studied here.

However, the reasons for the unique behavior of the activity coefficients with concentrations for each rare earth are not very well understood. However it is clear from Figure 5.28 the reason it has been so challenging to develop comprehensive activity coefficient models for molten salt systems. Not only does the activity coefficient vary by orders of magnitude difference but also the variation in activity coefficient with concentration seems to be unique for every element.

5.5 Summary

In this chapter, experimental data for the for activity four rare earth chlorides, $LaCl_3$, $CeCl_3$, $NdCl_3$, and $GdCl_3$, were presented. The activity of all four species was measured electrochemically. It was observed that the activity coefficient of the three species for which it was measured ($LaCl_3$, $CeCl_3$, and $GdCl_3$) varies with the concentrations of the respective chlorides. It is observed that the nature of change of the activity coefficient is unique to each species. For $LaCl_3$, the activity coefficient increases and subsequently decreases with concentration of salt. For $GdCl_3$ the activity coefficient decreases and subsequently increased with concentration. Finally, for $CeCl_3$, the activity coefficient increases linearly with concentration for most of the window tested.

It is also observed that the activity of the rare earth chlorides shows a strong dependence to the ionic radii of the corresponding rare earth metal. The smaller the ionic size of the species, the larger the deviation from ideal solution behavior observed. Further, if the activity of the four species is plotted on versus ionic radii, an exponential relationship is

observed.

The effect of presence of CsCl was also examined for three of the rare earth chlorides: $LaCl_3$, $CeCl_3$, and $GdCl_3$. It is reported that the activity coefficient of $LaCl_3$ increases in the presence of high concentrations of CsCl. The activity coefficient of $GdCl_3$ decreases with increasing CsCl concentrations. Finally, it is also observed that the presence of CsCl does not seem to influence the properties of $CeCl_3$ in the concentration window tested.

CHAPTER 6

GALVANIC DRAWDOWN OF UCl_3 USING $Gd/GdCl_3$ REDOX COUPLE

In the pyrochemical processing of spent fuel, the drawdown of actinides is an important unit operation to enable the recycling of salt and minimize waste. In this section, a new method for the drawdown of uranium(III) chloride from LiCl-KCl molten salt has been presented. Using the galvanic interaction present between the Gd/Gd(III) and U/U(III) redox reactions, it is should be possible to draw down the UCl_3 using gadolinium metal.

6.1 Motivation

To minimize the amount of waste from pyroprocessing that requires permanent deep geologic disposal, a sequence of two drawdown steps have been proposed and included in reference flowsheets.[19] The first step would be used to separate actinides from the electrorefiner waste salt. The second step would be used to separate rare earth fission products from the actinide-free product from the first drawdown operation. The remaining salt would mostly consist of eutectic LiCl-KCl and could be recycled to the electrorefiner. Actinides recovered in the first drawdown operation could likewise be returned to the electrorefiner salt. In theory, this would facilitate a high percentage of actinide recovery as metals on cathodes in the electrorefiner. While drawdown can involve a variety of different approaches based on converting the actinides or rare earths to insoluble species, it is most commonly proposed to achieve drawdown via reduction to the metallic state.[18,92–97]

While most of these studies have investigated electrochemical reduction of actinides and/or lanthanides on a cathode, Simpson et al.[97] studied the method of direct lithium metal addition to reduce lanthanide chlorides as shown in Equation 6.1.[97]

$$3Li_{(l)} + MCl_{3_{(l)}} \rightleftharpoons M_{(s)} + 3LiCl_{(l)} \tag{6.1}$$

Two problems were encountered with this approach–lack of selectivity and inability to easily collect the metal products. The selectivity issue is understandable given that the Li^+/Li reduction potential is more negative than all of the lanthanides in LiCl-KCl eutectic salt. The only way to control selectivity is via reagent-limited operation. But even that approach was shown to yield unsatisfactory results. In theory, cathodic reduction can solve both of these problems. Cathode potential can be controlled to selectively reduce the more electronegative metals, and metals can be collected as deposits on the electrode. But in a 2009 paper by Kwon et al.,[96] it was shown that cerium chloride is removed along with uranium chloride via electrochemical deposition in a mixture of LiCl-KCl-UCl_3-$CeCl_3$. In papers by Li et al.[98] from Idaho National Laboratory, it was shown that co-deposition of rare earths with actinides in liquid metal cathodes is also problematic.[98,99] Liquid metals such as cadmium and bismuth appear to stabilize both actinide and rare earths as reduced products, shifting their apparent reduction potentials to a narrow range.

During deposition, the activity of the reduced metal varies from one for pure metal cathode to potentially orders of magnitude lower in a liquid metal cathode. Driving uranium metal deposition onto a solid cathode, for example, requires that the potential be low enough to achieve the desired concentration in the salt. The problem with using lithium metal to draw down uranium is that it sets the equilibrium potential too low–sufficiently low to reduce rare earths as well as actinides. The problem with a liquid metal cathode is that the activity of dissolved actinides and lanthanides is so far away from one that the equilibrium potential shifts to favor co-deposition. Hypothetically, an ideal drawdown process would use a cathode with a constant potential to first reduce actinides and then reduce rare earths on a subsequent cathode. The problem with this approach is that anode design becomes complicated. An inert anode will generate Cl_2 gas, which is corrosive at the operating temperature of the electrorefiner. Reactive anodes have not been used traditionally in these processes and would likely put an impurity in the salt or create a gas stream that would need to be managed as in the case of Cl_2.

The alternative proposed here is to employ a galvanic couple for plating of uranium and transuranic species. The key feature in this process is to use a rare earth metal to generate an anodic surface, while the stainless steel basket it is contained within serves as the cathodic surface. Rare earths, such as Gd, have standard reduction potentials slightly more negative

than that of the actinides. They can essentially act as reducing agents, less powerful than lithium metal. This reduction can be done electrochemically to actually deposit the U metal onto an object that can be extracted from the electrorefiner. For example, that object may be a stainless steel basket.

This chapter presents the results of the first experiment in which this galvanic process was used to draw down UCl_3 from a surrogate ER salt mixture. The results are promising for developing a simple process for cleaning the ER salt of actinides in preparation for subsequent fission product extraction. Unlike the lithium drawdown process, this method provides a simple method for removing the reduced actinides from the salt and recycling them back to the electrorefiner.

6.2 Experimental Description

For this experiment, a mixture of LiCl-KCl-UCl_3-$MgCl_2$ was prepared in an alumina crucible (AdValue Technology). The initial concentrations of the salts based on ICP-MS data were 8 wt. % UCl_3, 1.33 wt. % $MgCl_2$ and balance LiCl-KCl eutectic salt. There was no $GdCl_3$ in the initial salt. This salt mixture was heated to 773 K in a Kerr electro-melt furnace. A Gd metal rod (6.35 mm x 25 mm; 99.9 % ESPI Metals) was placed in a perforated stainless steel basket. The inside of the steel basket was lined with a stainless steel mesh. The stem of the basket was inserted into an Autolab rotating disk electrode rotator (Metrohm). This rotator was mounted on a stand and clamp assembly atop the Kerr furnace. This rotator enabled the basket to be rotated continuously at 100 rpm throughout the experiment. Rotation should increase the overall reaction rate. No external current/potential was applied to drive the electrochemical reaction. Figure 6.1 shows the schematic of the experimental set-up used for this experiment.

6.3 Results

The experiment was performed for a total of 3 hours. After the initial insertion of the basket into the molten salt bath, the basket was rotated for an hour. At the end of an hour, the rotator was stopped and a salt sample was taken using a stainless steel all-thread. Then the basket rotation was continued. This process was repeated an additional two times at intervals of an hour each for a total test time of 3 hours. ICP-MS analysis was performed

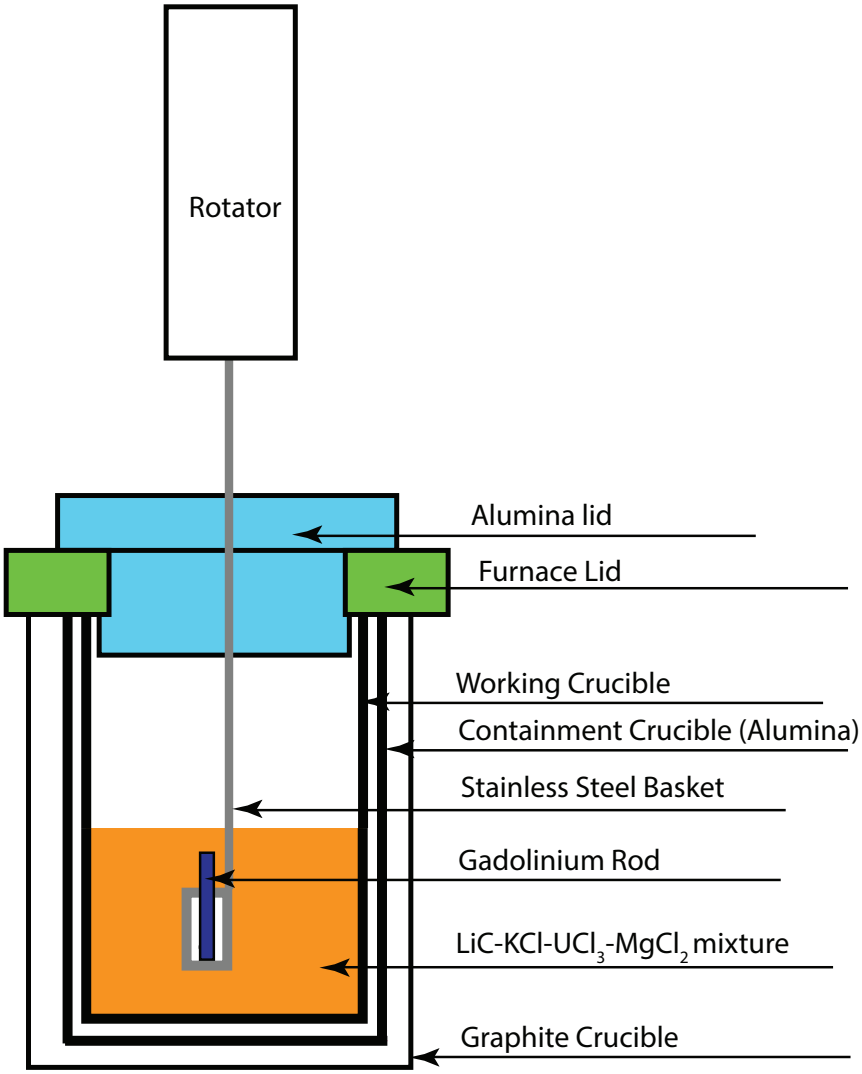

Figure 6.1. Schematic of the experimental set-up used for this study.

on these samples to determine concentration of Gd, U and Mg. The results are shown in Figure 6.2. The salt had an initial concentration of UCl_3 and $MgCl_2$ of 8 wt. % and 1.33 wt %, respectively. After an hour, almost all of the uranium from the salt had been plated out of the salt onto the steel basket, while the amount of $GdCl_3$ present in the salt markedly increased to 6.76 wt. %. As the test continued, the amount of $GdCl_3$ present in the salt continued to increase, while both UCl_3 and $MgCl_2$ concentration continued to decrease in salt. At the end of the third hour, a slight increase in the UCl_3 concentration in the salt was observed. The reason for this increase in concentration at the end of the experiment is

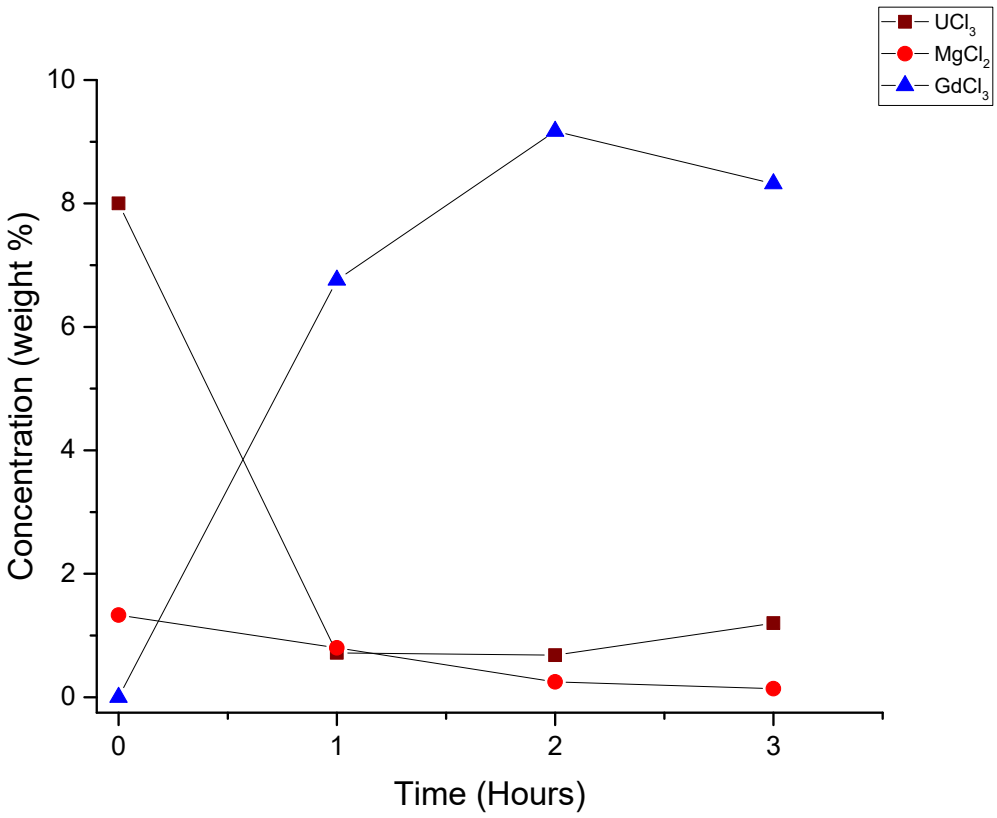

Figure 6.2. The concentration of UCl_3, $MgCl_2$ and $GdCl_3$ in the LiCl-KCl eutectic salt at 773 K tracked at 1-hour intervals.

unclear. Figures 6.3 and 6.4 show the images of the steel basket after an hour of testing. This black deposit on the steel basket was determined to be uranium metal by a Geiger counter, since uranium is the only radioactive species in the system.

At the end of the test, the salt was allowed to cool to room temperature, and the alumina crucible was broken to release the salt. It was observed that the bottom of the crucible was lined with black precipitate that was again determined to be uranium oxide with some traces of Gd metal present. This analysis was performed using x-ray diffraction analysis. The x-ray diffraction spectrum is shown in Figure 6.5. It can be observed from Figure 6.5 that the diffraction spectrum is quite noisy. The reason for this is believed to be the background from the Whatman filter paper that was used to initially filter out the solids from the liquids after the salt was dissolved in water. This process of dissolution, filtration

Figure 6.3. The side view of the basket showing uranium deposited after 1 hour of testing.

Figure 6.4. The top view of the basket showing uranium deposited after 1 hour of testing.

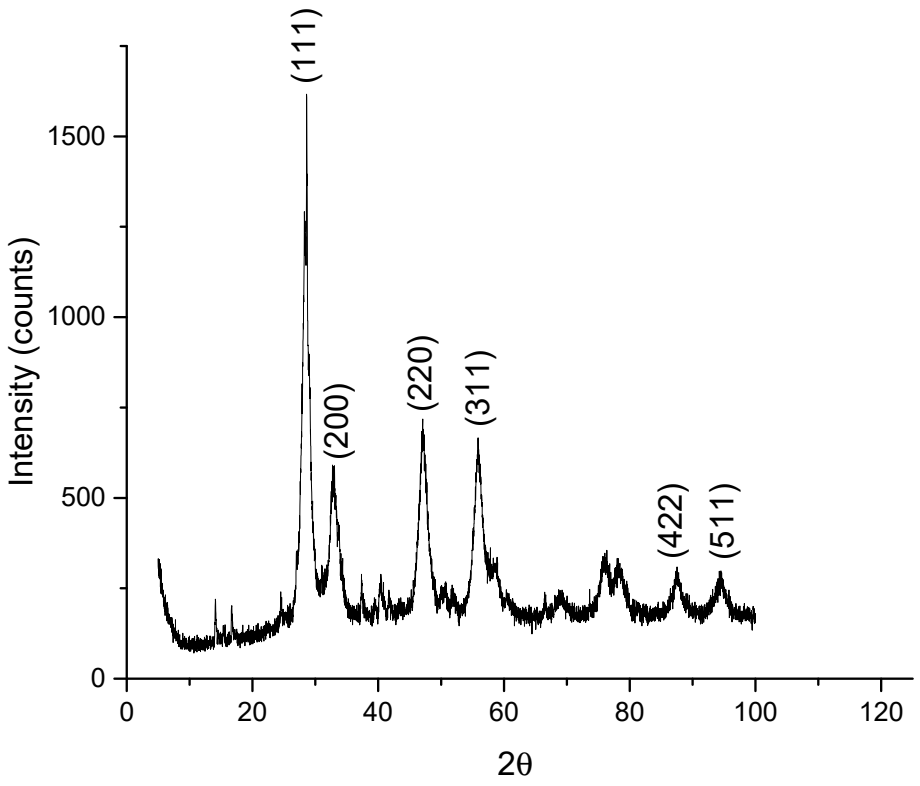

Figure 6.5. X-ray diffraction spectrum of UO_2.

and exposure to oxygen is believed to have caused the oxidation of the uranium metal to uranium oxide.

The findings reported here demonstrate the uranium drawdown can be effectively performed using a galvanic couple with a electrochemically less noble species like Gd metal. This has very important implications for the standpoint of pyroprocessing of spent fuel. If such a galvanic reduction process were to be deployed rather than the other options like electrowinning, there would be some significant advantages. First, the process equipment and operations cost would be reduced by employing a passive process that does not require active electrical control. Second, operation very close to the equilibrium reduction potential for Gd^{3+}/Gd would minimize the co-reduction of rare earths, which would enable them to be mostly extracted in the subsequent rare earth drawdown step. Any species that is less noble than the one used for the galvanic reduction will not reduce on the electrode. This enables

better control of the process and impurities. Recycling of rare earths to the electrorefiner would, thus, be minimized. Third, the reduced actinides could easily be recovered and recycled to the electrorefiner without handling liquid metal cathodes. Fourth, high processing rate can be achieved by optimizing salt mixing and rotation of the basket. As shown in the proposed flowsheet as shown in Figure 6.6, it is envisioned that the cathodic product obtained at the rare earth drawdown stage[19] can be recycled back to the actinide drawdown step to be used in the galvanic drawdown of actinides. There would, thus, be no need to use expensive rare earth metals as reactants, and the net effect on rare earth disposal would be zero. For efficient control over the galvanic drawdown process, accurate knowledge of the activity of the rare earths and the actinides is needed to enable the prediction of the reduction potentials under operational conditions.

6.4 Summary

In this chapter, using the activity data, it is demonstrated that UCl_3 can be drawn down using Gd metal. This experiment demonstrates that availability of high quality activity data opens up future avenues for further research and development giving researchers an additional lever of control over the process.

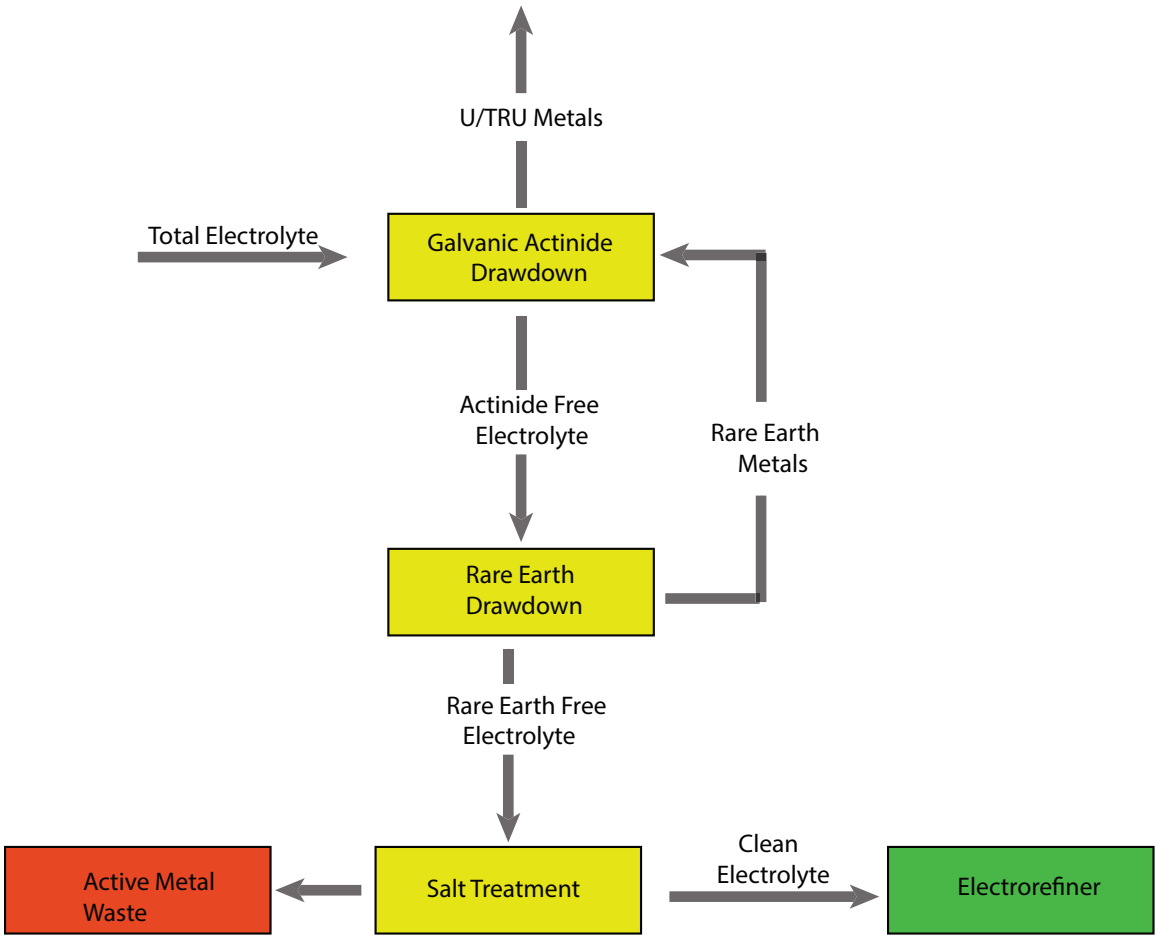

Figure 6.6. A proposed flowsheet showing recycling of rare earths for galvanic actinide drawdown.

CHAPTER 7

LIQUIDUS AND SOLIDUS DATA FOR LiCl-KCl-CsCl-$RECl_3$ MIXTURES

In this chapter, data will be presented for the phase diagram for the following quaternary systems:

1. LiCl−KCl−CsCl−$LaCl_3$ System
2. LiCl−KCl−CsCl−$GdCl_3$ System
3. LiCl−KCl−CsCl−$NdCl_3$ System

For the phase diagram studies, the concentration of CsCl varied from 0 to 1.40 mol% CsCl. The motivation for the study was to determine the effect of other fission products on the phase behavior of LiCl-KCl-$RECl_3$ mixtures. Neither the actinide nor the rare earth drawdown processes removes CsCl and other Group I/II fission products from the salt. Thus, their effect on phase behavior over a range of $RECl_3$ concentrations is of interest. As the concentration of CsCl will build up in the LiCl-KCl eutectic salt, CsCl will likely influence the behavior of the salt. Understanding the influence of the CsCl on the eutectic salt will enable us to set limits on the operating conditions for specific unit operations. This work differentiates from data published by Sridharan et al.[29] on LiCl-KCl-$LaCl_3$, LiCl-KCl-$CeCl_3$, and LiCl-KCl-$NdCl_3$ since Sridharan et al.[29] did not explore the influence of CsCl. Sridharan et al.[29] studied the LiCl-KCl-$ReCl_3$ ternary systems to very high concentrations of about 25 mol % $ReCl_3$. In this work a lower concentration window has been explored for quaternary LiCl-KCl-CsCl-$RECl_3$ systems. Furthermore, in the second section of the chapter, an attempt will be made to examine the activity data previously measured and the phase diagram together and draw a correlation between them if possible.

7.1 LiCl−KCl−CsCl−$LaCl_3$ Phase Diagram

The phase diagram for the LiCl-KCl-$LaCl_3$ system was previously studied and published in the literature.[29] The thermograms generated from the differential scanning calorimetry instrument for all of the systems have been documented in Appendix B.

Figure B.1 shows the thermograms for the LiCl-KCl-$LaCl_3$ with no CsCl present. As evident from Figures B.1, there is only one endothermic peak on the whole spectrum for the LiCl−KCl−$LaCl_3$ system. This means that the solidus and liquidus lines are the same. There is no 2-phase region in the phase diagram. Figure B.2 shows the heat flow signal for the LiCl−KCl−CsCl−$LaCl_3$ system with 0.69 mole % CsCl present. A major endothermic peak exists at about 350°C. However a small endothermic peak is observed at just above 300°C for all of the thermograms. A similar behavior is observed in the LiCl−KCl−CsCl−$LaCl_3$ system with 1.40 mol % CsCl present as shown in Figure B.3. However with 1.40 mol % CsCl present, the low temperature peak is more prominent than the corresponding peak in the quaternary system with 0.69 mol % CsCl. The low temperature peak present in the samples with CsCl present represents the solidus temperature for such systems while the main peak present at 350°C represents the liquidus temperature for the salt systems.

Using the thermograms generated, it possible to determine the temperatures of the endothermic events. This temperature is defined as the onset temperature of the endothermic event. For the samples with CsCl present, both the solidus and liquidus temperatures can be determined. Figure 7.1 shows the solidus and liquidus line for LiCl−KCl−$LaCl_3$ system as a function of $LaCl_3$ concentration. This system shows a eutectic behavior. Figure 7.1b and 7.1c show the solidus and liquidus line in the presence of 0.69 and 1.40 mole % CsCl respectively. It can be observed that now the system shows a peritectic behavior. Figure 7.2 shows the comparison of the liquidus temperatures for the three $LaCl_3$ subsystems. There is definitely a depression in the liquidus temperatures in the presence of 1.40 mole % CsCl.

7.2 LiCl−KCl−CsCl−$NdCl_3$ Phase Diagrams

Tests for this system were performed similar to the first system. The thermograms for the LiCl-KCl-CsCl-$NdCl_3$ system have been documented in Appendix B. It can be observed the thermograms that unlike for the LiCl-KCl-CsCl-$LaCl_3$ system, no low

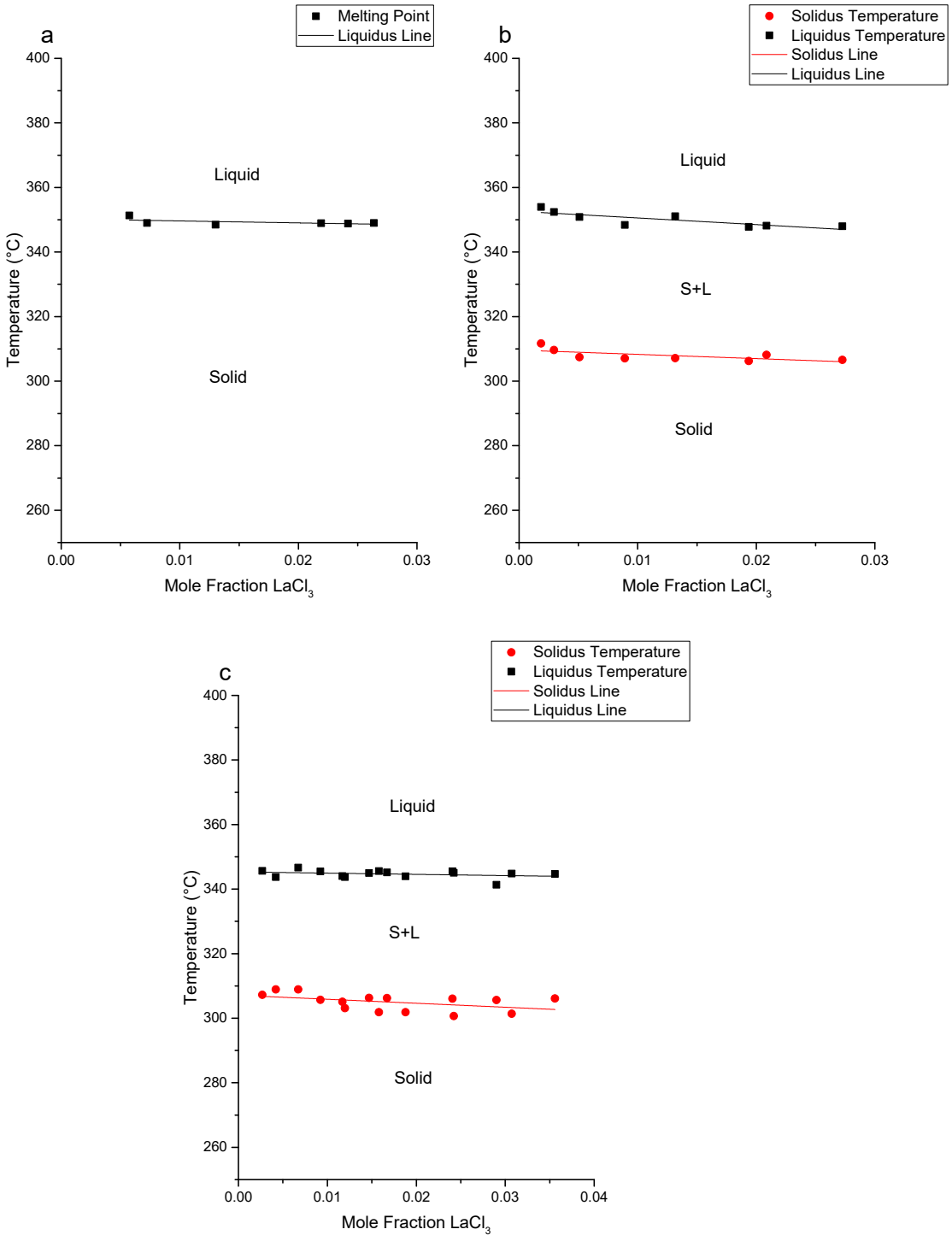

Figure 7.1. Solidus and liquidus lines for the LiCl-KCl-CsCl-$LaCl_3$ system. (a) 0 mol % CsCl, (b) 0.69 mol % CsCl, (c) 1.40 mol % CsCl.

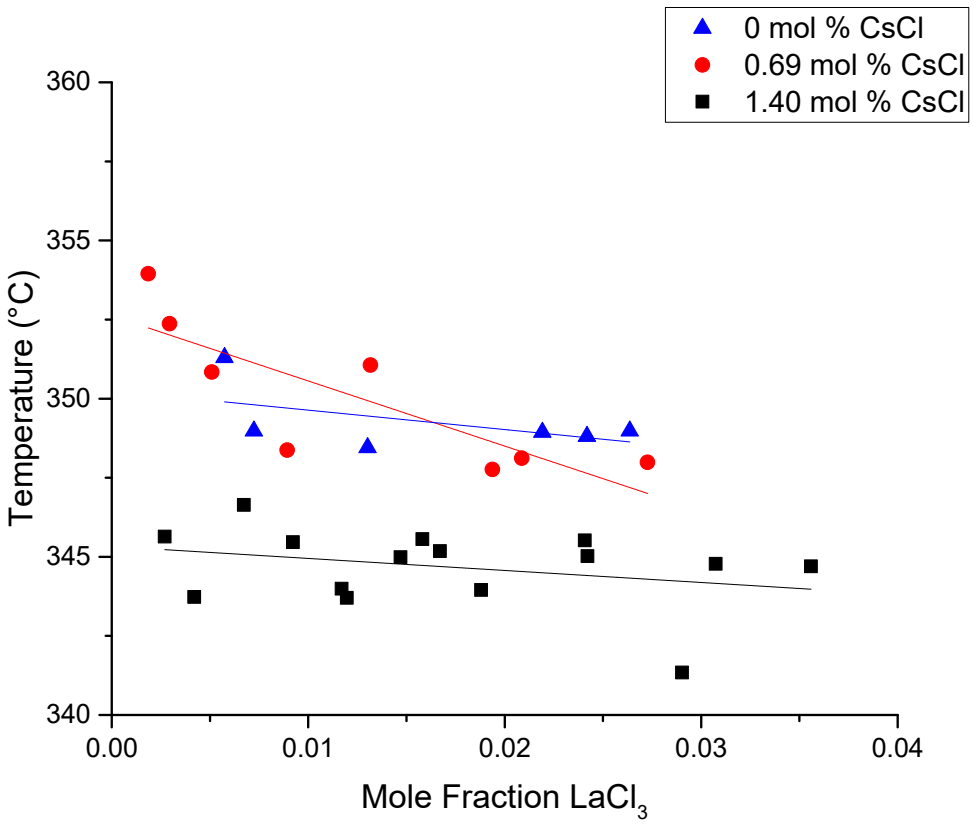

Figure 7.2. Comparison of liquidus temperatures for the LiCl-KCl-CsCl-$LaCl_3$ system at three concentrations of CsCl; 0, 0.69, and 1.40 mol % CsCl.

temperature peaks were observed for the LiCl-KCl-CsCl-$NdCl_3$ system. This indicates that unlike the LiCl-KCl-CsCl-$LaCl_3$ system, peritectic behavior is not quite observed for the LiCl-KCl-CsCl-$NdCl_3$ system. Figure 7.3 shows the liquidus line for this system. It can be observed that the presence of CsCl does seem to lower the liquidus temperatures. However, unlike the LiCl-KCl-CsCl-$LaCl_3$ system, no peritectic behavior is observed.

7.3 LiCl−KCl−CsCl−$GdCl_3$ Phase Diagrams

The thermograms for the LiCl-KCl-CsCl-$GdCl_3$ system have been documented in Appendix B. Figure B.7 shows the thermograms for the LiCl-KCl-$GdCl_3$ with no CsCl present. Figure B.7 shows that there is only a single endothermic peak present. Similar behavior is observed in thermograms of the LiCl-KCl-CsCl-$GdCl_3$ with 0.70 mol % CsCl present as

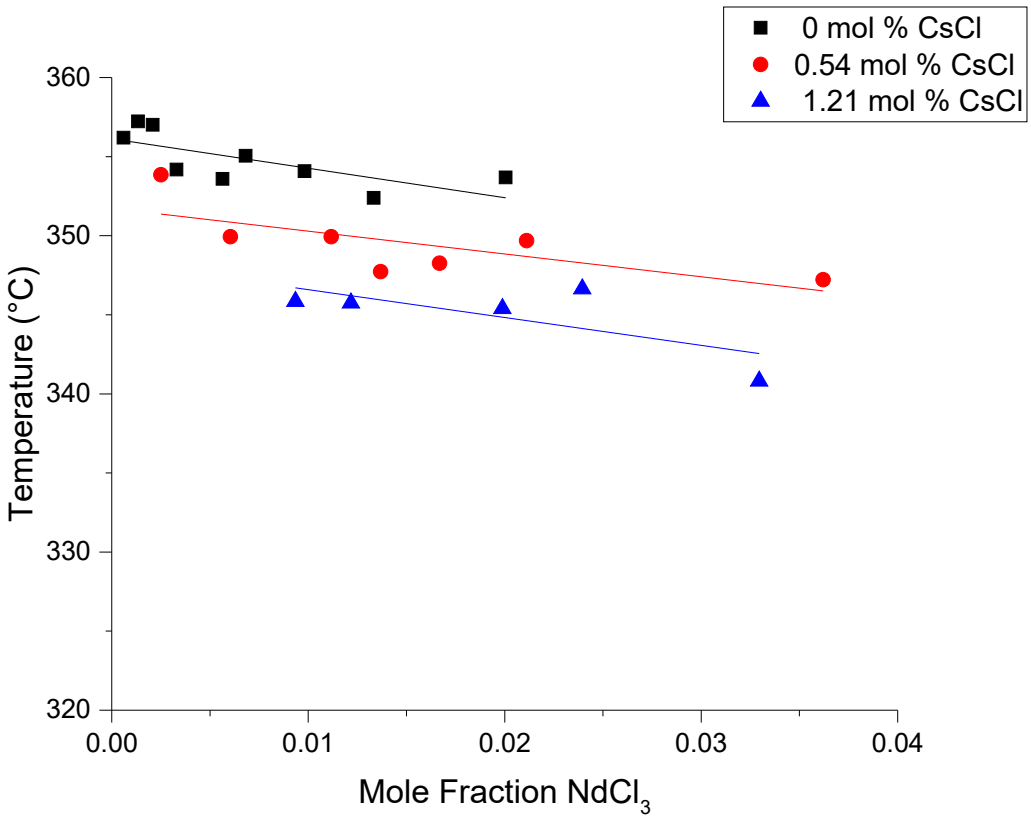

Figure 7.3. Liquidus lines for the LiCl-KCl-CsCl-$NdCl_3$ system for three concentrations of CsCl; 0, 0.54, and 1.21 mol % CsCl.

evident in Figure B.8. For the thermograms of the salts with 1.43 mol % CsCl, shown in Figure B.9, there is a low temperature peak observed at around 260°C. Strangely this peak is present only at the low concentrations of $GdCl_3$ and disappears at around 0.35 mol % $GdCl_3$. To confirm this behavior, duplicate samples were run for the low concentration samples with fresh calibration. They yielded similar results. This low temperature peak is more clearly observed in Figure B.10 in Appendix B.

Figure 7.4 shows the liquidus temperatures for all of the three sets of samples for the $GdCl_3$ system. It can be observed that the presence of CsCl does depress the liquidus temperatures of mixture slightly, although there seems to be no difference in the liquidus temperatures for the two concentrations of CsCl present.

Figure 7.5 shows the phase diagram for the LiCl-KCl-CsCl-$GdCl_3$ system with the 1.43 mol % CsCl present deduced from the thermograms. The x-axis is on log scale representing the mole fraction of $GdCl_3$ present. It is proposed that the initial portion shows peritectic behavior with a binary phase region present. The solid vertical line is added to represent the finding that at higher concentration of $GdCl_3$, the system returns to a eutectic behavior.

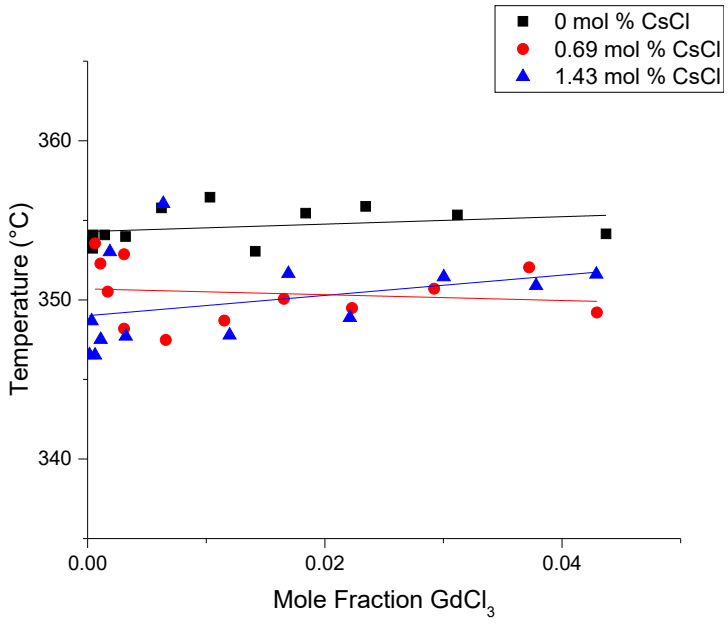

Figure 7.4. Comparison of liquidus temperatures for the LiCl-KCl-CsCl-$GdCl_3$ system for three concentrations of CsCl; 0, 0.69, and 1.43 mol % CsCl present.

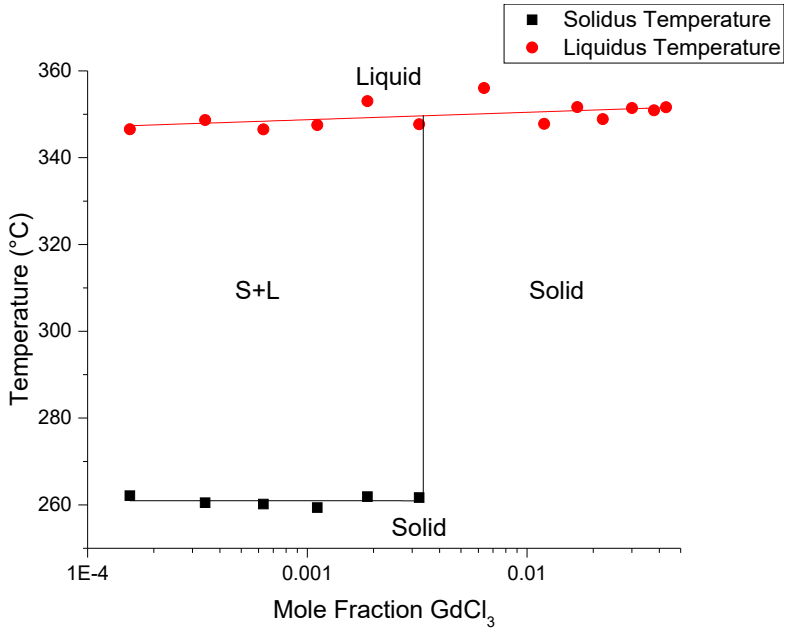

Figure 7.5. Solidus and liquidus lines for the LiCl-KCl-CsCl-$GdCl_3$ system with 1.43 mol % CsCl present.

7.4 Discussion

In the ensuing discussion, an attempt will be made to explain the reasons for the observed effects. Two pathways will be discussed, through the prism of thermodynamics and through the lens of coordination chemistry.

7.4.1 Le Chatelier-Shreder Equation

In general from the phase diagram data reported above, it can be concluded that the presence of CsCl depresses the liquidus temperature for all three systems studied here. In two of the systems, $LaCl_3$ and $GdCl_3$, a low temperature peak is additionally observed. The consistency of the depression in the liquidus temperatures with the addition of CsCl points to a common underlying phenomenon that may be contributing to the lowering of liquidus temperatures. This phenomenon is probably operative and effective to varying degrees in the three lanthanides.

The liquidus temperature can be predicted using the Le Chatelier-Shreder[100] relationship as shown in Equation 7.1. The Le Chatelier-Shreder equation draws a link between the liquidus temperatures and the activity of species.

$$T_{i,liq} = \frac{\Delta_{fus}H_i \, T_{fus,i}}{\Delta_{fus}H_i - RT_{fus,i} \ln a_i} \tag{7.1}$$

In Equation 7.1, the $T_{i,liq}$ is the liquidus temperature of species i which is a function of the enthalpy of fusion ($\Delta_{fus}H_i$) and activity ($\ln a_i$) of species i. Using this equation, it is possible to calculate liquidus temperature. For the systems LiCl-KCl-CsCl-$RECl_3$ salt mixtures tested for this work, it would be challenging to use this equation since there are four species that need to be considered: LiCl, KCl, CsCl, and $RECl_3$. Of these four species, the activity of only one species, $RECl_3$ is known. One way to look at this equation intuitively is to consider the system as a pseudo binary system made of LiCl-KCl-$RECl_3$ and CsCl, since the liquidus temperatures shows a depression from the baseline liquidus temperature of the LiCl-KCl-$RECl_3$ temperature. Now when CsCl is added to the ternary salt mixture, the activity of the LiCl-KCl-$RECl_3$ will decrease since its mole fraction decreases. In terms of Equation 7.1, this implies that the value of a_i decreases. This implies that the term $\ln a_i$ is a larger negative number. This means that the denominator in Equation 7.1 is larger causing the term, $T_{i,liq}$, on the left hand side to be smaller. This is consistent with the observations reported in this work.

Another possibility is to calculate the activity of all of the other species using the Gibbs-Duhem Equation. An attempt to do such calculations proved not to be successful. For using the Gibbs-Duhem equation to be successful, the system needs to be again evaluated as a pseudo binary system with $RECl_3$ and one species and LiCl-KCl-CsCl as the other pseudo species. In such calculations, it would only be able to calculate the activity composite LiCl-KCl-CsCl phase. However such calculations proved to be extremely challenging. When the activity coefficient of the known species, $RECl_3$, is determined as a function of electrolyte (LiCl-KCl-CsCl) mole fraction as a polynomial function, the coefficient fits huge numbers of the 10^8 order of magnitude. Hence the standard deviations for such coefficients of fit are very large for these calculations. This gives generally very inaccurate numbers for the activity of the base electrolyte. This has been a general criticism of the use of polynomial functions for representation of excess functions in the literature.[48]

7.4.2 Aspects of Coordination Chemistry

As discussed above, it is hard to discern the reasons for changes in phase behavior of molten salt systems. In this subsequent discussion, an attempt will be made to look at the phase behavior through the lens of coordination chemistry.

Before a specific discussion on the behavior of the particular rare earths is embarked upon, a general discussion on the influence of CsCl to the intermolecular structure of rare earth in molten salts is appropriate. The presence of alkali metals plays the role of network breaker with an increasing efficiency when going from Li to Cs, i.e., the octahedral network structure of $LnCl_6^{3-}$ (Ln: Lanthanide) that is known to be present in molten salts is broken with increasing efficiency going from Li to Cs. When an alkali chloride is added to a melt, the network is broken down by the incorporation of the added Cl^- ions into the coordination shells of the $LnCl_3$ ions. The extent to which this happens depends on the facility with which the alkali cations 'release' their Cl^- ions; Cs^+ is expected to do this to a greater extent than other alkali ions and from this perspective is a better structure breaker.[101]

The addition of CsCl into an LiCl-KCl-$RECl_3$ molten salt mixture thus introduces into the salt mixture a species (Cs) of the same chemical family, alkali metal, as the base salt albeit one that is a more powerful structure breaker than Li and K already present in the salt. In addition, the Cs^+ ion is much larger than either the Li or K ions.[2] This large ionic size also seems to play an important role in altering the behavior lanthanides in molten salt systems.

Rollet and Salanne[86] presented evidence to draw the conclusion that since alkali metals are structure breakers, they isolate the $LnCl_6^{3-}$ species present in the molten salt. Furthermore, the bigger the alkali earth species, the stronger the decrease in the coordination number of anion around the cation. These general observations are also true for other rare earth halides - alkali halide combinations.[102]

First looking at the LiCl-KCl-CsCl-$LaCl_3$ mixtures, two important observations can be made. First, at the low CsCl concentration of 0.70 mol %, the peak of the low temperature endothermic event is small and does seem to get bigger with increasing $LaCl_3$ concentration (see Figure B.2). Another observation is that for the LiCl-KCl-CsCl-$LaCl_3$ mixtures with 1.40 mol % CsCl, the peak of the low temperature endothermic event is much more prominent than the comparable peaks with of the mixtures with 0.70 mol % CsCl (see Figure

B.3. It is clear from these sets of data that at high CsCl and high $LaCl_3$ concentrations there seem to be some intermolecular interactions that cause the low temperature endothermic event peaks to be more prominent.

If the activity coefficient data for $LaCl_3$ is taken into account, it seems to reinforce the findings from the phase diagrams. From Figure 5.9, it is clear that the open circuit potential (and by extension activity) of $LaCl_3$ is influenced heavily at both high CsCl and high LaC_3 concentration similar to the conclusions from the thermograms.

This confirmed influence of CsCl on both the activity and the phase diagrams can be potentially explained by some existing literature. While there has been no study to date on the LiCl-KCl-CsCl-$LaCl_3$ systems, there have been a number of studies[85,101] performed on binary $LaCl_3-CsCl$ molten salt mixtures. Okamoto et al.[85] reported that the introduction of CsCl into pure $LaCl_3$ melt causes the coordination number of Cl^- to decrease from 8 to a limiting case of 6 (octahedral structure) with increasing CsCl concentration. This finding concurs with the conclusions that were drawn by Rollet and Salanne[86] that the bigger the alkali earth species the stronger the decrease in the coordination number of anion around cation. The strong propensity of CsCl to break up the structure of $LaCl_3$ will also be present when the $LaCl_3$ is dissolved in LiCl-KCl eutectic salt. The presence of two alkali metals, Li and K, already disrupts the structure of $LaCl_3$ to a certain extent. However the introduction of a CsCl likely aggravates this disruption further. This would be the reason for the change in behavior of the LiCl-KCl-$LaCl_3$ system when CsCl is introduced from a coordination chemistry standpoint.

Interestingly, Okamoto et al.[85] also noted that based on related works[103,104] other trivalent metal ions show different behavior when mixed with alkali halides. Ions smaller than La^{3+}, like Y^{3+} or Dy^{3+}, which form six coordinate chloride crystals, appear not to change their coordination number on dilution in alkali chlorides. This indicates that not even all lanthanides behave identically underscoring the complexity of these studies in drawing meaningful interpretations.

The closely related system of $NdCl_3$-ACl (A = Li, Na, K, Cs) is much harder to comment on since it has been studied by only a handful of authors.[105–107] The $NdCl_3$ also shows an octahedral structure with $NdCl_6^{3-}$ ions[105] in the presence of alkali ions like Cs^+. The reason this system behaves vastly differently from the $LaCl_3$ system is not well understood.

For the $GdCl_3$-ACl system, again an octahedral $GdCl_6^{3-}$ structure has been reported in the literature.[108,109] Though no studies are present on the $GdCl_3$-CsCl system, studies on the $GdCl_3$-KCl[108] and $GdCl_3$-LiCl-KCl[109] systems exist. It is hard to conclude much from either of these two studies on the possible interactions of CsCl with $GdCl_3$. However on the phase diagram behavior and the general interaction of lanthanides with CsCl some information can be hypothesized. In the phase diagrams, a lower temperature peak is observed only at high CsCl and low $GdCl_3$ concentrations. This indicates that if CsCl does break the network structures of $GdCl_3$, it is probably more effective at high Cs/Gd ratios.

In the above discussion, it is recognized that the explanations and potential conclusions may be incomplete. However given the complex nature of the systems studied here and the unique behavior of each rare earth, it is hard to ascertain the exact causes for the various phenomena observed and reported here.

7.5 Summary

In this chapter, the solidus and liquidus temperatures for three quaternary system were studied and reported. These systems were the LiCl-KCl-CsCl-$RECl_3$ (RE = La, Nd, and Gd) mixtures. It is observed that the presence of CsCl causes a slight depression in the liquidus temperature for all of the three rare earth chlorides when compared to the corresponding ternary system liquidus temperatures in the absence of any CsCl. The $LaCl_3$ quaternary system (with CsCl) manifests a peritectic behavior as opposed to eutectic behavior of ternary systems (no CsCl).

The $GdCl_3$ quaternary system shows a peritectic behavior only in a limited concentration windows, at low $GdCl_3$ and high CsCl concentrations. The $NdCl_3$ system shows a eutectic behavior throughout the concentrations range tested in this work, albeit with a slight depression in the liquidus temperatures in the presence of CsCl.

CHAPTER 8

CONCLUSIONS

Within the broad theme of minimization of waste generated in the pyrochemical processing of spent nuclear fuel, this dissertation pursues research into three subject areas: waste disposal using H-Y zeolite, activity of rare earth chlorides and quaternary phase diagram development for LiCl-KCl-CsCl-$RECl_3$ systems.

The treatment of the salt waste using H-Y zeolite was investigated in the first part of this work. It was demonstrated that the ion exchange was successfully performed between the anions in the eutectic salt and H-Y zeolite. This results in the evolution of HCl gas. This evolution of HCl will result in reduction of the mass of the final waste form. However the leach tests demonstrate that much of the salt easily leaches from the zeolite. This is evidence of unreacted chloride salt. Further the maximum loading that was achieved was about 50 % of theoretical maximum. Additional improvements need to be made to improve both the efficiency of loading and to make the waste form more leach resistant.

Experimental data derived from EMF measurements provide compelling data that the activity coefficients of the three rare earth chlorides are heavily dependent on concentration. This reveals the error that other researchers have made by reporting a single apparent reduction potential, which implies that there is a single low concentration activity coefficient. No evidence was observed to support the hypothesis that activity coefficient approaches a constant at infinite dilution.

From the activity measurements of the four rare earth chlorides, a definite correlation with ionic radius was observed. It is evident that the lanthanides show a larger negative deviation from ideal solution behavior with decreasing ionic size, i.e., the smaller the size of the radius of the metal, the greater the departure from ideal solution behavior for the rare earth chlorides. In some cases, CsCl interacts with rare earth chlorides in LiCl-KCl to affect their activity at a fixed mole fraction. This complicates the prediction of activity and

reduction potentials during an electrochemical drawdown process applied to electrorefiner salt.

Stable reference electrodes can be prepared using a rare earth metal in equilibrium with a salt mixture saturated with the corresponding rare earth chloride. This allows for almost direct measurement of activities via EMF measurements. The only adjustments needed are for correcting rare earth chloride standard states from solid to liquid. Using the activity data, a scoping study in this work showed that it is possible to successfully drawdown uranium(III) chloride from LiCl-KCl using an electrochemical galvanic couple established between the U/UCl_3 and $Gd/GdCl_3$ redox couples.

The phase diagrams for the LiCl-KCl-CsCl-$RECl_3$ were developed. In general it is seen that the presence of CsCl depresses the liquidus temperature slightly for all of the systems tested. Additionally, the phase diagram for the LiCl-KCl-CsCl-$LaCl_3$ departs from eutectic to peritectic behavior in the presence of CsCl, showing a solidus line at around 300°C and liquidus line at around 350°C. The phase diagrams for LiCl-KCl-CsCl-$NdCl_3$ continue to manifest eutectic behavior in the presence of CsCl. However the LiCl-KCl-CsCl-$NdCl_3$ does show a few degree depression in the melting point in the presence of CsCl. For the LiCl-KCl-CsCl-$GdCl_3$ system, the system departs from eutectic to peritectic behavior at low $GdCl_3$ concentrations (below 0.35 mol %) and high CsCl concentration (1.43 mol %). Above the 0.35 mol % $GdCl_3$, the system reverts back to eutectic behavior.

APPENDIX A

ELECTROCHEMICAL DATA

Table A.1. Experimental data for the LiCl-KCl-$LaCl_3$ at 773 K

Sample ID	X_{LaCl_3}	X_{CsCl}	OCP
	mol %	mol %	V vs. Cl^-/Cl_2
8-02	0.04	0	-3.297
8-03	0.06	0	-3.294
8-04	0.09	0	-3.280
8-05	0.19	0	-3.258
8-06	0.27	0	-3.240
8-07	0.43	0	-3.233
8-08	0.57	0	-3.223
8-09	0.72	0	-3.213
8-10	1.30	0	-3.209
8-11	2.19	0	-3.206
8-12	2.42	0	-3.202
8-13	2.64	0	-3.200

Table A.2. Experimental data for the LiCl-KCl-CsCl-$LaCl_3$ at 773 K

Sample ID	X_{LaCl_3}	X_{CsCl}	OCP
	mol %	mol %	V vs. Cl^-/Cl_2
11-03	0.03	0.68	-3.297
11-04	0.05	0.68	-3.291
11-05	0.09	0.68	-3.279
11-06	0.13	0.67	-3.268
11-07	0.19	0.67	-3.259
11-08	0.29	0.69	-3.245
11-09	0.51	0.68	-3.230
11-10	0.89	0.71	-3.220
11-11	1.32	0.70	-3.213
11-12	1.94	0.74	-3.204
11-13	2.09	0.72	-3.202
11-14	2.73	0.75	-3.192

Table A.3. Experimental data for the LiCl-KCl-CsCl-$LaCl_3$ at 773 K

Sample ID	X_{LaCl_3}	X_{CsCl}	OCP
	mol %	mol %	V vs. Cl^-/Cl_2
14-01	0.18	1.35	-3.257
14-02	0.25	1.33	-3.251
14-03	0.24	1.34	-3.251
14-04	0.32	1.35	-3.245
14-05	0.42	1.37	-3.238
14-06	0.67	1.36	-3.222
14-07	1.20	1.44	-3.200
14-08	1.58	1.43	-3.190
14-09	1.88	1.43	-3.185
14-10	2.42	1.50	-3.181
14-11	3.07	1.49	-3.182

Table A.4. Experimental data for the LiCl-KCl-$GdCl_3$ at 773 K

Sample ID	X_{GdCl_3}	X_{CsCl}	OCP
	mol %	mol %	V vs. $Gd/GdCl_{3(l)}$
18Gd-02	0.02	0	-0.369
18Gd-03	0.04	0	-0.366
18Gd-04	0.05	0	-0.366
18Gd-05	0.14	0	-0.358
18Gd-06	0.32	0	-0.346
18Gd-07	0.62	0	-0.333
18Gd-08	1.03	0	-0.321
18Gd-09	1.41	0	-0.313
18Gd-10	1.84	0	-0.305
18Gd-11	2.34	0	-0.297
18Gd-12	3.12	0	-0.284
18Gd-13	4.37	0	-0.265

Table A.5. Experimental data for the LiCl-KCl-CsCl-$GdCl_3$ at 773 K

Sample ID	X_{GdCl_3}	X_{CsCl}	OCP
	mol %	mol %	V vs. $Gd/GdCl_{3(l)}$
20Gd-02	0.03	0.70	-0.386
20Gd-03	0.06	0.70	-0.380
20Gd-04	0.11	0.70	-0.373
20Gd-05	0.17	0.70	-0.365
20Gd-06	0.31	0.70	-0.352
20Gd-07	0.66	0.70	-0.335
20Gd-08	1.15	0.70	-0.322
20Gd-09	1.66	0.69	-0.312
20Gd-10	2.23	0.69	-0.301
20Gd-11	2.92	0.68	-0.289
20Gd-12	3.72	0.68	-0.275
20Gd-13	4.29	0.67	-0.266
20Gd-14	4.29	1.31	-0.273
20Gd-15	4.29	1.92	-0.276
20Gd-16	4.29	2.59	-0.279
20Gd-17	4.29	3.53	-0.282

Table A.6. Experimental data for the LiCl-KCl-$CeCl_3$ at 773 K

Sample ID	X_{CeCl_3}	X_{CsCl}	OCP
	mol %	mol %	V vs. $Ce/CeCl_{3(l)}$
25Ce-01	0.01	0	-0.358
25Ce-02	0.04	0	-0.331
25Ce-03	0.08	0	-0.314
25Ce-04	0.14	0	-0.298
25Ce-05	0.21	0	-0.289
25Ce-06	0.36	0	-0.275
25Ce-07	0.75	0	-0.256
25Ce-08	1.36	0	-0.239
25Ce-09	2.11	0	-0.226
25Ce-10	2.99	0	-0.214
25Ce-11	3.83	0	-0.205
25Ce-12	4.66	0	-0.197
25Ce-13	4.66	0.66	-0.198
25Ce-14	4.66	1.92	-0.196

Table A.7. Experimental data for the LiCl-KCl-$NdCl_3$ at 773 K

Sample ID	X_{NdCl_3}	X_{CsCl}	OCP
	mol %	mol %	V vs. Cl^-/Cl_2
18Nd-01	0.06	0	-3.241
18Nd-02	0.13	0	-3.223
18Nd-03	0.21	0	-3.214
18Nd-04	0.33	0	-3.203
18Nd-05	0.56	0	-3.195
18Nd-06	0.68	0	-3.187
18Nd-07	0.98	0	-3.182
18Nd-08	1.33	0	-3.174
18Nd-09	2.00	0	-3.166
18Nd-10	2.82	0	-3.158

APPENDIX B

PHASE DIAGRAM THERMOGRAMS

In this appendix, the raw thermograms generated for the phase diagram work that was presented in this work has been presented for four rare earth chlorides: $LaCl_3$, $NdCl_3$, $GdCl_3$, and $CeCl_3$.

B.1 Lanthanum Chloride System

In this section, the phase diagrams for the LiCl−KCl−CsCl−$LaCl_3$ system are presented: Figures B.1, B.2, and B.3.

B.2 Neodymium Chloride System

In this section, the phase diagrams for the LiCl−KCl−CsCl−$NdCl_3$ system are presented: Figures B.4, B.5, and B.6.

B.3 Gadolinium Chloride System

In this section, the phase diagrams for the LiCl−KCl−CsCl−$GdCl_3$ system are presented: Figures B.7, B.8, B.9, and B.10.

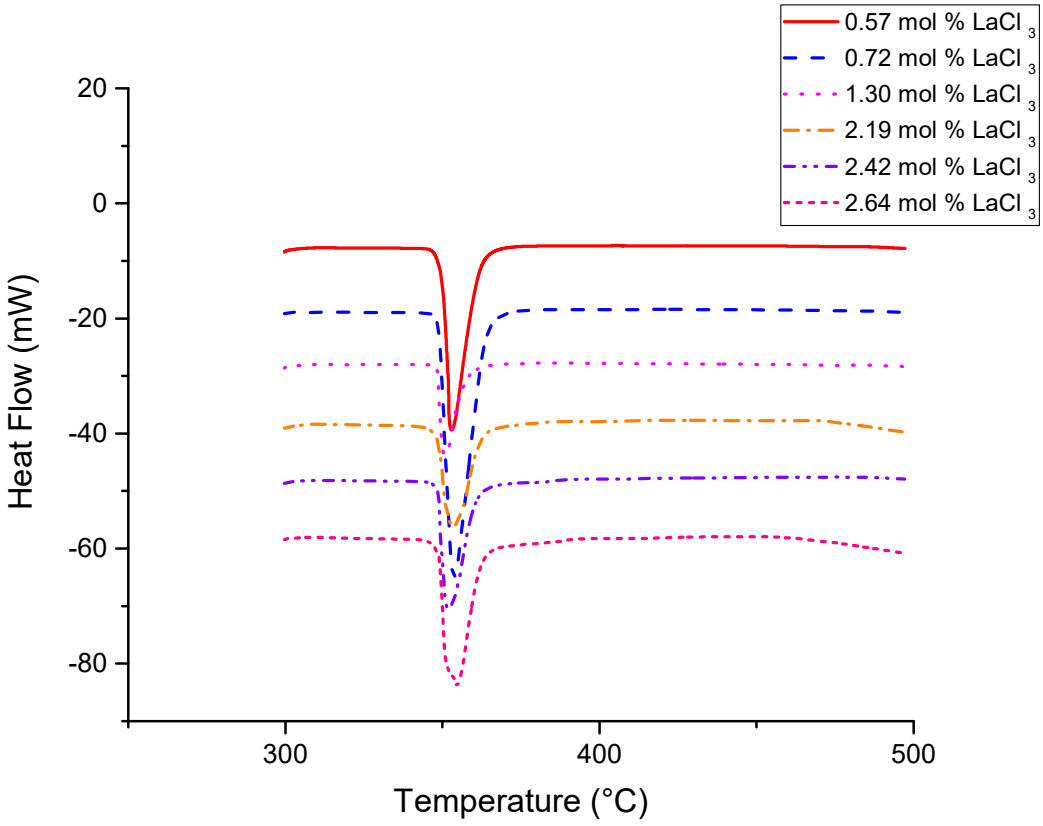

Figure B.1. Heat flow versus temperature curves generated from the TGA/DTA instrument for the LiCl−KCl−$LaCl_3$ system.

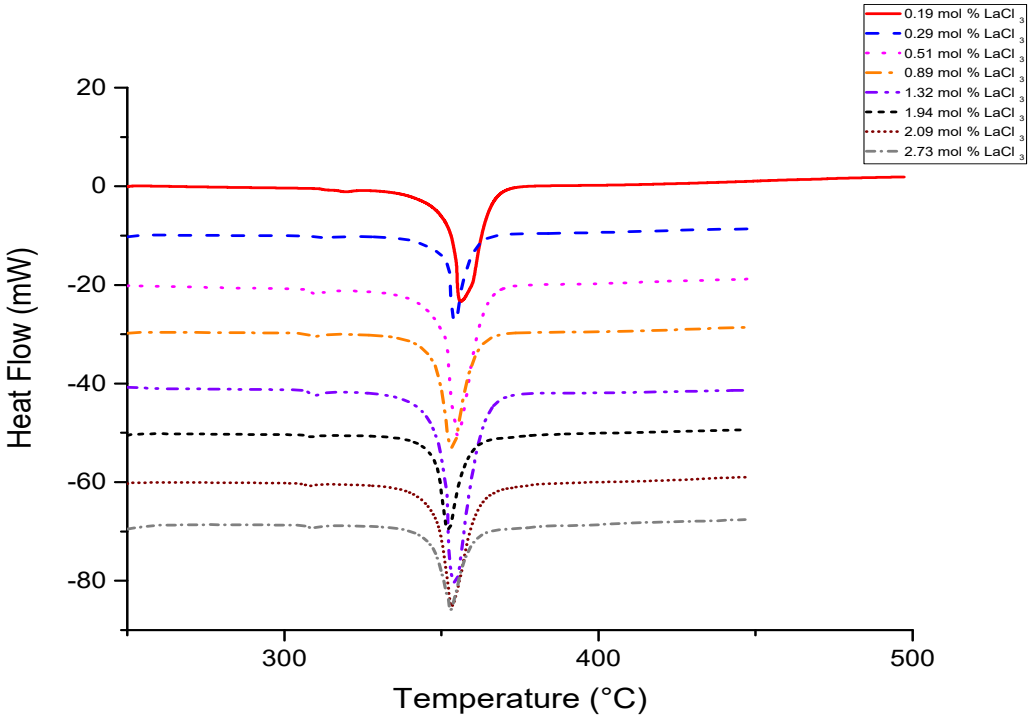

Figure B.2. Heat flow versus temperature curves generated from the TGA/DTA instrument for the LiCl−KCl−CsCl−$LaCl_3$ system with 0.69 mole % CsCl present.

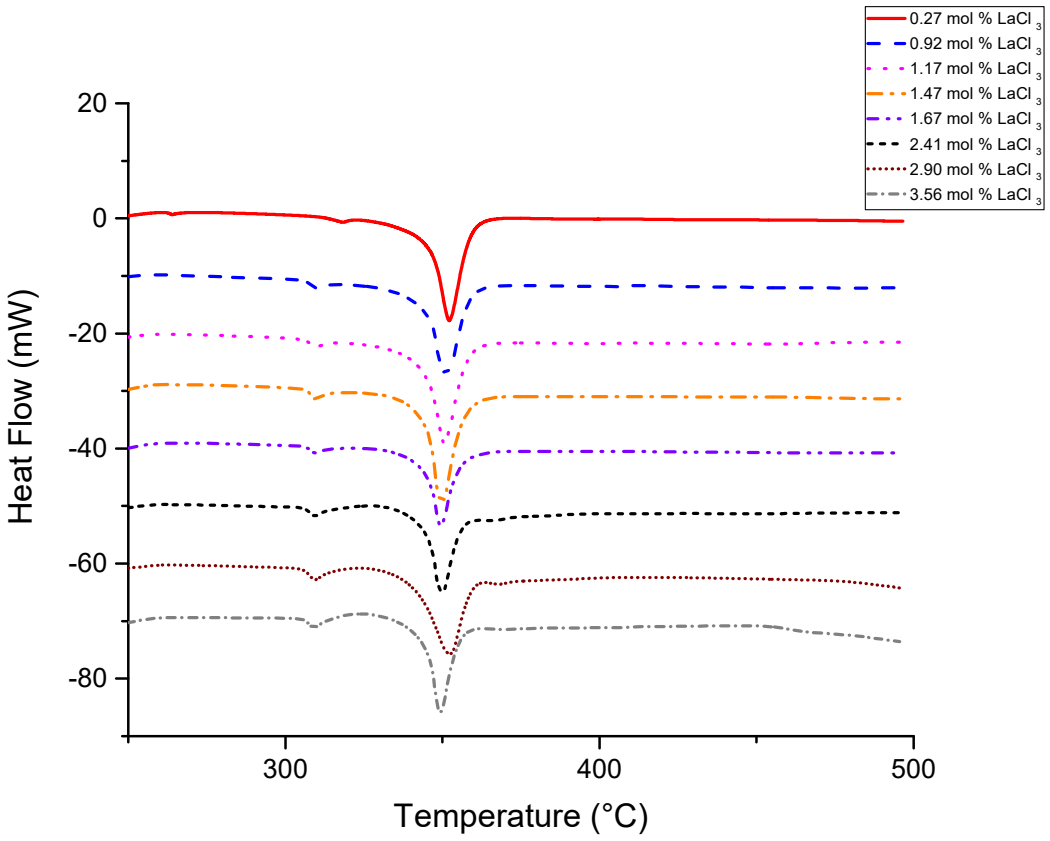

Figure B.3. Heat flow versus temperature curves generated from the TGA/DTA instrument for the LiCl−KCl−CsCl−$LaCl_3$ system with 1.40 mole % CsCl present.

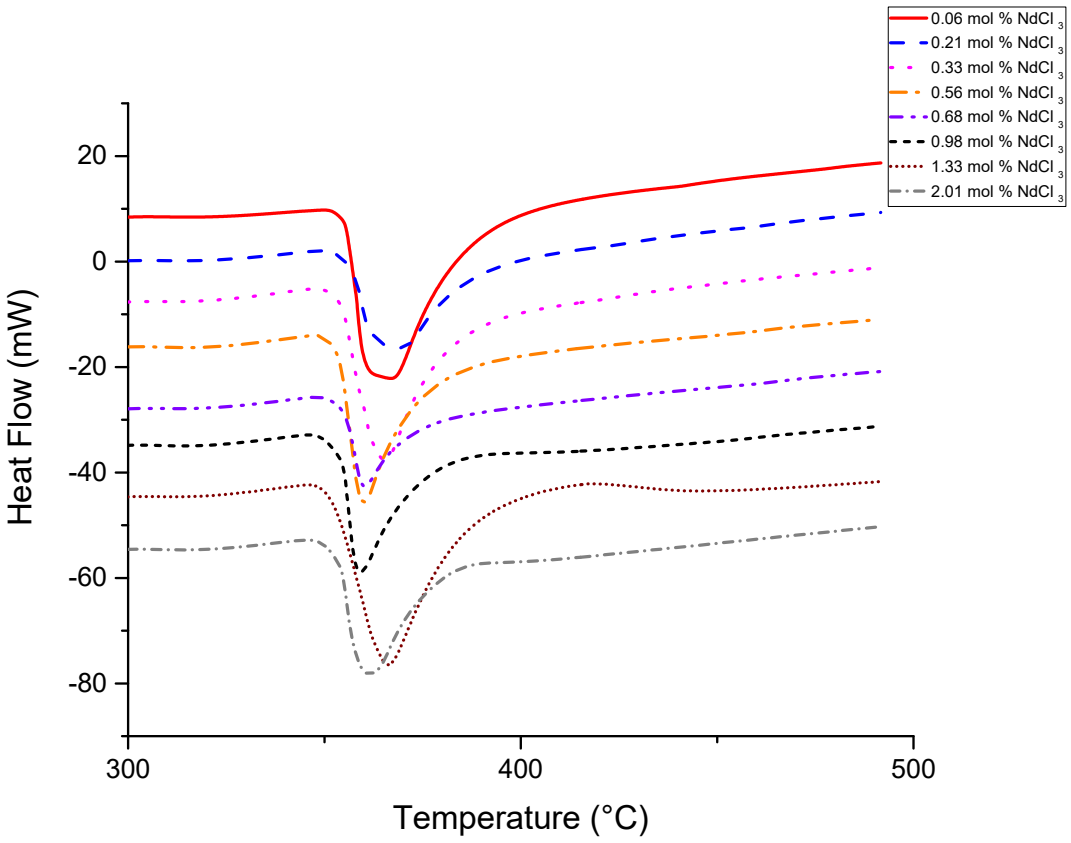

Figure B.4. Heat flow versus temperature curves generated from the TGA/DTA instrument for the LiCl−KCl−$NdCl_3$ system

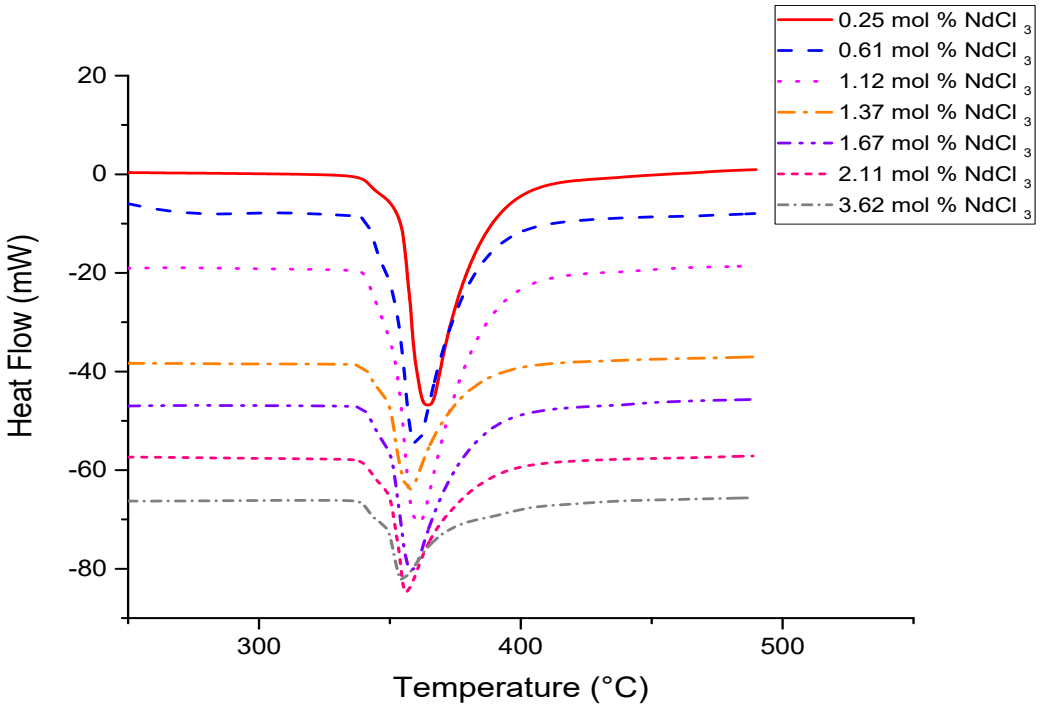

Figure B.5. Heat flow versus temperature curves generated from the TGA/DTA instrument for the LiCl−KCl−CsCl−$NdCl_3$ system with 0.54 mol % CsCl present

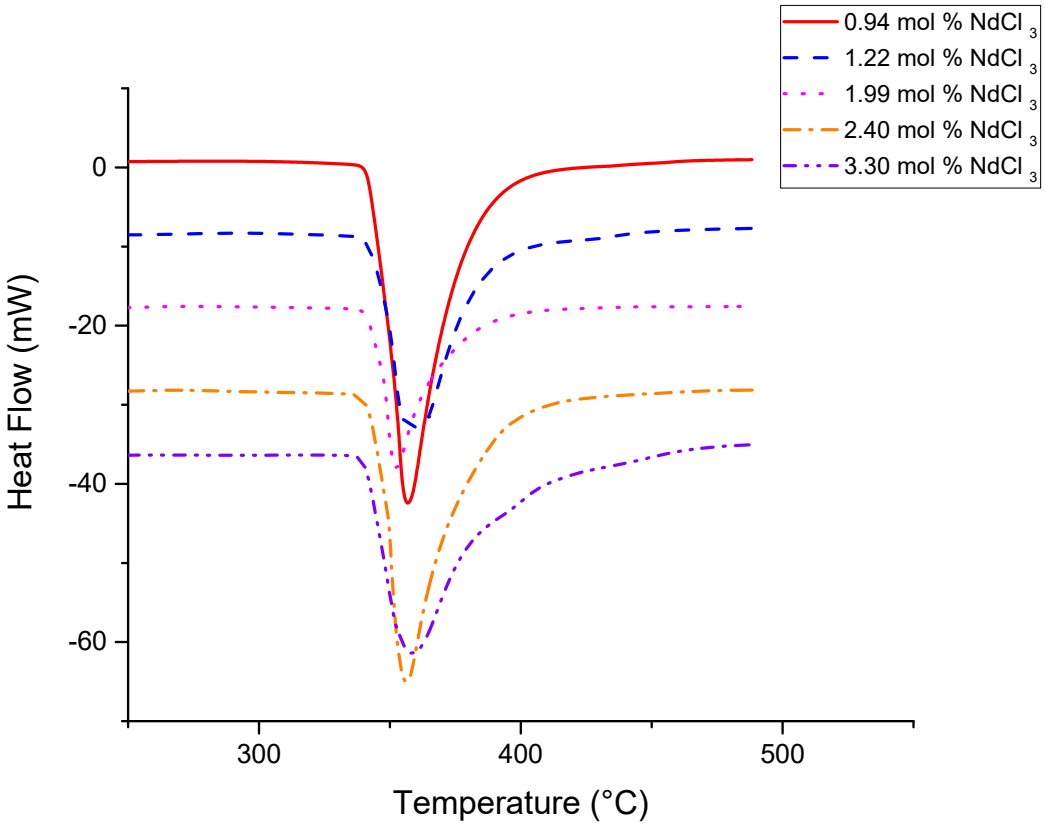

Figure B.6. Heat flow versus temperature curves generated from the TGA/DTA instrument for the LiCl−KCl−CsCl−$NdCl_3$ system with 1.21 mole % CsCl present.

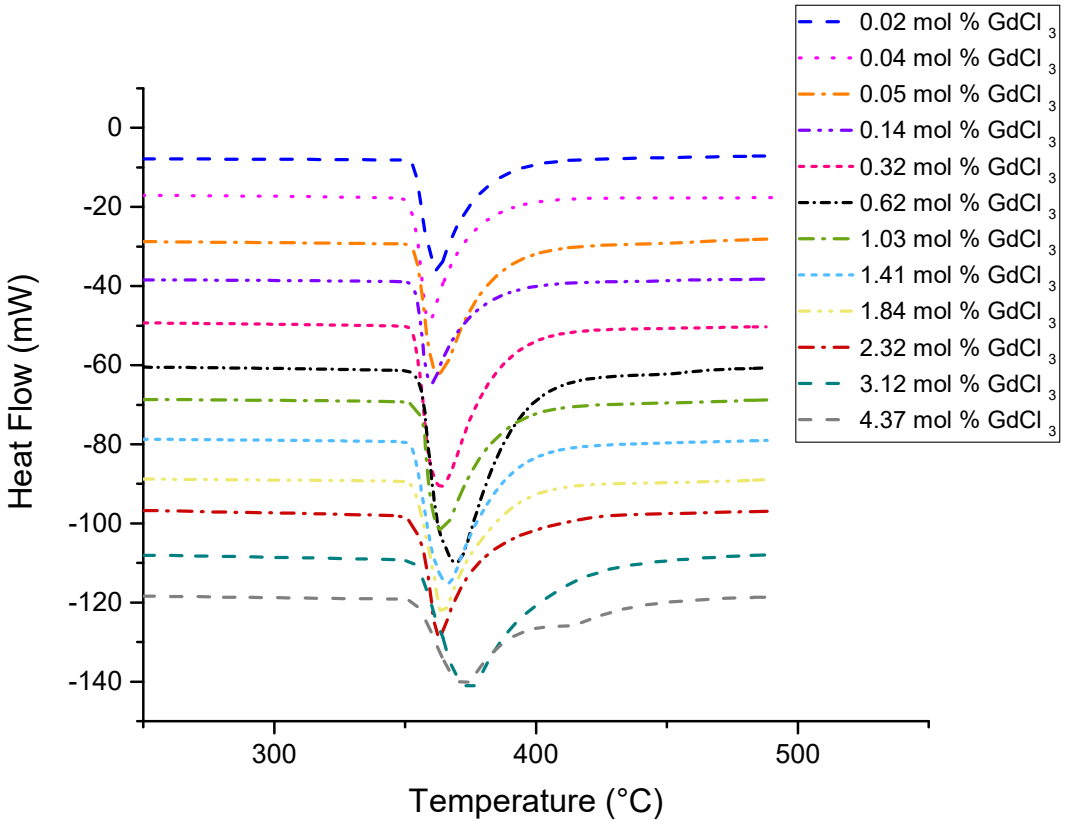

Figure B.7. Heat flow versus temperature curves generated from the TGA/DTA instrument for the LiCl−KCl−$GdCl_3$ system.

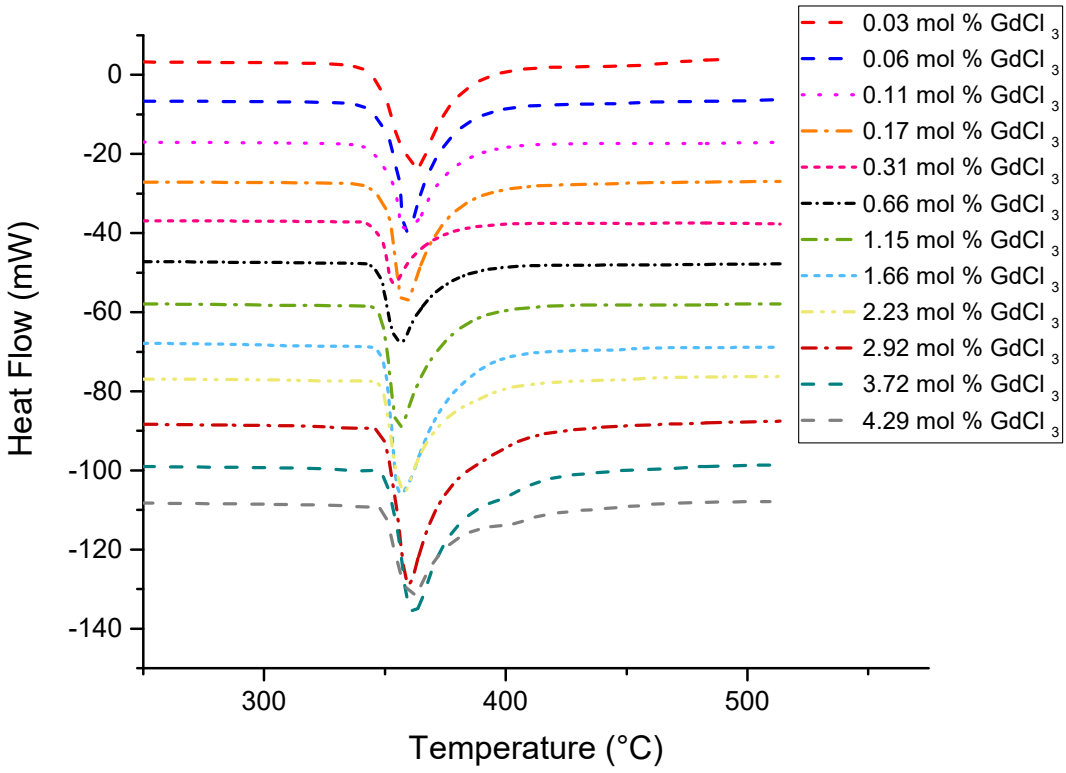

Figure B.8. Heat flow versus temperature curves generated from the TGA/DTA instrument for the LiCl−KCl−CsCl−$GdCl_3$ system with 0.69 mol % CsCl present.

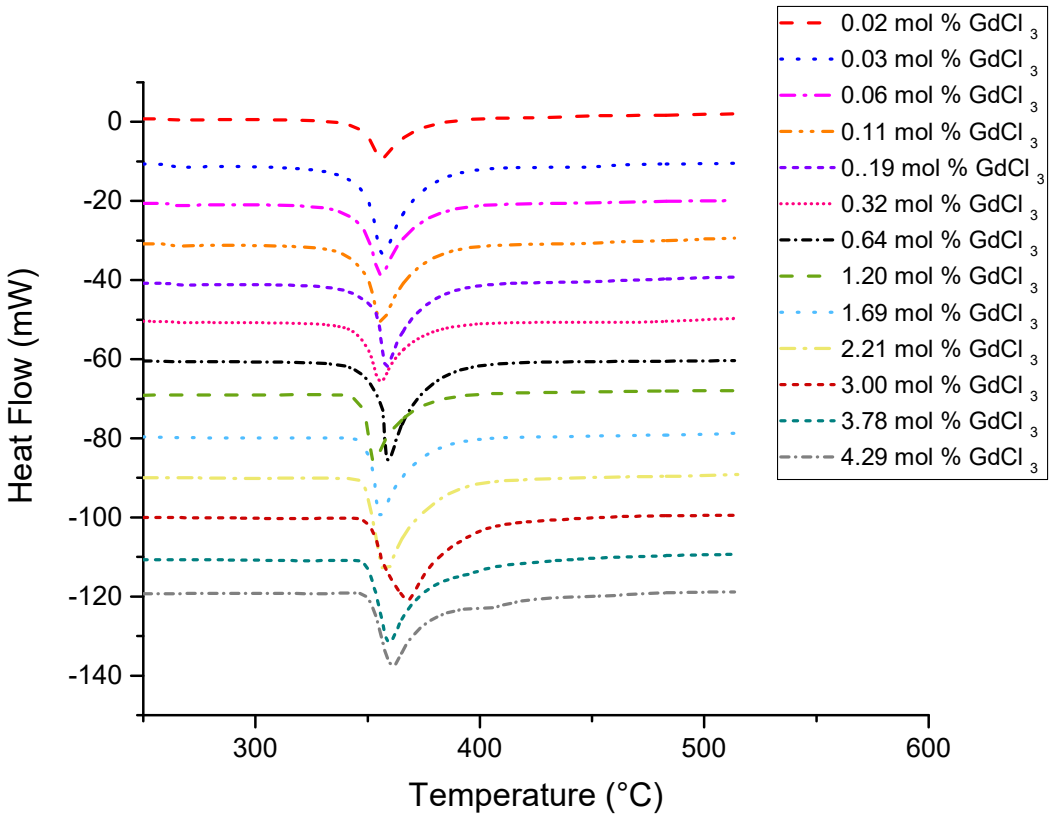

Figure B.9. Heat flow versus temperature curves generated from the TGA/DTA instrument for the LiCl−KCl−CsCl−$GdCl_3$ system with 1.43 mol % CsCl present.

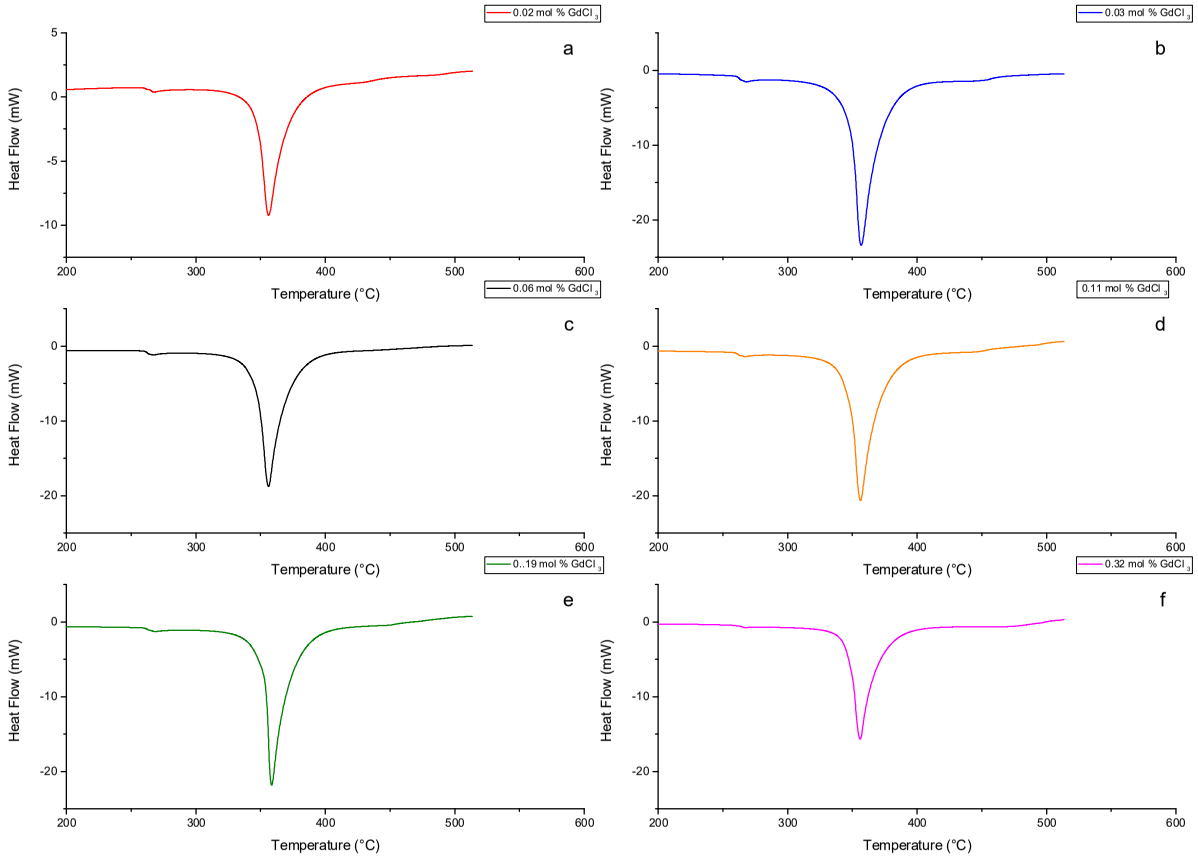

Figure B.10. Heat flow versus temperature curves generated from the TGA/DTA instrument for the LiCl−KCl−CsCl−$GdCl_3$ system with 1.43 mol % CsCl present showing a low temperature peak which represents the solidus temperature for this system.

REFERENCES

[1] Lewin, R.; Harrison, M. In *Reprocessing and Recycling of Spent Nuclear Fuel*; Taylor, R., Ed.; Woodhead Publishing Series in Energy; Woodhead Publishing: Oxford, 2015; pp 373 – 413.

[2] Database of Ionic Radii. http://abulafia.mt.ic.ac.uk/shannon/ptable.php.

[3] Roston, E. *The Carbon Age: How Life's Core Element Has Become Civilization's Greatest Threat*; Walker Books: New York, 2010.

[4] Council, N. R. *Advancing the Science of Climate Change*; The National Academies Press: Washington, DC, 2010.

[5] IPCC, *Climate Change 2014–Impacts, Adaptation and Vulnerability*; Cambridge University Press: New York, 2014.

[6] IEA, *Key World Energy Statistics*; International Energy Agency: France, 2015.

[7] Lovasic, Z. *IAEA Report: IAEA-TECDOC-1587*; Blackwell Publishing: Vienna, 2008.

[8] Willit, J.; Miller, W.; Battles, J. *Journal of Nuclear Materials* **1992**, *195*, 229–249.

[9] Cassayre, L.; Malmbeck, R.; Masset, P.; Rebizant, J.; Serp, J.; Soucek, P.; Glatz, J.-P. *Journal of Nuclear Materials* **2007**, *360*, 49–57.

[10] Uozumi, K.; Iizuka, M.; Kato, T.; Inoue, T.; Shirai, O.; Iwai, T.; Arai, Y. *Journal of Nuclear Materials* **2004**, *325*, 34–43.

[11] Johnson, T.; Li, S.; Marsden, K.; Goff, C., K. M. with Solbrig; Westphal, B. R. *Pyroprocessing progress at Idaho national Laboratory*; 2007.

[12] Lee, J.; Kang, Y.; Hwang, S.; Lee, H.; Kim, E.; Park, S. *Nuclear Technology* **2008**, *162*, 107–116.

[13] Lee, J.; Oh, K.; Kang, Y.; Hwang, S.; Lee, H.; Shim, J.; Kim, E.; Park, S. *Nuclear Technology* **2009**, *165*, 370–379.

[14] Magill, J.; Berthou, V.; Haas, D.; Galy, J.; Schenkel, R.; Wiese, J.; Heusener, G.; Tommasi, J.; Youinou, G. *Nuclear Energy-London* **2003**, *42*, 263–278.

[15] Souček, P.; Malmbeck, R.; Mendes, E.; Nourry, C.; Glatz, J.-P. *Journal of Radioanalytical and Nuclear Chemistry* **2010**, *286*, 823–828.

[16] Souček, P.; Malmbeck, R.; Nourry, C.; Glatz, J.-P. *Energy Procedia* **2011**, *7*, 396–404.

[17] Song, K.-C.; Lee, H.-S.; Hur, J.-M.; Kim, J.-G.; Ahn, D.-H.; Cho, Y.-Z. *Nuclear Engineering and Technology* **2010**, *42*, 131–144.

[18] Kinoshita, K.; Inoue, T.; Fusselman, S.; Grimmett, D.; Roy, J.; Gay, R.; Krueger, C.; Nabelek, C.; Storvick, T. *Journal of Nuclear Science and Technology* **1999**, *36*, 189–197.

[19] Williamson, M.; Willit, J. *Nuclear Engineering and Technology* **2011**, *43*, 329–334.

[20] Plambeck, J. A. *Journal of Chemical & Engineering Data* **1967**, *12*, 77–82.

[21] Tang, H.; Pesic, B. *Electrochimica Acta* **2014**, *119*, 120–130.

[22] Lantelme, F.; Berghoute, Y. *Journal of the Electrochemical Society* **1999**, *146*, 4137–4144.

[23] Masset, P.; Konings, R. J.; Malmbeck, R.; Serp, J.; Glatz, J.-P. *Journal of Nuclear Materials* **2005**, *344*, 173–179.

[24] Castrillejo, Y.; Bermejo, M.; Barrado, E.; Martınez, A.; Arocas, P. D. *Journal of Electroanalytical Chemistry* **2003**, *545*, 141–157.

[25] Tang, H.; Pesic, B. *Journal of The Electrochemical Society* **2014**, *161*, D429–D436.

[26] Caravaca, C.; De Cordoba, G.; Tomas, M.; Rosado, M. *Journal of Nuclear Materials* **2007**, *360*, 25–31.

[27] Marsden, K. C.; Pesic, B. *Journal of The Electrochemical Society* **2011**, *158*, F111–F120.

[28] Zhang, M.; Han, W.; Zhang, M.; Li, Y.; Zhu, F.; Xue, Y. *Chemical Research in Chinese Universities* **2014**, *30*, 489–494.

[29] Sridharan, K.; Martin, S.; Mohammadian, M.; Sager, J.; Allen, T.; Simpson, M. *Thermal Properties of LiCl-KCl Molten Salt for Nuclear Waste Separation*; 2012; Department of Energy's Nuclear Energy University Program final report project No. 09-780.

[30] Nakamura, K.; Kurata, M. *Journal of Nuclear Materials* **1997**, *247*, 309–314.

[31] Battisti, T. J.; Goff, K. M.; Bateman, K. J.; Simpson, M. F.; Lind, J. P. *Proceedings of 5th Topical DOE Spent Nuclear Fuel and Fissile Materials Management* **2002**, 17–20.

[32] Goff, K.; Simpson, M.; Bateman, K.; Esh, D. *Transactions of the American Nuclear Society* **1997**, *77*.

[33] Simpson, M. F.; Goff, K. M.; Johnson, S. G.; Bateman, K. J.; Battisti, T. J.; Toews, K. L.; Frank, S. M.; Moschetti, T. L.; O'Holleran, T. P.; Sinkler, W. *Nuclear Technology* **2001**, *134*, 263–277.

[34] Simpson, M. F.; Battisti, T. J. *Industrial & Engineering Chemistry Research* **1999**, *38*, 2469–2473.

[35] Morrison, M. C.; Bateman, K. J.; Simpson, M. F. Scale-Up of Ceramic Waste Forms for the EBR-II Spent Fuel Treatment Process. International Pyroprocessing Research Conference, Idaho National Laboratory, INL/CON-10-19439. 2010.

[36] Priebe, S.; Bateman, K. *Nuclear Technology* **2008**, *162*, 199–207.

[37] Simpson, M. F.; Sachdev, P. *Nuclear Engineering and Technology* **2008**, *40*, 175–182.

[38] Wang, Y.; Rath, J.; Hansen, F.; Lee, J. H.; Jove-Colon, C.; McMahon, K.; Swift, P. Closing the Nuclear Fuel Cycle with Salt. 13th International High-Level Radioactive Waste Management Conference. 2011.

[39] Benedict, R.; Goff, M.; Teske, G.; Johnson, T. *Journal of Nuclear Science and Technology* **2002**, *39*, 749–752.

[40] Jia, C.; Massiani, P.; Beaunier, P.; Barthomeuf, D. *Applied Catalysis A: General* **1993**, *106*, L185–L191.

[41] Nassar, E. J.; Serra, O. A. *Materials Chemistry And Physics* **2002**, *74*, 19–22.

[42] Breck, D. W. Molecular sieve-metal agglomerates and their preparation. 1965; US Patent 3,181,231.

[43] Allensworth, J. R.; Simpson, M. F.; Yim, M.-S.; Phongikaroon, S. *Nuclear Technology* **2013**, *181*, 337–348.

[44] Guggenheim, E. A. *Amsterdam, North-Holland, 1985, 414 p.* **1985**,

[45] Guggenheim, E. *The Journal of Physical Chemistry* **1929**, *33*, 842–849.

[46] Rockwood, A. L. *ChemPhysChem* **2015**, *16*, 1978–1991.

[47] Robinson, R. A.; Stokes, R. H. *Electrolyte Solutions*; Courier Corporation, 2002.

[48] Pelton, A. D.; Bale, C. W. *Metallurgical Transactions A* **1986**, *17*, 1057–1063.

[49] Debye, P.; Hückel, E. *Physikalische Zeitschrift* **1923**, *24*, 185–206.

[50] Orgel, L. E. *An Introduction to Transition-Metal Chemistry: Ligand-Field Theory*; John Wiley and Sons, Inc., New York, 1966.

[51] Gruen, D. M.; Osteryoung, R. A. *Annals of the New York Academy of Sciences* **1960**, *79*, 897–907.

[52] Laitinen, H. A.; Liu, C. H. *Journal of the American Chemical Society* **1958**, *80*, 1015–1020.

[53] Bard, A. J.; Faulkner, L. R. *Electrochemical Methods: Fundamentals and Applications*; Wiley New York: New York, Vol. 2.

[54] Barin, I. *Thermochemical Data of Pure Substances, Third Edition*; Wiley-VCH Verlag GmbH: Germany, 1995.

[55] Blander, M. *Thermodynamic Properties of Molten Salt Solutions*; Oak Ridge National Laboratory: Oak Ridge, TN, 1986.

[56] Prausnitz, J. M.; Lichtenthaler, R. N.; de Azevedo, E. G. *Molecular Thermodynamics of Fluid-Phase Equilibria*; Prentice Hall PTR: New Jersey, 1998.

[57] Bagri, P.; Bastos, T.; Simpson, M. F. *ECS Transactions* **2016**, *75*, 489–495.

[58] Bagri, P.; Simpson, M. F. *Journal of Nuclear Materials* **2016**, *482*, 248–256.

[59] Yang, L.; Hudson, R. G. *Journal of The Electrochemical Society* **1959**, *106*, 986–990.

[60] Shirai, O.; Nagai, T.; Uehara, A.; Yamana, H. *Journal of Alloys and Compounds* **2008**, *456*, 498–502.

[61] Näfe, H. *Berichte der Bunsengesellschaft für physikalische Chemie* **1994**, *98*, 1281–1286.

[62] Inman, D.; Hills, G.; Young, L.; Bockris, J. *Annals of the New York Academy of Sciences* **1960**, *79*, 803–829.

[63] Gabbott, P. *Principles and Applications of Thermal Analysis*; Blackwell Publishing: New Jersey, 2008.

[64] Salanne, M.; Simon, C.; Turq, P.; Madden, P. A. *The Journal of Physical Chemistry B* **2008**, *112*, 1177–1183.

[65] Zhang, J. *Journal of Nuclear Materials* **2014**, *447*, 271–284.

[66] Shirai, O.; Uehara, A.; Fujii, T.; Yamana, H. *Journal of Nuclear Materials* **2005**, *344*, 142 – 145, Proceedings of the 11th International Symposium on Thermodynamics of Nuclear Materials.

[67] Kuznetsov, S.; Hayashi, H.; Minato, K.; Gaune-Escard, M. *Journal of Nuclear Materials* **2005**, *344*, 169 – 172, Proceedings of the 11th International Symposium on Thermodynamics of Nuclear Materials.

[68] Bagotsky, V. S. *Fundamentals of Electrochemistry*; John Wiley & Sons: New Jersey, 2005; Vol. 44.

[69] Milchev, A. *Electrocrystallization: Fundamentals of Nucleation and Growth*; Springer Science & Business Media: New York, 2002.

[70] Wang, Y.; Zhou, W.; Zhang, J. *Journal of Nuclear Materials* **2016**, *478*, 61 – 73.

[71] Pitzer, K. S. *The Journal of Physical Chemistry* **1973**, *77*, 268–277.

[72] Pitzer, K. S.; Mayorga, G. *The Journal of Physical Chemistry* **1973**, *77*, 2300–2308.

[73] Pitzer, K. S.; Mayorga, G. *Journal of Solution Chemistry* **1974**, *3*, 539–546.

[74] Pitzer, K. S.; Kim, J. J. *Journal of the American Chemical Society* **1974**, *96*, 5701–5707.

[75] Pitzer, K. S. *Journal of Solution Chemistry* **1975**, *4*, 249–265.

[76] Papatheodorou, G. *Inorganic and Nuclear Chemistry Letters* **1975**, *11*, 483–490.

[77] Iwadate, Y.; Matsuura, H.; Kajinami, A.; Takase, K.; Ohtori, N.; Umesaki, N.; Fujita, R.; Mizuguchi, K.; Kofuji, H.; Myochin, M. *Electrochemistry* **2009**, *77*, 736–740.

[78] Wasse, J. C.; Salmon, P. S. *Journal of Physics: Condensed Matter* **1999**, *11*, 1381.

[79] Wasse, J. C.; Salmon, P. S.; Delaplane, R. G. *Physica B: Condensed Matter* **2000**, *276–278*, 433 – 434.

[80] Wasse, J. C.; Salmon, P. S. *Journal of Physics: Condensed Matter* **1999**, *11*, 9293.

[81] Saboungi, M.-L.; Price, D. L.; Scamehorn, C.; Tosi, M. P. *EPL (Europhysics Letters)* **1991**, *15*, 283.

[82] Okamoto, Y.; Hayashi, H.; Ogawa, T. *Japanese Journal of Applied Physics* **1999**, *38*, 156.

[83] Okamoto, Y.; Shiwaku, H.; Yaita, T.; Narita, H.; Tanida, H. *Journal of Molecular Structure* **2002**, *641*, 71 – 76.

[84] Okamoto, Y.; Madden, P. *Journal of Physics and Chemistry of Solids* **2005**, *66*, 448 – 451, Proceedings of the 11th International Conference on High Temperature Materials Chemistry (HTMC-XI).

[85] Okamoto, Y.; Suzuki, S.; Shiwaku, H.; Ikeda-Ohno, A.; Yaita, T.; Madden, P. A. *The Journal of Physical Chemistry A* **2010**, *114*, 4664–4671, PMID: 20225902.

[86] Rollet, A.-L.; Salanne, M. *Annu. Rep. Prog. Chem., Sect. C: Phys. Chem.* **2011**, *107*, 88–123.

[87] Bard, A. J.; Faulkner, L. R. *Electrochemical Methods: Fundamentals and Applications, 2nd Edition*; Wiley New York: New York, 2001.

[88] Fusselman, S. P.; Roy, J. J.; Grimmett, D. L.; Grantham, L. F.; Krueger, C. L.; Nabelek, C. R.; Storvick, T. S.; Inoue, T.; Hijikata, T.; Kinoshita, K.; Sakamura, Y.; Uozumi, K.; Kawai, T.; Takahashi, N. *Journal of The Electrochemical Society* **1999**, *146*, 2573–2580.

[89] Cantor, S. *The Journal of Physical Chemistry* **1961**, *65*, 2208–2210.

[90] Blander, M. *Molten Salt Chemistry*; Interscience Publishers: New York, 1964.

[91] Yang, L.; Hudson, R. *Transactions of the American Institute of Mining and Metallurgical Engineers* **1959**, *215*, 589–601.

[92] Kurata, M.; Sakamura, Y.; Hijikata, T.; Kinoshita, K. *Journal of Nuclear Materials* **1995**, *227*, 110–121.

[93] Ackerman, J. P.; Settle, J. L. *Journal of Alloys and Compounds* **1993**, *199*, 77–84.

[94] Kobayashi, T. *Journal of Nuclear Science and Technology* **2006**, *43*, 819–823.

[95] Yoo, J.-H.; Lee, H.-S.; Kim, E.-H. *Nuclear Engineering and Technology* **2007**, *39*, 663–672.

[96] Kwon, S. W.; Ahn, D. H.; Kim, E. H.; Ahn, H. G. *Journal of Industrial and Engineering Chemistry* **2009**, *15*, 86–91.

[97] Simpson, M. F.; Yoo, T. S.; Labrier, D.; Lineberry, M.; Shaltry, M.; Phongikaroon, S. *Nuclear Engineering and Technology* **2012**, *44*, 767–772.

[98] Li, S. X.; Herrmann, S.; Goff, K.; Simpson, M.; Benedict, R. *Nuclear Technology* **2009**, *165*, 190–199.

[99] Li, S. X.; Herrmann, S. D.; Simpson, M. F. *Nuclear Technology* **2010**, *171*, 292–299.

[100] Danek, V. *Physico-Chemical Analysis of Molten Electrolytes*; Elsevier, 2006.

[101] Glover, W. J.; Madden, P. A. *The Journal of Chemical Physics* **2004**, *121*, 7293–7303.

[102] Chrissanthopoulos, A.; Zissi, G. D.; Papatheodorou, G. N. *Zeitschrift für Naturforschung A* **2005**, *60*, 739–748.

[103] Okamoto, Y.; Akabori, M.; Motohashi, H.; Shiwaku, H.; Ogawa, T. *Journal of Synchrotron Radiation* **2001**, *8*, 1191–1199.

[104] Inoue, T.; Sakamura, Y.; Gaune-Escard, M. *Nato Science Series* **2002**, *52*, 249.

[105] Fujii, T.; Nagai, T.; Sato, N.; Shirai, O.; Yamana, H. *Journal of Alloys and Compounds* **2005**, *393*, L1–L5.

[106] Photiadis, G.; Brresen, B.; Papatheodorou, G. *Journal of the Chemical Society, Faraday Transactions* **1998**, *94*, 2605–2613.

[107] Fukasawa, K.; Uehara, A.; Nagai, T.; Fujii, T.; Yamana, H. *Journal of Nuclear Materials* **2011**, *414*, 265–269.

[108] Chrissanthopoulos, A.; Papatheodorou, G. *Physical Chemistry Chemical Physics* **2000**, *2*, 3709–3714.

[109] Okamoto, Y.; Shiwaku, H.; Yaita, T.; Suzuki, S.; Gaune-Escard, M. *Journal of Molecular Liquids* **2013**, *187*, 94–98.